

multi-Risk sciEnce for resilienT commUnities undeR a changiNgclimate

Codice progetto MUR: **PE00000005** – CUP LEAD PARTNER: **E63C22002000002**



Deliverable title: Harmonized modelling approach for multi-hazard physical and functional vulnerability

Deliverable ID: DV 5.3.2

Due date: November, 2024 (M24)

Submission date: November 30th, 2024

AUTHORS

Mariano Di Domenico, Gerardo M. Verderame, Marta Del Zoppo (UNINA DIST); Luca Pozza, Francesca Ferretti (UNIBO); Sergio Lagomarsino (UNIGE), Roberto Castelluccio, Rossella Marmo (UNINA DICEA), Cristina Visconti, Valeria D'Ambrosio, Ferdinando Di Martino (UNINA DIARC)

Technical references

Project Acronym	RETURN
Project Title	multi-Risk sciEnce for resilienT commUnities undeR a changiNg climate
Project Coordinator	Domenico Calcaterra UNIVERSITA DEGLI STUDI DI NAPOLI FEDERICO II domcalca@unina.it
Project Duration	December 2022 – November 2025 (36 months)

Deliverable No.	DV 5.3.2 - Harmonized modelling approach for multi-hazard physical and functional vulnerability
Dissemination level*	
Work Package	5.3- Multi-risk vulnerability and impact assessment and forecasting
Task	5.3.2 - Physical vulnerability of urban assets to multiple hazards
Lead beneficiary	UNINA
Contributing beneficiary/ies	UNINA, UNIBO, UNIGE

* PU = Public

PP = Restricted to other programme participants (including the Commission Services)

RE = Restricted to a group specified by the consortium (including the Commission Services)

CO = Confidential, only for members of the consortium (including the Commission Services)

Document history

Version	Date	Lead contributor	Description
0.1	26.07.2024	Gerardo M. Verderame and Mariano Di Domenico (UNINA DIST)	First draft
0.2	15.11.2024	Marta Del Zoppo (UNINA DIST); Roberto Castelluccio, Rossella Marmo (UNINA DICEA), Cristina Visconti, Valeria D'Ambrosio, Ferdinando Di Martino (UNINA DIARC)	First draft
0.3	25.11.2024	Luca Pozza, Francesca Ferretti (UNIBO); Sergio Lagomarsino (UNIGE)	Critical review and proofreading; Task Extended description
0.4	30.11.2024	Gerardo M. Verderame and Mariano Di Domenico (UNINA DIST)	Edits for approval
1.0	30.11.2024	All authors	Final version

Table of contents

Technical references.....	2
Document history.....	3
Table of contents	4
1. Introduction.....	5
2. Vulnerability under single hazards	17
2.1. Geophysical hazards.....	17
2.1.1. Seismic vulnerability.....	17
2.1.1.1. Seismic hazard	17
2.1.1.2. Methods for the assessment of physical vulnerability of structures.....	21
2.1.1.3. Specificity related to buildings social function.....	48
2.1.1.4. Dynamic seismic vulnerability	56
2.1.2. Tsunami vulnerability.....	59
2.1.2.1. Description of Hazard.....	59
2.1.2.2. Physical and functional vulnerability assessment methods for residential buildings	59
2.2. Climate hazards	64
2.2.1. Urban heat waves vulnerability	64
2.2.1.1. Description of Hazard.....	64
2.2.1.2. Physical and functional vulnerability assessment methods for residential buildings	65
Authors contribution	77

1. Introduction

Buildings are composed of several technical elements which are expected to respond to a set of user's needs, meet legal requirements and provide certain performance levels. With regard to the building envelope, this is commonly meant to provide privacy and security for people, to address the need for comfortable indoor environments, and to function for a certain period of time without excessive maintenance costs (Silva et al., 2016). These needs guide the design process and lead to requirements definition and performance assessment of the envelope technical elements. However, building envelopes are subject to an inevitable degradation process which velocity depends on the external forces acting on them.

The interest in technical elements service life and performance assessment is justified by several factors, including the awareness that the design quality and the global costs of a building depend on the entire life cycle of the building, i.e., the design, the construction, the operational and the demolition phases; the knowledge of the economic losses and environmental impacts associated with a damaged or low-performance envelope; the understanding of how failures of building technical elements can trigger potentially harmful events to people. On this latter point, it has been observed (Castelluccio et al., 2024) that envelope technical elements are particularly fragile elements, and they are prone to collapse under several circumstances, such as high wind and heavy rain, but also low-intensity seismic events. Also, the envelope technical elements interact with the external environment in a way that they may become a threat to people. This is the case of a detached portion of a façade when overlooking a crowded public place (Moghtadernejad et al., 2014; Ruggiero et al., 2021; Ruiz et al., 2019).

It becomes relevant to assess the vulnerability of building envelope technical elements against a set of hazards of interest, i.e., it is relevant to assess the propensity of an envelope to report damage in a specific context. Such a vulnerability assessment should be performed in a way that the identification of where to intervene to ensure that the interventions will have the largest possible beneficial impact in terms of vulnerability reduction becomes easy. For example, it would be beneficial to know if the propensity of the envelope to report damage when subject to an external force is due to its physical condition or its technological characteristics, moreover, knowing which technical element is more prone to damage compared to others and why it is so would help guiding preventive or emergency interventions.

This contribution introduces a method for assessing the vulnerability of building envelope technical elements against a set of natural hazards of interest, such as earthquake, wind, rain, and solar exposure. This is part of a bigger research aimed at assessing the people's safety risk triggered by damaged technical elements. This is why the vulnerability assessment focuses on the technical elements' propensity to be physically damaged, up to collapse and detachment from the envelope.

Analysed technical elements

The analysed technical elements are those composing the building envelope. The description of the technical elements of interest was retrieved from the Return Taxonomy (Deliverable n. 5.2.1), as depicted in Figure 1, and it comprises attribute 14 – roof shape, attribute 20 – exterior wall, attribute 21 – openings/windows, attribute 22 – cornice construction technique, attribute 24 – household drain system material. These attributes provide for the technical elements' technological characterisation and detailing. For example, a roof cornice is characterised by its construction technique, and several sub-attributes concerning the intrados and extrados shape, the face height, and the finishing description (Table 1). The readers can find the full description of the taxonomy in Deliverable n. 5.2.1

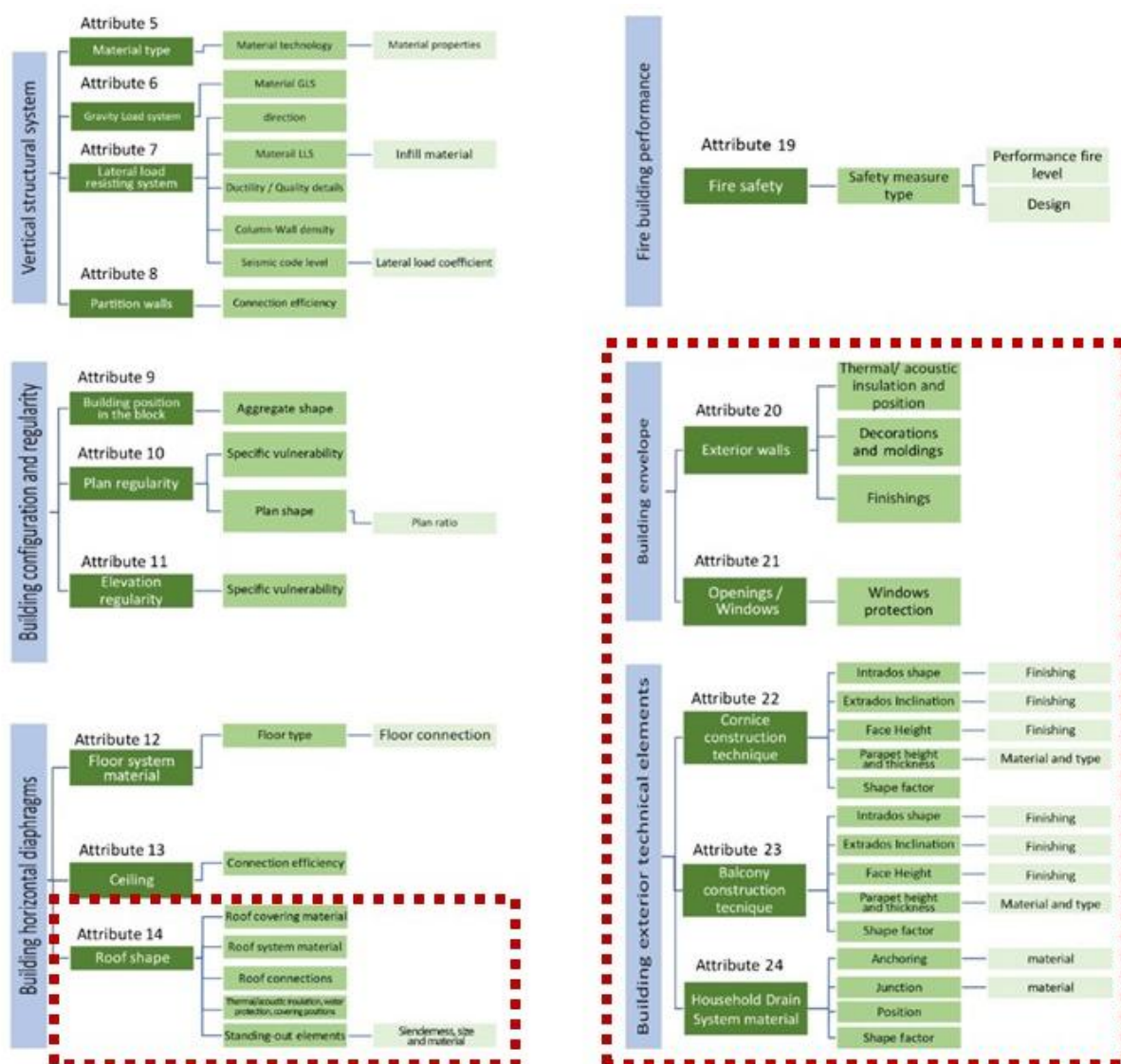


Figure 1. Attributes of interest (in red boxes)

Table 1. Cornice description according to the Return Taxonomy

Attribute 22	
ID	Cornice construction technique
--	Unknown cornice construction technique shape
CMG	Masonry, generic
CMM	With metal cantilever
CCC	Cast-in-place Reinforced Concrete
CCP	Precast Reinforced Concrete
CS	Steel
CP	Polystyrene /FRP / Polyurethane

CW	Wood		
CC	Composite/other		
ID	22.1 Intrados shape	ID	22.1.1 Finishing
--	Unknown Intrados shape	--	Unknown Intrados finishing
CIS	Shaped Intrados	CIP	Plaster finishing
CIF	Flat Intrados	CIB	Brut
ID	22.2 Extrados inclination	ID	22.2.1 Finishing
	Unknown extrados inclination		Unknown extrados
0	Flat extrados	CENP	Extrados without protection
5	up to 5°	CEW	Extrados with waterproof membrane only
15	up to 15°	CEWT	Extrados with waterproof membrane and clay tiles or stone slabs
16	more than 16°	CEWM	Extrados with waterproof membrane and metal sheet
		CET	Extrados with clay tiles or stone slabs only
		CEM	Extrados with metal sheet only
ID	22.3 Face height	ID	22.3.1 Finishing
--	Unknown Face Height	--	Unknown Face finishing
0	No face	CFP	Plaster finishing
10	up to 10cm	CFB	Brut
30	up to 30cm	CFD	Decorated
31	more than 31cm		
ID	22.4 Parapet shape	ID	22.4.1 Parapet material
--	No Parapet	--	Unknown
--	Unknown	CPMA	Masonry
CPCS	Continuous and stocky	CPRC	Concrete/ Reinforced concrete
CPCL	Continuous and slender	CPST	Steel
CPDS	Discontinuous and stocky	CPWO	Wood
CPDL	Discontinuous and slender	CPCO	Composite/Combined
ID	22.5 Shape factor		
--	Unknown shape factor		

CSF1	$H > L$		
CSF2	$H = L$		
CSF3	$H < L$		
CSF4	$H < < L$		

Hazards deriving from damaged technical elements

In line with international standards on the vulnerability of the so-called “non-structural elements” (FEMA E-74, 2012) there are at least three main categories of hazardous events triggered by damaged technical elements: safety, functional and economic losses. Regarding life safety, it is possible to mention at least injuries and fatalities, cascading damage to other objects, and road/escape/emergency route obstruction.

Functional losses may become the result of direct damage to technical elements or of the consequences produced by their damage. Functional losses are strictly related to economic losses. For example, a high-tech facility may have contents that are worth many times the value of the building's technical elements, it must be ensured, then, that these are not compromised by damaged technical elements.

Finally, costs associated with damaged technical elements can be very extensive. This is due to repair costs and downtime.

Table 2 reports the categories and some types of hazardous events triggered by damaged technical elements. It is worth noticing that any type of event can be translated into monetary loss, for example, injuries can be monetised through hospital treatment costs, downtimes can be translated into hours of work lost and related costs, etc.

Table 2. Examples of hazards triggered by damaged technical elements

Category	Type
Safety loss	Injuries and fatalities
	Road/route obstruction
	Damage to objects
Functional loss	Downtime (e.g., due to closed commercial activity)
	Additional travel time
	Number of evacuated buildings
Economic loss	Repair costs
	Costs of downtimes
	Costs of shelters

As the focus of this contribution is on building envelope technical elements and the extent to which they can become a threat to the surroundings, the authors have developed a vulnerability assessment method to estimate the propensity of the technical elements to report damage, fall and become a hazard for people. Thus, the

vulnerability assessment focuses on estimating technical elements' physical damage, while associated functional and economic losses may become the focus of future studies.

Vulnerability assessment method

Two possible approaches can be adopted to determine the propensity of a technical element to suffer damage when subject to external forces: qualitative and quantitative. The latter relies on digital simulations or empirical methods aimed to define elements' fragility curves, the former is to be used when a high-level comprehensive understanding of the topic under analysis is needed before proceeding with more detailed studies. Considering that the topic of building envelope technical elements vulnerability is relatively new, the authors adopted a qualitative approach, through the review of scientific findings, international and national guidelines, technical reports, and expert opinion. This way a preliminary assessment of elements' vulnerability against several hazards was performed, providing a solid foundation for more detailed studies.

The approach is built upon the analysis of documented damages of the envelope technical elements due to the hazards of interest, the consequent identification of vulnerability factors, and, finally, the introduction of a vulnerability grading system which can be used to compare different technical elements vulnerability per their technological characteristics and degradation level.

Vulnerability factors

First, the way each hazard can damage each exposed envelope technical element has been studied to determine potential vulnerability factors. If the available studies and sources were not sufficient to draw a clear profile of the behavior of a specific element, vulnerability factors were determined by analogy with documented behavior. Then an on-off matrix has been developed to identify the attributes and sub-attributes, i.e., the parts of the technical elements, which contribute to the vulnerability of the element against the hazards of interest. Table 3 reports an extract of the on-off matrix with regard to the roof cornice. The text below briefly exposes the results of the conducted analysis and provides a summary of the identified vulnerability factors (Table 4).

Reports and technical documentation on the vulnerability of building elements in the event of an earthquake have been used to identify the main vulnerability factors, such as those published by the Civil Protection Department in Italy (De Sortis et al., 2009), the Pacific Earthquake Engineering Research Center (Taghavi & Miranda, 2003) and the Federal Emergency Management Agency (FEMA E-74, 2012). The main causes of damage to an element during an earthquake are related to fragility, mass and deformability, which represent, then, the main vulnerability factors. For example, the analysis of the vulnerability of cornices in an earthquake considers both the construction technique and the shape factor of the cornice. The construction technique is closely related to the fragility and mass of the cornice, while the form factor affects its deformability.

Heavy rain, in particular, causes significant damage to building envelopes, as it can lead to water infiltration. In water-permeable or cracked materials, water penetrates the element, generating degradation phenomena that can even lead to the collapse of the finishes themselves (Bourcet J., et al., 2023). In addition, the shape of the element, such as the roof shape or the household drainage system element dimension, influences the ability to withstand heavy rainfall, as flat surfaces may lead to water stagnation and small drainage elements can become pressurized, and consequently fail (Papathoma-Köhle et al. 2023). The junction of the household drain system, given the different response of the system when increasing the fatigue provoked by intense rainfall events, plays a fundamental role in the determination of the vulnerability. As easily identifiable, the greater the anchoring solidity, the lower the vulnerability. Thus, the absence of a water-proofing layer, the high-water permeability of the finishings and the element's shape factor, including hydraulic capacity, represent the main vulnerability factors.

Solar exposure can generate deterioration phenomena of the technical elements of the envelope due to excessive deformations, which can lead to cracks and element collapse depending on the coefficient of thermal expansion, and photo-oxidation, which causes materials to become brittle and to potentially premature failure depending on the materials chemical structure (Kaewunruen et al., 2022). In addition, the rising temperatures require high-thermal performance building envelopes (Cabeza & Chàfer, 2020; Dong et al., 2023). Thus, the

main vulnerability factors against solar exposure and high temperatures are the coefficient of thermal expansion, the propensity to be photo-oxidated, and the thermal conductivity. Apart from the elements' intrinsic characteristics, the absence of shading and protection devices against direct solar exposure is an additional vulnerability factor to be considered when assessing the envelope's propensity to report damage due to high temperatures and solar exposure.

As far as wind is concerned, this can cause damage to the envelope technical elements due to the high pressures exerted, both positive and negative. The shape factor of the element, especially of the roofs, plays an important role, as the wind pressure changes according to the geometric configuration of the element. Negative pressures, which occur at the windward edges and corners of the roof, are responsible for most wind-induced damage (Estephan et al., 2021). In the case of discontinuous roof coverings, wind can cause the roof covering to detach, especially when the tiles are not well anchored to the substrate or when the metal panels are subjected to high suction forces (e.g. when the area of the element is large and the mass of the element is small) (Estephan et al., 2021). In addition, some impact resistance is required to reduce the damage caused by wind-propelled debris on the envelope surfaces (Smith & Masters, 2015). Thus, the main vulnerability factors to wind forces are the shape factor, the mass, the type of anchoring, low surface resistance and the fragility of the material.

Table 3. Parts of the cornice which contribute to the vulnerability of the element to different hazards

Element parts	Earthquake	Rainfall	High temperatures/solar exposure	Wind
22. Cornice construction technique	✓	✓	✓	✓
22.1 Intrados shape				
22.1.1 Intrados finishing	✓	✓		✓
22.2 Extrados inclination		✓		
22.2.1 Extrados finishing	✓	✓	✓	✓
22.3 Face height				
22.3.1 Face finishing	✓	✓	✓	✓
22.4 Parapet shape	✓			✓
22.4.1 Parapet material	✓	✓	✓	✓
22.5 Cornice shape factor	✓			✓

Table 4. Summary of identified vulnerability factors per hazard

Hazard	Potential vulnerability factors
Earthquake	Fragility, shape factor, mass
Rainfall	Shape factor (including hydraulic capacity), absence of water-proofing layer, high-water permeability material



High temperatures/solar exposure	Coefficient of thermal expansion, coefficient of thermal conductivity, chemical reactivity to photo-oxidation, absence of shading and protective devices against direct solar exposure
Wind	Fragility, shape factor, mass, surface resistance

Vulnerability grading system

Both, the Return taxonomy and the vulnerability factors exposed before are to be used to perform the vulnerability assessment of a specific element against a specific hazard. Indeed, once the vulnerability factors were identified, they were used to compare several technological solutions, as described by the Return taxonomy, accordingly. Also, while performing the vulnerability assessment, the taxonomy was reduced by considering the sub-attributes which play a major role in terms of vulnerability. You can always decide to detail the vulnerability analysis and to consider the entire set of sub-attributes included in the taxonomy, but the more the attributes, the more complex will be the analysis, leading to increased computational time with the risk of jeopardising the applicability of the overall approach.

For example, a first simplified vulnerability analysis of roof cornices against earthquakes can include the cornice construction technique (attribute n°22), the parapet material and shape factor (sub-attributes n°22.4 and n°22.4.1) and the shape factor of the roof cornice (sub-attribute n° 22.5). This is because the main reasons for a cornice to fail in case of an earthquake are related to its fragility, mass and deformability. This means that a steel cornice, without a parapet and a very small shape factor, is less vulnerable to earthquakes than a masonry cornice, with a slender masonry parapet and high shape factor. A more detailed analysis could include the finishings of the intrados, face and extrados too (sub-attributes n°22.1.1, n°22.2.1, n°22.3.1), taking into account their fragility and their fixing solutions. This means that an elastic and monolithic finishing, such as a waterproof membrane, is less vulnerable to earthquakes than a fragile and composite finishing, such as clay tiles.

Another vulnerability factor which is not described in the Return taxonomy, but is included in the proposed vulnerability assessment method, is the physical condition of the element, it is to say its degradation level. Indeed, the poorer the physical condition the more likely the element will report damage when a hazardous event occurs.

In the end, the vulnerability of a technical element was deemed to be dependent on two main factors: technological characteristics and the degradation level. Thus, for each hazard, it was possible to define a vulnerability grade ($V_{et,i}$) at the element scale based on technological characteristics ($V'_{et,i}$) adjusted by the degradation level ($\beta_{et,i}$) as per Figure 2.

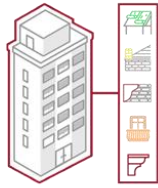
The element vulnerability was described by means of a qualitative scale to express a low, moderate, high or very high propensity of an element to suffer damage when subject to an external force. However, as the assessment method requires the combination of the two vulnerability driver factors (technological vulnerability and degradation condition), these factors were measured on a semi-quantitative scale.

More specifically, the technological vulnerability is expressed on a four-point scale ranging from low (equal to 1), moderate (equal to 2), high (equal to 3) and very high (equal to 4). An example of technological vulnerability assessment is reported in Table 5 concerning the vulnerability of roof cornices against the set of natural hazards of interest. The propensity of a cornice to suffer damage when subject to external forces depends on the vulnerability factors identified before which are driven by the element's construction characteristics, including construction technology, materials and geometry. For example, in the case of an earthquake, masonry roof cornices were deemed to be more vulnerable than reinforced concrete cornices, which were assumed to be more vulnerable than steel cornices.

To assess the degradation condition of the envelope technical elements the authors mainly referred to the well-known UNI 11182:2006 to describe the forms of alteration and degradation of natural and artificial stones, including reinforced concrete, metals and wood anomalies in the analysis too. Anomalies were assessed considering their severity (ranging from absent/very mild, to severe) and their extent (expressed in percentage of area occupied by the anomaly out of the element area). The severity mainly refers to the type of performance alteration caused by the anomaly, thus a very mild or absent anomaly is an aesthetic alteration of the element (such as, graffiti), a mild anomaly is a superficial alteration (such as, haircracking), an advanced anomaly is able to compromise the mechanical properties of the element (such as, corrosion or presence of vegetation), while a severe anomaly has already led or it is about to lead the element to collapse (e.g., detachment from support, missing parts). The degradation condition coefficient varies from 1 to 4, corresponding to absent or very mild anomalies to severe anomalies occupying the entire element surface.

Element vulnerability

$V'_{et,i}$ = Technological vulnerability



Vulnerability depending upon material properties, shape factors, technological characteristics

$$V_{et,i} = V'_{et,i} \times \beta_{et,i}$$

$\beta_{et,i}$ = Degradation condition



$$\beta_{et,i} = A_j \times \alpha_j$$

A_j = Anomaly incidence

α_j = Anomaly severity

Vulnerability depending upon the severity and the occupied surface of observed anomalies



Figure 2. Facade analysis based on technological elements and degradation characterization

ID	Attribute	Vulnerability grade per hazard			
	22 Cornice construction technique	Earthquake	Heavy Rain	High Temp.	Wind
--	Unknown				
CMG	Masonry, generic	Very high	Very high	Low	Low
CMM	With metal cantilever	High	High	Low	Low
CCC	Cast-in-place Reinforced Concrete	Moderate	Moderate	Low	Low
CCP	Precast Reinforced Concrete	High	Moderate	Low	Low
CS	Steel	Low	Low	Very high	Moderate
CP	Polystyrene /FRP / Polyurethane	Low	Moderate	Very high	Very high
CW	Wood	Low	Very high	Low	High
CC	Composite / other	Very high	Very high	Very high	Very high
	22.1.1 Intrados Finishing	Earthquake	Heavy Rain	High Temp.	Wind
--	Unknown Intrados finishing				
CIP	Plaster finishing	Moderate	Moderate	Moderate	
CIB	Brut	Low	Very high	Very high	
CID	Decorated	Very high	Low	Low	
	22.2 Extrados inclination	Earthquake	Heavy Rain	High Temp.	Wind
--	Unknown extrados inclination				
0	Flat extrados		Very high		
5	Up to 5°		High		
15	Up to 15°		Moderate		
16	More than 15°		Low		
	22.2.1 Extrados Finishing	Earthquake	Heavy Rain	High Temp.	Wind
--	Unknown extrados				
CENP	Extrados without protection	Low	Very high	Very high	Low
CEW	Extrados with waterproof membrane only	Low	Low	High	Moderate
CEWT	Extrados with waterproof membrane and clay tiles or stone slabs	Very high	Low	Low	Very high
CEW M	Extrados with waterproof membrane and metal sheet	Moderate	Low	High	Very high

CET	Extrados with clay tiles or stone slabs only	Very high	High	Low	Very high
CEM	Extrados with metal sheet only	Moderate	High	Very high	Very high
	22.3.1 Face Finishing	Earthquake	Heavy Rain	High Temp.	Wind
--	Unknown Face finishing				
CFP	Plaster finishing	Moderate	Moderate	Moderate	
CFB	Brut	Low	Very high	Very high	
CFD	Decorated	Very high	Low	Low	
	22.5 Shape factor	Earthquake	Heavy Rain	High Temp.	Wind
--	Unknown shape factor				
CSF1	$H > L$	Low			Low
CSF2	$H = L$	Low			Low
CSF3	$H < L$	High			High
CSF4	$H < < L$	Very high			Very high
	22.4 Parapet shape	Earthquake	Heavy Rain	High Temp.	Wind
--	Unknown shape				
CPCS	Continuous and stocky	Low			High
CPCL	Continuous and slender	Very high			Very high
CPDS	Discontinuous and stocky	Low			Low
CPDL	Discontinuous and slender	High			Low
	22.4.1 Parapet material	Earthquake	Heavy Rain	High Temp.	Wind
--	Unknown material				
CPMA	Masonry	Very high	Very high	Low	Low
CPRC	Concrete / Reinforced concrete	Moderate	Moderate	Moderate	Low
CPST	Steel	Low	Low	Very high	Moderate
CPWO	Wood	Low	Very high	Moderate	Very high
CPCO	Combined/Composite	Very high	Very high	Very high	Very high

In the end, the element vulnerability can assume values ranging from 1 (low technological vulnerability and absence of anomalies) to 16 (very high technological vulnerability combined with extensive severe degradation). It is worth noticing that the degradation condition weighs way more than the technological characteristics when it comes to estimating the propensity of an element to suffer damage if subject to an external force. This idea relies on statistical analysis conducted at the national level on data concerning the emergency interventions performed by the Italian fire brigades which prove that poor physical condition was the main cause of intervention, independently from geographic area and natural hazard.

The value assigned to the element vulnerability (from 1 to 16) can be expressed on a qualitative scale for better interpretation, where an element is deemed to have a low vulnerability against a specific hazard when the vulnerability value varies from 1 to 3.99 (green-coloured), a moderate vulnerability for values ranging from 4 to 6.99 (yellow-coloured), a high vulnerability for values ranging from 7 to 10.99 (orange-coloured), and a very high vulnerability for higher values (red-coloured).

The results that you can get from this vulnerability assessment method consist of a structured way of comparing different elements based on their vulnerability grades. Based on this comparison, you can understand if a building envelope is consistently vulnerable to a specific hazard, and thus requires major renovation interventions (such as, refurbishment of the entire facade) or if minor localised interventions are needed (for example, replacing the roof cornice water-proofing membrane only). An example of a façade vulnerability map is reported in Figure 3 where you can easily identify the areas of major concern in case of an earthquake.

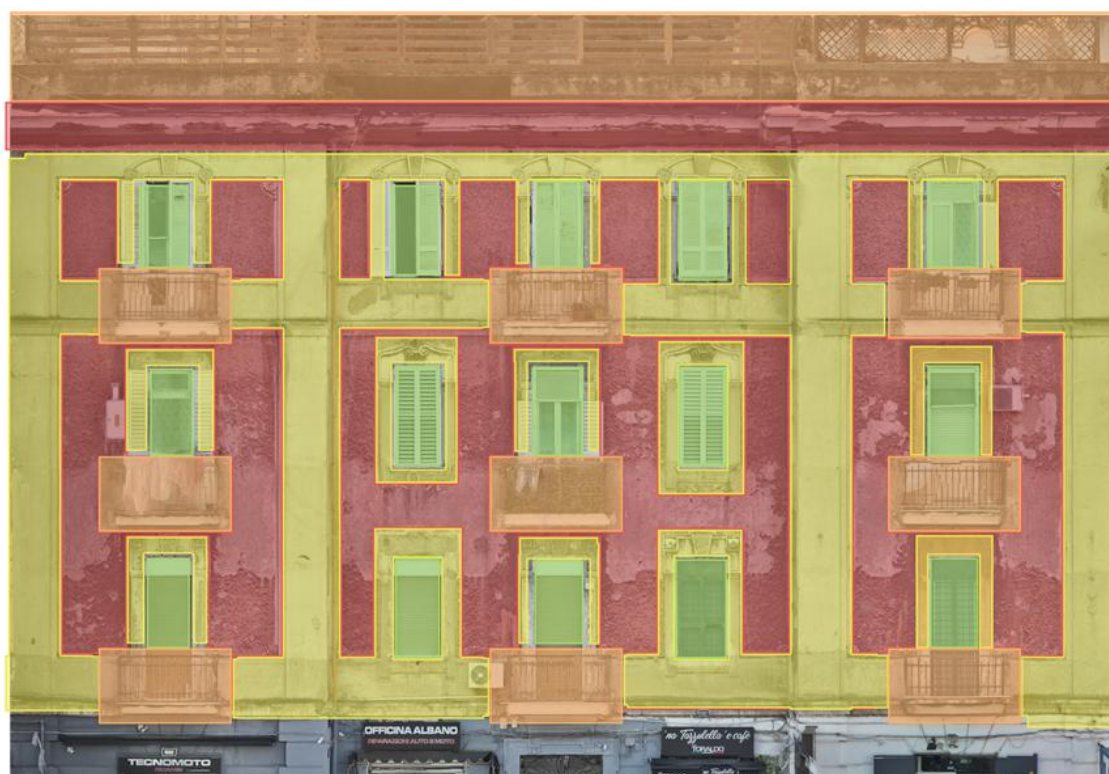


Figure 3. Example of façade vulnerability map in case of an earthquake

2. Vulnerability under single hazards

2.1. Geophysical hazards

2.1.1. Seismic vulnerability

2.1.1.1. Seismic hazard

Earthquake or seism or earth tremor is classified as Geohazard GH0001 according to the Hazard Information Profile (USGS 2020). According to the United States Geological Survey (USGS), as reported by the Hazard Information Profile, “Earthquake is a term used to describe both sudden slip on a fault, and the resulting ground shaking and radiated seismic energy caused by the slip, or by volcanic or magmatic activity, or other sudden stress changes in the Earth”.

Other deliverables may include information and details about the geophysical origin of tectonic earthquakes, i.e., about the fact that the shaking felt on the earth surface is due to sudden (potentially after a rupture) slip on a fault. In this deliverable, earthquake is investigated as a phenomenon striking people, buildings, infrastructures, communities, with highly detrimental effects. In other words, what happens below roughly 30 meters down below the Earth's surface is not of interest. Also, note that this report is focused on tectonic earthquakes, while earth tremors may be also due to volcanic activity, fracking, and other forms of energy release from the Earth crust.

According to Hazard Information Profile, between 1994 and 2013, earthquakes and their related hazards (both primary and secondary) caused nearly 750,000 deaths, surpassing the fatalities from all other natural disasters combined (CRED, 2015). While technology to reduce earthquake hazards is not yet available, the risks to buildings, infrastructure, and human populations can be mitigated through seismic retrofitting of existing structures, stricter adherence to seismic safety building codes, and avoiding construction on cliff faces, soft soils, or near active faults.

As it is well known, earthquakes manifests with a sudden motion of the ground lasting from few seconds up to a couple of minutes. This movement can be described as a ground displacement or acceleration changing in time. Nowadays, displacement and accelerations can be measured, thus allowing the identification of earthquake intensity through quantitative Intensity Measure (IM). In the past, earthquake intensity was qualitatively identified via the effects that it had on people and structures. Namely, some earthquakes are felt only by instruments, while some others, in the history, provoked thousands and thousands of deaths, injuries, total destruction of structures, devastation of territory, modification of ground surface shape: this is the rationale behind the well-known Mercalli-Cancani-Sieberg macro-seismic intensity scale (from level I to level XII), formalized between the end of XIX and the beginning of XX century, and modified (modified MCS) by Wood and Neumann in 1931 and by Richter in 1956.

Despite macro-seismic intensity has been a fundamental tool for the reconstruction of the history of seismicity for earthquake-prone areas (and, thus, of their seismic hazard), quantitative measures are paramount for the characterization of the seismic hazard of an area with a probabilistic approach and, finally, for the assessment of seismic risk.

Richter Magnitude (M), dating from 1935, is a quantitative measure of the earthquake intensity. For its calculation, a registration of the seismic motion is needed, as it is defined as the logarithm of the amplitude of the seismic waves registered by a seismograph with certain features. A more objective definition of seismic magnitude is Moment Magnitude M_W , which is related via empirical logarithmic formulations to the energy released, or radiated, by the earthquake, which is a physical property of the phenomenon basically independent on the instrument that registered it. Moment magnitude is a number varying from 1 to 10.



Despite Magnitude (in one of its various definitions) is widely used by Civil Protection and Emergency Management institutions, as well as in the scientific literature, especially in the geological and geophysical area, the IM preferred from the engineering point of view is the Peak Ground Acceleration (PGA), i.e., the maximum acceleration imposed to the ground by the earthquake, or the Pseudo-Spectral Acceleration (Sa or PSA) of a generic Single Degree of Freedom (SDOF) system with fixed vibration period and damping ratio placed on the shaking ground.

A comparison between MCS scale, Richter Magnitude Scale and PGA values is shown in Table 6, according to USGS.

Table 6. Comparison between MCS intensity, Richter Magnitude (according to USGS) and PGA (Worden et al. 2011).

modified MCS intensity	Richter Magnitude	Approximate PGA	Shaking description according to MCS
I	up to 3.9	0.0005 g	Not felt. Not felt except by very few under especially favorable conditions.
II	up to 3.9	0.003 g	Weak. Felt only by a few people at rest, especially on upper floors of buildings. Delicately suspended objects may swing.
III	up to 3.9	0.003 g	Weak. Felt quite noticeably by people indoors, especially on upper floors of buildings: Many people do not recognize it as an earthquake. Standing vehicles may rock slightly. Vibrations are similar to the passing of a truck, with duration estimated.
IV	up to 4.9	0.028 g	Light. Felt indoors by many, outdoors by few during the day: At night, some are awakened. Dishes, windows, and doors are disturbed; walls make cracking sounds. Sensations are like a heavy truck striking a building. Standing vehicles are rocked noticeably.
V	up to 4.9	0.062 g	Moderate. Felt by nearly everyone; many awakened: Some dishes and windows are broken. Unstable objects are overturned. Pendulum clocks may stop
VI	up to 5.9	0.12 g	Strong. Felt by all, and many are frightened. Some heavy furniture is moved; a few instances of fallen plaster occur. Damage is slight.
VII	up to 5.9	0.22 g	Very strong. Damage is negligible in buildings of good design and construction; but slight to moderate in well-built ordinary structures; damage is considerable in poorly built or badly designed structures; some chimneys are broken. Noticed by motorists.
VIII	up to 6.9	0.40 g	Severe. Damage slight in specially designed structures; considerable damage in ordinary substantial buildings with partial collapse. Damage great in poorly built structures. Fall of chimneys, factory stacks, columns, monuments, walls. Heavy furniture overturned. Sand and mud ejected in small amounts. Changes in well water. Motorists are disturbed.
IX	up to 6.9	0.75 g	Violent. Damage is considerable in specially designed structures; well-designed frame structures are thrown off-kilter. Damage is great in substantial buildings, with partial collapse. Buildings are shifted off foundations. Liquefaction occurs. Underground pipes are broken.
X	over 6.9	> 1.39 g	Extreme. Some well-built wooden structures are destroyed; most masonry and frame structures are destroyed with foundations. Rails are bent. Landslides considerable from river banks and steep slopes. Shifted sand and mud. Water splashed over banks.
XI	over 6.9	> 1.39 g	Extreme. Few, if any, (masonry) structures remain standing. Bridges are destroyed. Broad fissures erupt in the ground. Underground pipelines

			are rendered completely out of service. Earth slumps and land slips in soft ground. Rails are bent greatly.
XII	over 6.9	> 1.39 g	Extreme. Damage is total. Waves are seen on ground surfaces. Lines of sight and level are distorted. Objects are thrown upward into the air.

PSA and PGA are the same only if PSA is calculated for a SDOF with vibration period virtually equal to zero; otherwise, they may be significantly different. The function relating PSA to the vibration period T , at given damping ratio, is called Pseudo-Acceleration Response Spectrum. An example PSA Response Spectrum is shown in Figure 4.

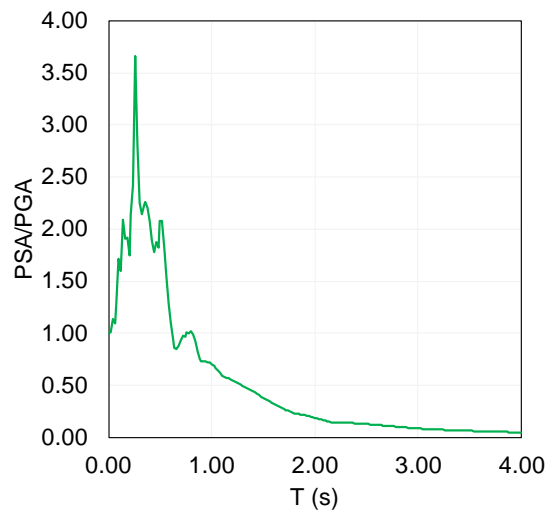


Figure 4. Pseudo-acceleration response spectrum (example).

Typically, PSA is the most adopted IM for seismic hazard assessment (and vulnerability, as shown in the next sections) characterization in current structural engineering, but this basically depends on the objective of seismic hazard analysis and on the object of seismic vulnerability analysis (for example, for risk analysis of spatial infrastructures, such as pipelines networks, Peak Ground Velocity is nowadays a preferred IM).

Once PSA at a certain vibration period is selected as IM, the seismic hazard of an earthquake-prone area is represented by a hazard curve obtained via a Probabilistic Seismic Hazard Analysis (PSHA). Basically, as a result of this analysis, one can obtain, for a certain area, the relationship between the IM values and the probability of exceeding that intensity measure value in a year, that under certain common hypotheses can be confused with the rate of exceedance of that intensity measure in a year, $\lambda(\text{IM})$. The inverse of the rate of exceedance is named return period, TR , which is average time interval between events exceeding the specific value of interest of the selected IM. Example of hazard curves for different sites are shown in Figure 5.

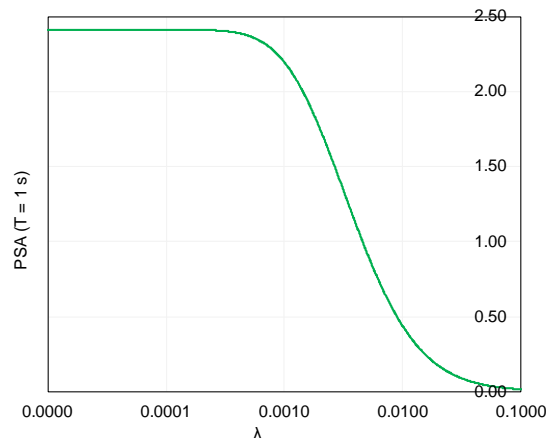


Figure 5. Hazard curve for L'Aquila (Italy) site relating the pseudo-spectral acceleration at $T=1$ s with the rate of exceedance. Curve calculated by using REASSESS (Chioccarelli et al. 2018). PSA expressed in g units.

Once a hazard curve is selected as representative of the seismic hazard of a specific site of interest, vulnerability assessment of structures allows describing, potentially with a probabilistic approach, the relationship between increasing IM values and the effect of the occurrence of an earthquake with that IM to the structure or set of structures of interest. This effect is typically a damage level, or damage state, that can range from absent/slight to total, corresponding to structural real collapse. Damage thresholds are expressed as a function of an Engineering Demand Parameters (e.g., top or interstorey displacement demand). Threshold values of the EDP are determined based on experimental or mechanical studies (Elnashai 2006) In fact, vulnerability expresses the propensity or predisposition of an individual, a community, infrastructure, assets or systems (including ecosystems) to be adversely affected by hazards (UNDRR, 2016).

Based on the above discussion, hazard analysis allows the assessment of the probability of exceedance of a certain IM in a certain site; vulnerability analysis allows the assessment of the probability of attaining or exceeding a certain damage level for a certain structure at varying IM. The appropriate combination of hazard analysis and vulnerability analysis allows the assessment of the probability of exceeding or attaining a certain damage level for a structure in case of earthquake in a certain site.

The association of a certain impact to the exceedance of damage levels (e.g. in terms of deaths, injuries, economic losses, etc.) is the object of the exposure analysis. As it is well known, the combination of hazard, vulnerability, and exposure analysis provides estimates of seismic risk, i.e., of the probability of observing or exceeding certain consequences (number of deaths, number of displaced people, number of injured, amount of money that must be spent for recovery etc.) due to the impact of an earthquake event on a structure or on a set of structures.

The Global Earthquake Model Foundation created a global map of earthquake hazard and risk (GEM, 2018) and is releasing the national and regional models that support it. Many of GEM's hazard models have been developed by or in partnership with national governments for use in seismic design regulations in building codes.

This section of this deliverable is dedicated to methods adopted for the assessment of seismic vulnerability of structures. Section 2 focuses on methods proposed in the literature for the assessment of physical vulnerability (empirical, mechanical, hybrid, judgment-based). Section 3 focuses on specificity, within vulnerability assessment, related to the social functions of buildings (i.e., the differences in vulnerability assessment for residential, educational, hospital, cultural heritage

buildings). Section 4 investigates the recent topic of dynamic vulnerability assessment, i.e., how vulnerability against a hazard (seismic hazard, in this case) is changed by the occurrence of other hazardous events or by other natural phenomena (e.g., aging, degradation, etc.).

2.1.1.2. Methods for the assessment of physical vulnerability of structures

As already stated, vulnerability expresses the propensity or predisposition of an individual, a community, infrastructure, assets or systems (including ecosystems) to be adversely affected by hazards (UNDRR, 2016).

Different methods for the assessment of physical vulnerability of structures exist. A key difference exists between empirical and analytical methods of assessing vulnerability: empirical methods rely on observing damage experienced by specific building types during previous earthquakes to estimate expected damage, while analytical methods use a model with direct physical interpretation to establish the relationship between seismic intensity and expected damage.

The reliability and significance of observed data enable empirical methods to realistically predict expected damage, as long as these methods are applied to building stocks with similar characteristics to those used in their development. However, empirical methods have several disadvantages. They fail to account for the vibration characteristics of buildings and do not explicitly model the various sources of uncertainty, preventing the removal of uncertainty in the seismic demand from the vulnerability assessment. Seismic intensity is often defined using a macroseismic measure, which is itself derived from observed damage, making seismic intensity and damage interdependent (Crowley et al., 2009). Additionally, collecting data on building damage after an earthquake, which is essential for developing empirical relationships between seismic intensity and expected damage, has several shortcomings. These include inconsistent data availability, leading to greater statistical reliability for lower damage/ground motion ranges compared to higher ones, and errors from inadequately filled post-earthquake assessment forms (Colombi et al., 2008). Furthermore, empirical methods cannot model the influence of retrofit solutions on vulnerability, which stems from improvements in structural response.

Conversely, using an algorithm to evaluate structural vulnerability allows for a detailed and transparent consideration of various building stock characteristics and explicitly accounts for uncertainties in the assessment process. An analytical approach enables the inclusion of structures with different or new construction practices in the vulnerability assessment and considers the impact of retrofitting on the response of existing structures. Additionally, analytical methods benefit from advancements in seismic hazard assessment, such as the creation of seismic hazard maps using spectral ordinates (e.g., INGV-DPC S1, 2007), rather than relying on macroseismic intensity or PGA. However, analytical methods generally require more detailed data and greater computational effort compared to empirical methods. Therefore, the actual increase in accuracy when using analytical methods should be validated through comparison with observed damage data.

There are critical issues to consider when applying analytical methods. These include the confidence in a numerical model's ability to accurately predict the response of real structures and the correlation between the assumed analytical damage index (e.g., interstorey drift or a cyclic damage index) and actual structural damage. Additionally, many collapses observed after seismic events result from construction errors and deficiencies, which are typically not accounted for in analytical models (e.g., Verderame et al., 2010).

Empirical and analytical methods can complement each other, as seen in "hybrid" methods. Furthermore, relationships between seismic intensity and expected damage for different structural typologies can also be based on expert judgment.

A very comprehensive and detailed review of seismic vulnerability assessment methodologies can be found in (Calvi et al., 2006). More recently, updated state-of-the-art reviews with comparison of the application of different vulnerability assessment methods were proposed by D'Ayala et al. (2015) and by Ceroni et al. (2020).

In the following, main vulnerability assessment procedures are illustrated.

2.1.1.2.1. Empirical methods

First developments of seismic vulnerability assessment of building stocks took place in 1970s, through empirical methods based on macroseismic intensity; at the time, the major part of hazard maps adopted this kind of measure for the seismic intensity.

Different types of empirical methods for the seismic vulnerability assessment of buildings can be distinguished:

- Damage Probability Matrices (DPMs), expressing in a discrete form the conditional probability of reaching a damage level $D = j$ due to a ground motion of intensity $I = i$, $P_{ij} = P [D = j | I = i]$;
- vulnerability functions, expressing in a continuous form the probability $P_{ij} = P [D \geq j | I = i]$;
- methods based on a so-called “Vulnerability Index”;
- screening methods.

Damage Probability Matrices

First DPMs have been proposed in (Whitman et al., 1973), see Figure 6 for a given structural typology. In this DPM the probability of being in a given state of structural and non-structural damage is provided. For each damage state, the damage ratio is provided too, representing the ratio between the cost of repair and the cost of replacement. These DPMs are compiled for different structural typologies based on the damage observed in over 1600 buildings after the 1971 San Fernando earthquake.

Damage State	Structural Damage	Non-structural Damage	Damage Ratio (%)	Intensity of Earthquake				
				V	VI	VII	VIII	IX
0	None	None	0-0.05	10.4	-	-	-	-
1	None	Minor	0.05-0.3	16.4	0.5	-	-	-
2	None	Localised	0.3-1.25	40.0	22.5	-	-	-
3	Not noticeable	Widespread	1.25-3.5	20.0	30.0	2.7	-	-
4	Minor	Substantial	3.5-4.5	13.2	47.1	92.3	58.8	14.7
5	Substantial	Extensive	7.5-20	-	0.2	5.0	41.2	83.0
6	Major	Nearly total	20-65	-	-	-	-	2.3
7	Building condemned		100	-	-	-	-	-
8	Collapse		100	-	-	-	-	-

Figure 6. Damage Probability Matrix proposed by Whitman et al. (1973) (from (Calvi et al., 2006))

Braga et al. (1982) proposed the first European version of DPMs based on the damage observed after the 1980 Irpinia earthquake. Three vulnerability classes (A, B and C) corresponding to different

building typologies are defined, and the seismic intensity measure is based on the Medvedev-Sponheuer-Karnik (MSK) scale.

DPMs proposed by Braga et al. (1982) are improved by Di Pasquale et al. (2005) changing the seismic intensity measure from the MSK to the Mercalli-Cancani-Sieberg (MCS) scale and dividing class C into two sub-classes to differentiate between good masonry (C1) and RC buildings (C2) (see Figure), as described in (Di Pasquale and Orsini, 1997). Furthermore, the number of buildings is replaced by the number of dwellings in order to use the original inventory from the 1991 census of the Italian National Institute of Statistics (*Istituto Nazionale di Statistica*, ISTAT).

The DPMs from (Braga et al., 1982) are also adapted for the town of Potenza by Dolce et al. (2003), adding the vulnerability class D, which represents the buildings constructed since 1980, and expressing the seismic intensity according to the European Macroseismic Scale (EMS-98) (Grünthal, 1998).

Table I. Vulnerability classes vs. horizontal and vertical structural elements.

Horizontal structure	Vertical structure			
	Masonry walls			R.C.
	Field stone	Hewn stone	Bricks	
Vaults	A	A	A	\
Wood	A	A	B	\
Steel & vaults	B	B	C1	\
R.C.	B	C1	C1	C2

Table II. Vulnerability classes vs. age for masonry buildings.

Age	Vulnerability class		
	A	B	C1
< 1919	0.74	0.23	0.03
'19-'45	0.52	0.40	0.08
'46-'60	0.25	0.47	0.28
'61-'71	0.04	0.31	0.65
'72-'91	0.02	0.19	0.79

Figure 7. Vulnerability classes adopted in (Di Pasquale et al., 2005)

According to EMS-98 scale six vulnerability building classes (A to F, see Figure 8) are defined, then for each class a qualitative description ("few", "many" and "most", see Figure 9) of the proportion of buildings suffering a given level of damage (1 to 5, see Figure 10) is provided as a function of the seismic intensity level, ranging from V to XII. Hence, DPMs are implicitly defined in EMS-98 scale. Nevertheless, they are incomplete (the proportion of buildings suffering a given damage level for a given seismic intensity is not provided for all possible combinations of damage levels and seismic intensities) and vague (proportion of buildings is described only qualitatively).

Type of Structure		Vulnerability Class					
		A	B	C	D	E	F
MASONRY	rubble stone, fieldstone	○					
	adobe (earth brick)	○	—				
	simple stone	—	○				
	massive stone		—	○	—		
	unreinforced, with manufactured stone units	—	○	—			
	unreinforced, with RC floors		—	○	—		
	reinforced or confined			—	○	—	
REINFORCED CONCRETE (RC)	frame without earthquake-resistant design (ERD)	—	—	○	—		
	frame with moderate level of ERD		—	—	○	—	
	frame with high level of ERD			—	—	○	—
	walls without ERD		—	○	—		
	walls with moderate level of ERD			—	○	—	
	walls with high level of ERD				—	○	—
STEEL	steel structures			—	—	○	—
WOOD	timber structures		—	—	○	—	

○ most likely vulnerability class; — probable range;
.....range of less probable, exceptional cases

Figure 8. Vulnerability classes according to EMS-98 scale (Grünthal, 1998)

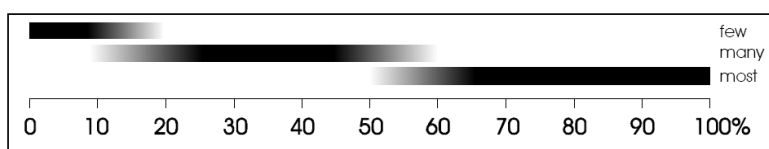


Figure 9. Definition of quantities “few”, “many” and “most” according to EMS-98 scale (Grünthal, 1998)

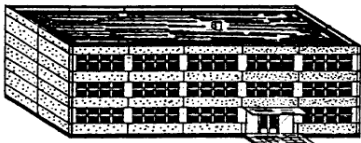
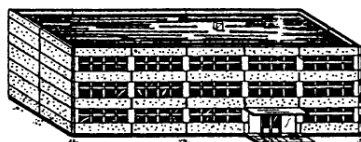
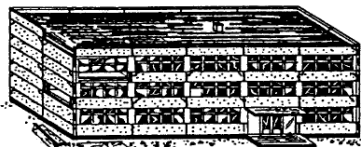
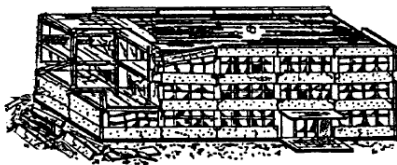

Classification of damage to buildings of reinforced concrete	
	<p>Grade 1: Negligible to slight damage (no structural damage, slight non-structural damage)</p> <p>Fine cracks in plaster over frame members or in walls at the base.</p> <p>Fine cracks in partitions and infills.</p>
	<p>Grade 2: Moderate damage (slight structural damage, moderate non-structural damage)</p> <p>Cracks in columns and beams of frames and in structural walls.</p> <p>Cracks in partition and infill walls; fall of brittle cladding and plaster. Falling mortar from the joints of wall panels.</p>
	<p>Grade 3: Substantial to heavy damage (moderate structural damage, heavy non-structural damage)</p> <p>Cracks in columns and beam column joints of frames at the base and at joints of coupled walls. Spalling of concrete cover, buckling of reinforced rods.</p> <p>Large cracks in partition and infill walls, failure of individual infill panels.</p>
	<p>Grade 4: Very heavy damage (heavy structural damage, very heavy non-structural damage)</p> <p>Large cracks in structural elements with compression failure of concrete and fracture of rebars; bond failure of beam reinforced bars; tilting of columns.</p> <p>Collapse of a few columns or of a single upper floor.</p>
	<p>Grade 5: Destruction (very heavy structural damage)</p> <p>Collapse of ground floor or parts (e. g. wings) of buildings.</p>

Figure 10. Definition of damage grades to RC buildings according to EMS-98 scale (Grünthal, 1998)

Giovinazzi and Lagomarsino (2004) and Lagomarsino and Giovinazzi (2006), within RISK-UE Project, start from these matrices and overcome their limits of incompleteness and vagueness, then relate the obtained DPMs to the building stock through a vulnerability index

Continuous vulnerability curves with or without Vulnerability Index

Relationships between seismic intensity and expected damage based on empirical data can also be derived in a continuous form.

Orsini (1999) elaborates the data of the damage survey carried out after the 1980 Irpinia earthquake in order to evaluate, for each municipality, a value of seismic intensity according to the Parameterless

Scale of Intensity (PSI) proposed by Spence et al. (1991). The main hypothesis at the basis of the PSI model is that the intensity at which the structures belonging to a single vulnerability class overcome a given damage threshold is continuously distributed according to a Gaussian model. The use of PSI allows the definition of continuous vulnerability functions depending on a macroseismic intensity parameter, tackling the problem that macroseismic intensity is not a continuous variable. After determining PSI values for each municipality, Orsini (1999) proposes vulnerability curves for apartment units as a function of this continuous parameter.

Sabetta et al. (1998) derive vulnerability curves depending on PGA, Arias Intensity and effective peak acceleration based on the elaboration of about 50000 building damage surveys from past Italian earthquakes, by calculating for each municipality a mean damage index as the weighted average of the frequencies of each damage level for each structural class.

Rota et al. (2008) select more than 91000 damage survey forms from past Italian earthquakes out of a total amount of 164000 ones, (i) disregarding the data affected by important information missing and (ii) including only data related to municipalities surveyed for at least 60%, thus avoiding a biased sample. The authors subdivide these data into 23 different building typologies and 10 ground motion intervals. Both PGA and Housner intensity are considered as ground motion parameters; their values are estimated for each municipality using the attenuation law of Sabetta and Pugliese (1987, 1996) for rock conditions, with the parameters (magnitude and epicentral coordinates) of the earthquake of interest. The adopted damage scale is similar to the EMS-98 scale, consisting of five levels of damage plus the case of no damage. DPMs are extracted from the data for all of the 23 considered vulnerability classes, according to the defined damage scale and seismic intensity scale. Hence, continuous vulnerability curves are obtained by fitting with lognormal distributions the data evaluated in form of DPMs; also, when carrying out this fitting, for each sample (given a building class, a seismic intensity and a damage level) the inverse of the estimated standard deviation is used as a weight expressing the reliability of the single sample.

It is to be noted that when the seismic intensity is measured by means of a parameter related to the spectral acceleration or spectral displacement at the fundamental period of vibration (e.g., Rossetto and Elnashai, 2003), different from macroseismic intensity or PGA, the vulnerability curves show a better prediction capacity, because taking into consideration the relationship between the frequency content of the ground motion and the dynamic characteristics of the building stock.

The “Vulnerability Index” method is first proposed in (Benedetti and Petrini, 1984; GNDT, 1993). The index I_v is evaluated by means of a field survey form where “scores” K_i (from A to D) are assigned to eleven parameters having a high influence on building vulnerability (see Table 7); then, the index is defined as the weighted sum

$$I_v = \sum_{i=1}^{11} K_i W_i \quad (1.2.3.1)$$

according to the importance assigned to each parameter.

Table 7. Partial indicators of structural vulnerability.

Indicator	Specification for masonry buildings	Specification for RC buildings
Type and organization of the resisting system	Effectiveness of connections, box behaviour	Design code, availability of structural drawings
Quality and technology of the resisting system	Homogeneity and quality of masonry	Including typology of the resisting system and quality of materials
Conventional strength	Simplified assessment of lateral strength	Not present
Position of the buildings and foundations	Soil conditions and foundation typology	0.028 g
Horizontal structure	Stiffness and connection to vertical structure of floor slabs	Number and typology
Plan regularity		Not present
Elevation regularity		Present as “vertical structures” characterization
Distance between resisting systems		Not present
Top roof type	Sloping or flat	Sloping or flat
Non structural elements		
Conservation	Potential presence of damage and/or degradation	Potential presence of damage and/or degradation

Based on observed damage data from past earthquakes, for different values of this vulnerability index a relationship can be calibrated between seismic intensity and damage ratio (i.e., the ratio between the cost of repair and the cost of replacement) (see Figure 11).

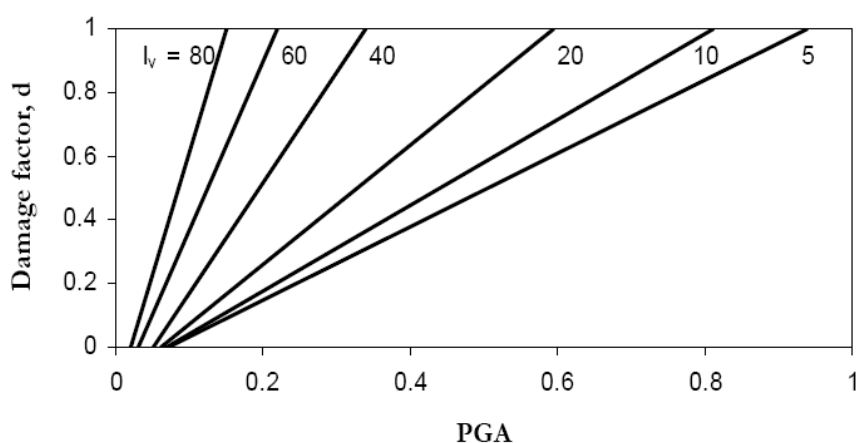


Figure 11. Vulnerability functions to relate damage ratio and PGA for different values of vulnerability index (adapted from Guagenti and Petrini (1989)) (from (Calvi et al., 2006))

The use of Vulnerability Index Method was quite widespread; it was also adopted in different projects such as RISK-UE (Mouroux and Le Brun, 2006) and “Progetto Catania” (Faccioli et al., 1999; Faccioli and Pessina, 2000).

As already stated, Giovinazzi and Lagomarsino (2004) and Lagomarsino and Giovinazzi (2006), within RISK-UE Project, start from DPM matrices based on EMS-98 scale and overcome their limits of incompleteness and vagueness, then relate the obtained DPMs to the building stock through a vulnerability index.

More specifically, the Authors propose a macroseismic method and a mechanical method. The mechanical method is described in the section dedicated to analytical methods of this deliverable. The two methods are then cross-validated. For the application of both methods, the building typology classification shown in Figure 12 is proposed.

Typologies	Building types
Unreinforced Masonry	M1 Rubble stone
	M2 Adobe (earth bricks)
	M3 Simple stone
	M4 Massive stone
	M5 U Masonry (old bricks)
	M6 U Masonry – r.c. floors
Reinforced/confined masonry	M7 Reinforced/confined masonry
Reinforced Concrete	RC1 Concrete Moment Frame
	RC2 Concrete Shear Walls
	RC3 Dual System

Figure 12. Proposal for a European building typology classification by Lagomarsino and Giovinazzi (2006)

Also, sub-typologies are defined: masonry buildings are furtherly distinguished for the horizontal structure (vaults, slabs, etc.); pilotis sub-typology is defined for RC structures. For all buildings, a further sub-typology is defined based on the building hight (RC) or number of floors (masonry), as well as based on the level of seismic design in terms of seismic action and ductility class.

Within the macroseismic approach, a Vulnerability index V and a Ductility index Q are assigned to each of the abovementioned structural typologies and subtypologies. These two numbers are the parameters of a continuous vulnerability function relating the expected damage grade (a continuous number between 0 and 5, according to EMS-98) with the macroseismic intensity. The vulnerability curves are obtained by transforming, using a fuzzy approach, the linguistic DPMs defined by EMS-98 scale in fuzzy crisp functions.

$$\mu_D = 2.5 \left[1 + \tanh \left(\frac{I + 6.25V - 13.1}{Q} \right) \right]$$

Gueguen et al. (2007) propose a vulnerability index method useful for vulnerability assessment in moderate-to-low seismic hazard regions. In this case, six structural parameters are required: 1. Material (masonry, RC, wood, steel, adobe, mixed); 2. Soil type (slope or flat, rock or sediment); 3. Age of construction; 4. Roof type (flat or sloping); 5. Plan regularity (yes or no); 6. Elevation regularity (yes or no). A potential seventh parameter is considered if the structure belongs to a block, since it individuates the position of the structure in the block. A number is associated to the possible letteral value assumed by these structural parameters, as well as a weight to each parameter. The linear combination of weights and values define a vulnerability index. However, vulnerability indices are also used to calculate vulnerability curves (they become a parameter of the curve) relating the damage grade to the macroseismic intensity.

The SAVE Method by Zuccaro and Cacace (2015) refines the EMS-98 typological classification by calibrating it based on damage observed in Italian buildings after eight significant earthquakes between 1980 and 2002. This method assesses building vulnerability through a synthetic damage parameter (SPD), which is influenced by the type of vertical resistant elements and further modified by 11 additional parameters related to the building's seismic behavior. Vulnerability is categorized into four classes (Av, Bv, Cv, Dv), which align with EMS vulnerability classes (AEMS to EEMS). The method takes into account dependencies between parameters to avoid overestimation and defines new vulnerability classes based on corrected SPD ranges: Class A ($SPD \geq 2.0$), Class B ($1.7 \leq SPD < 2.0$), Class C ($1.4 \leq SPD < 1.7$), and Class D ($1.0 \leq SPD < 1.4$).

Recently, Rosti et al. (2022) and Ferranti et al (2024), among others, proposed classical empirical vulnerability assessment methods aided, for the analysis of empirical data, by machine learning techniques.

Screening methods

According to the Japanese Seismic Index Method (JBDPA, 1990), the seismic performance of the building is represented by a seismic performance index, I_s , evaluated by means of a screening procedure. The procedure can be carried out according to three different levels of detail. I_s is calculated for each storey in every frame direction according to the following expression:

$$I_s = E_0 S_D T \quad (1.2.4.1)$$

where E_0 , S_D and T correspond to the basic structural performance, to the structural design and to the time-dependent deterioration of the building, respectively. E_0 is given by the product between C and F , respectively representing the ultimate strength and the ductility of the building, depending on the failure mode, the total number of storeys and the position of the considered storey. S_D accounts for irregularity in stiffness and/or mass distribution. A field survey is needed to define T . The calculated seismic performance index I_s is compared with the seismic judgement index I_{s0} to determine the degree of safety of the building. I_{s0} represents a storey shear force and is given by

$$I_{s0} = E_s ZGU \quad (1.2.4.2)$$

where E_s conservatively increases with the decreasing accuracy of the screening procedure, Z is a zone index modifying the ground motion intensity assumed at the site of the building, G accounts for local effects such as ground-building interaction or stratigraphic and topographic amplification and U is a kind of importance factor depending on the function of the building. In the 1998 revised version of the Japanese Building Standard Law the index I_{s0} is taken as the spectral acceleration (in terms of g) at the period of the considered building, and it should be distributed along the height of the structure according to a triangular distribution.

Preliminary assessment methods based on screening procedures have been proposed in Turkey, too, during last years. Some methods require the dimensions of the lateral load resisting elements to be defined: the “Priority Index” proposed by Hassan and Sozen (1997) is a function of a wall index (area of walls and infill panels divided by total floor area) and a column index (area of columns divided by total floor area); the “Capacity Index” proposed by Yakut (2004) depends on orientation, size and material properties of the lateral load-resisting structural system as well as the quality of workmanship and materials and other features such as short columns and plan irregularities. The Seismic Safety Screening Method (SSSM) by Ozdemir et al. (2005) derives from the Japanese Seismic Index Method (JBDPA, 1990): in this method, too, the seismic capacity of a building is represented by a seismic index value which is a function of structural strength and ductility; this index value has to be

compared with a seismic demand index value – representing the seismic hazard of the zone where the building is located – for assessing the degree of safety of the building.

2.1.1.2.2. Analytical methods

GNDT (1993) work was already described in the previous section dedicated to empirical methods. However, if a sufficient number of information is available, a mechanical approach is proposed for RC buildings: in this case, the vulnerability index is calculated as the difference between the design PGA for high seismicity zones according to the code and an estimate of the PGA corresponding to the attainment of the building capacity evaluated with an approximate and simplified approach.

Singhal and Kiremidjian (1996) estimate vulnerability curves and DPMs for different RC frames (from Low-Rise, Mid-Rise and High-Rise classes, respectively) through nonlinear dynamic analyses and using the Monte Carlo simulation technique (see Figure 13).

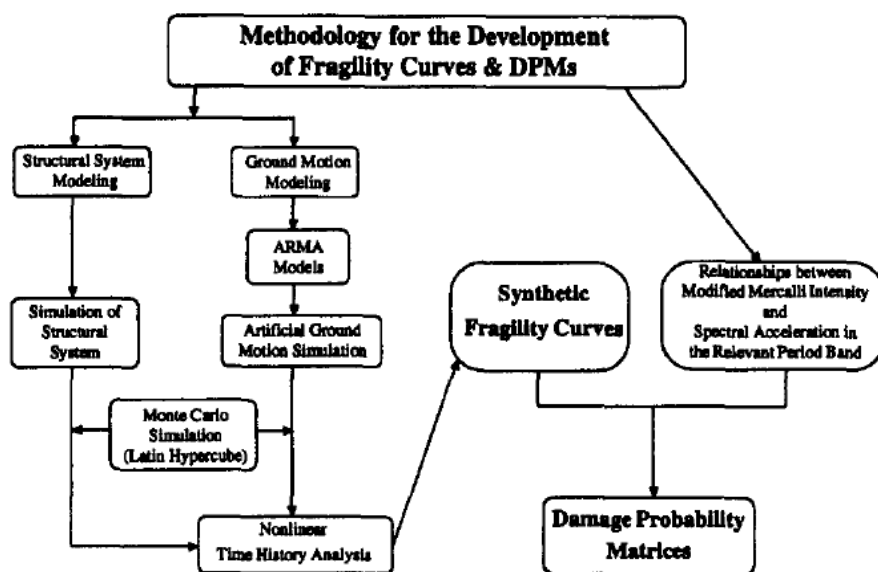


Figure 13. General framework of the methodology adopted in (Singhal and Kiremidjian, 1996)

The uncertainties associated with structural capacities and demands are modelled. Uncertainty in capacity is simulated assuming as random variables the compressive strength of concrete and the yield strength of steel. Uncertainty in seismic demands is accounted for by simulating 100 artificial time histories. Then, the conditional probability of reaching or exceeding a damage state given a ground motion intensity is determined by the Monte Carlo simulation method. 100 Latin hypercube samples are used for the nonlinear dynamic analyses at each ground motion level (expressed in terms of spectral acceleration value). After performing nonlinear dynamic analyses, for each level of ground motion the statistics of the Park and Ang (1985) damage index are used to obtain the parameters of a lognormal probability distribution function at that ground motion level (see Figure 14).

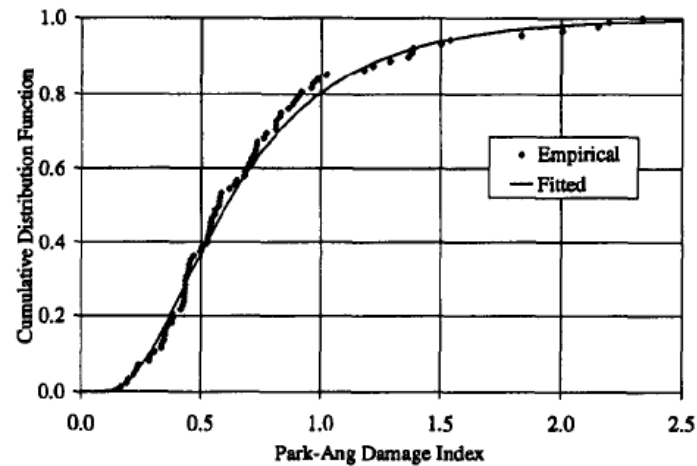


Figure 14. Probability distribution of Park and Ang's damage index at $S_a=3g$ (Singhal and Kiremidjian, 1996)

The lognormal probability functions at each level of ground motion are then used to obtain the probabilities of reaching or exceeding a damage state, adopting given threshold values for the different damage states (see Figure 15).

Damage state (1)	Range of the Park and Ang index (2)
Minor	0.1–0.2
Moderate	0.2–0.5
Severe	0.5–1.0
Collapse	>1.0

Figure 15. Ranges of Park and Ang's damage index for different damage states (Singhal and Kiremidjian, 1996)

Discrete points representing the probabilities of different damage states for a given spectral acceleration value are evaluated from the probability distributions of the damage measure. Hence, smooth vulnerability curves are obtained fitting lognormal distribution functions to these points (see Figure 16).

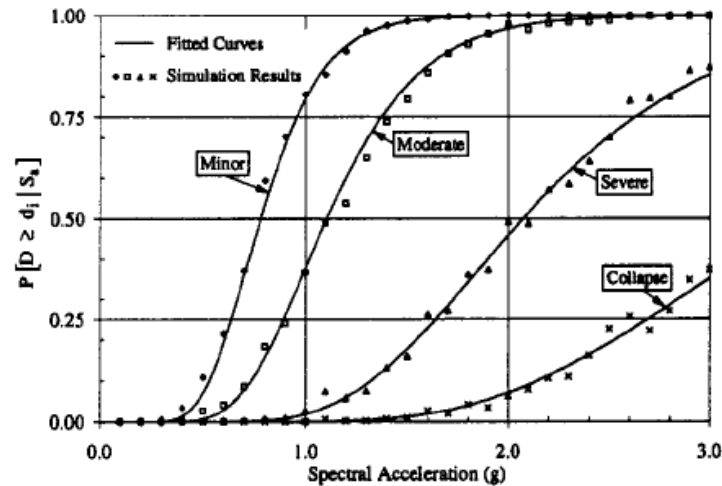


Figure 16. Vulnerability curves for Mid-Rise frames (Singhal and Kiremidjian, 1996)

The relationship between the Modified Mercalli Intensity (MMI) and the average spectral acceleration (that is, the conditional probability of a spectral acceleration at a specified MMI value) in each period band, which is assumed to be lognormal, is developed in the paper based on average spectral acceleration values of the ground motions recorded on firm sites and the MMI values from these earthquakes at the respective recording stations (see Figure 17).

Finally, DPMs are evaluated from the fragility curves by calculating the probability of reaching or exceeding a given damage state for a given MMI intensity (see Figure 18). This probability is obtained by convolving (i) the probability of reaching or exceeding the given damage state for a specified MMI and spectral acceleration and (ii) the conditional probability of a spectral acceleration at specified MMI.

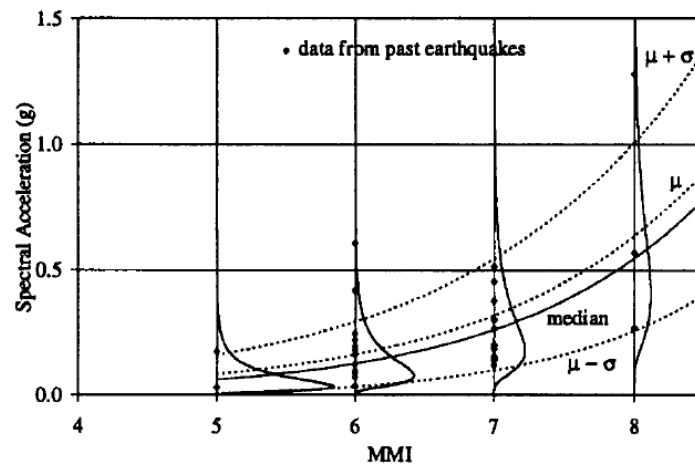


Figure 17. Correlation between MMI intensity and spectral acceleration over period range 0.5-0.9 s (Singhal and Kiremidjian, 1996)

Damage state (1)	Modified Mercalli Intensity						
	VI (2)	VII (3)	VIII (4)	IX (5)	X (6)	XI (7)	XII (8)
None	99.0	93.5	70.0	24.5	1.6	—	—
Minor	0.7	4.2	15.8	23.0	6.1	0.1	—
Moderate	0.3	2.1	12.0	36.6	33.7	4.9	0.2
Severe	—	0.2	1.9	12.5	34.6	22.3	1.8
Collapse	—	—	0.3	3.4	24.0	72.7	98.0

Figure 18. Damage Probability Matrix for Mid-Rise frames (Singhal and Kiremidjian, 1996)

A similar approach is adopted in (Masi, 2003), where three main structural typologies are examined: bare frames, regularly infilled frames and pilotis frames, designed for gravity loads only. Structural models are generated through a simulated design procedure considering current practice and codes in force at the age of construction. Nonlinear dynamic analyses with ground motions of various levels of intensity are carried out. Based on the obtained results, each type of building can be assigned to a different vulnerability class of EMS-98 scale.

Rossetto and Elnashai (2005) derive vulnerability curves for a low-rise infilled RC frame with inadequate seismic provisions according to the following methodology: a population of 25 buildings is generated from a single building through consideration of material parameter uncertainty; uncertainty in demand is accounted for through the use of 30 different accelerograms; for each of the generated buildings, an adaptive pushover analysis is carried out, and the performance point is found following the Capacity Spectrum framework of assessment, for all the accelerograms; a damage scale experimentally calibrated to maximum inter-storey drift is adopted. Hence, the results of the population assessment are used to generate second-order response surfaces, one for each damage state. Vulnerability curves are generated from response surfaces through re-sampling. The derived curves show good correlation with observational post-earthquake damage statistics.

In (Cosenza et al., 2005) a procedure to evaluate the seismic capacity of a building class is proposed that enables to reduce dispersion of results depending on the level of knowledge. A building class is defined in terms of age of construction and number of storeys. The level of knowledge of the building stock is accounted for through a “specification” of building classes in different orders depending on the level of knowledge of the parameters. RC rectangular shaped frame buildings are considered.

For each class, a number of building models is generated by means of a simulated design procedure, based on the probabilistic distribution of the structural (geometrical and mechanical) parameters. Seismic capacity is determined in terms of base shear coefficient and global drift for each of the generated buildings of the building class, through a mechanics-based approach: $3n_z$ predefined mechanisms, where n_z is the number of storeys, are considered (see Figure 19) and the corresponding base shear, V_{bi} , is calculated for each mechanism assuming a linear distribution of horizontal seismic forces.

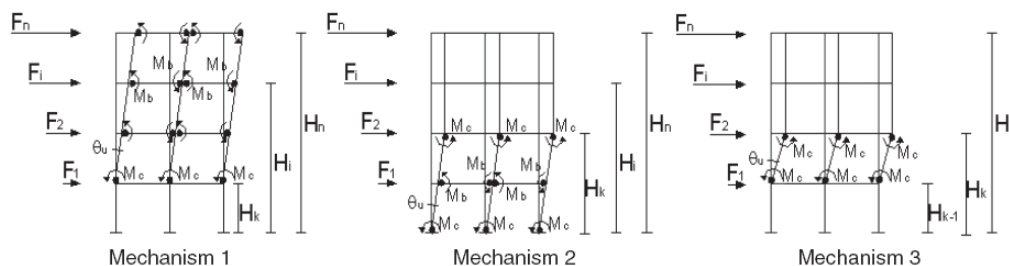


Figure 19. Predefined collapse mechanisms (Cosenza et al., 2005)

The ultimate roof displacement Δ_{ui} is determined as a function of the ultimate rotation θ_u of the structural elements:

$$\Delta_{u,1} = \theta_u \cdot (H_n - H_k) \quad (1.3.1)$$

$$\Delta_{u,2} = \theta_u \cdot H_k \quad (1.3.2)$$

$$\Delta_{u,3} = \theta_u \cdot (H_k - H_{k-1}) \quad (1.3.3)$$

The collapse mechanism is identified by the lowest value of V_{bi} . Then, the capacity of the building is finally evaluated in terms of base shear coefficient $C_{b,i}$ (= ratio between the base shear $V_{b,i}$ and the seismic weight W) and corresponding lateral (drift) _{u} _{i} (= ratio between the ultimate roof displacement $\Delta_{u,i}$ and the building height H_n) for the determined collapse mechanism:

$$C_{b,i} = \frac{V_{b,i}}{W} \quad (1.3.4)$$

$$(\text{drift}_u)_i = \frac{\Delta_{u,i}}{H_n} \quad (1.3.5)$$

Starting from the capacity of the analyzed buildings, the response surface method is adopted and the influence of each parameter is investigated. Capacity curves expressing the probability of having a capacity lower than the assigned value are obtained through a Monte Carlo simulation technique. The influence of the knowledge level on the probability of reaching a fixed capacity threshold is shown, too.

However, this study only provides cumulative frequency distributions of capacity parameters (base shear coefficient and ultimate roof drift) within a building class. No vulnerability curve, relating a seismic demand measure to the probability of reaching or exceeding a given damage state, is provided.

In (Iervolino et al., 2007) a complete seismic risk assessment framework is presented, where the mechanisms-based approach is overcome.

In order to investigate the building class capacity, n geometrical and mechanical characteristics of the buildings are identified as random variables. Then, a possible range of variation and a corresponding “scanning step” are assumed for each one of these variables. A simulated design procedure, a nonlinear FE modelling of the structure and a Static PushOver (SPO) analysis are carried out for all of the resulting combinations of values. Hence, response surfaces are obtained for the capacity parameters T (period), C_s (strength) and C_d (displacement capacity) of the equivalent SDOF system (see Figure 20), expressed as function of the assumed random variables.

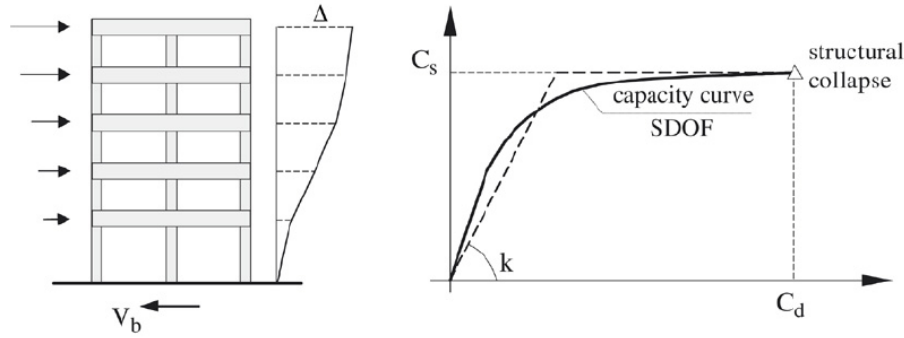


Figure 20. Capacity parameters (Iervolino et al., 2007)

Seismic demand is provided by Probabilistic Seismic Hazard Analysis (PSHA).

Hence, a calculation of seismic risk can be carried out through a Monte Carlo simulation technique, according to the following steps:

- sampling of N values of the n input random variables describing different geometrical and mechanical building characteristics according to the Probability Density Functions (PDFs) respectively assigned;
- evaluation of N arrays of capacity parameters $\{T, C_s, C_d\}$ as a function of the sampled random variables by linearly interpolating between the points obtained from the SPO analyses;
- sampling of N values of elastic spectral displacement demand $S_{d,e}$ according to the probability distribution given by the PSHA;
- evaluation of the corresponding N values of *median* inelastic displacement demand $S_{d,i} = S_{d,e} \cdot C_R$ according to the Capacity Spectrum Method assessment procedure (Fajfar, 1999);
- sampling of N values of the random variable ε_{C_R} representing the variability of the inelastic displacement demand, according to the assigned PDF, thus giving the N final values of the displacement demand $D = S_{d,i} \cdot \varepsilon_{C_R}$;
- comparison between the N values of displacement capacity C_d and the corresponding N values of displacement demand D , thus leading to the number N_f of buildings for which the capacity is exceeded by the demand;

- estimation of the failure probability as
$$P_f = \frac{N_f}{N}$$
.

HAZUS (HAZard in United States) is an earthquake loss estimation methodology including many components. It was developed by the Federal Emergency Management Agency (FEMA) under agreements with the National Institute of Building Sciences (NIBS) (FEMA, 2001; Kircher et al., 1997a; Kircher et al., 1997b; Whitman et al., 1997).

Estimates of building damage are used as inputs to other damage modules. Most importantly, building damage is used as an input to a number of loss modules (see Figure 21).

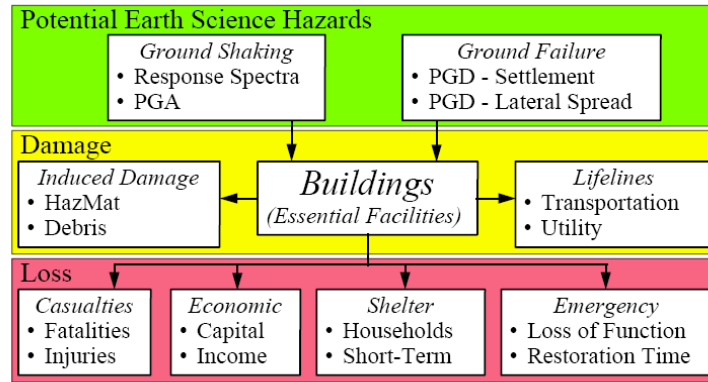


Figure 21. Building-related modules of HAZUS methodology (FEMA, 2001)

HAZUS damage functions for ground shaking have two basic components: capacity curves and fragility curves.

Capacity curves are defined by two control points: the yield capacity and the ultimate capacity. The yield capacity accounts for design strength, redundancies in design, conservatism in code requirements and expected (rather than nominal) strength of materials. Design strengths of model building types are based on the requirements of US seismic code provisions or on an estimate of lateral strength for buildings not designed for earthquake loads. The ultimate capacity represents the maximum strength of the building when the global structural system has reached a full mechanism. Up to yield, the building capacity curve is assumed to be linear with stiffness based on an estimate of the expected “elastic” period of the building. From yield to the ultimate point, the capacity curve transitions in slope from an essentially elastic state to a fully plastic state. The capacity curve is assumed to remain plastic past the ultimate point (see Figure 22).

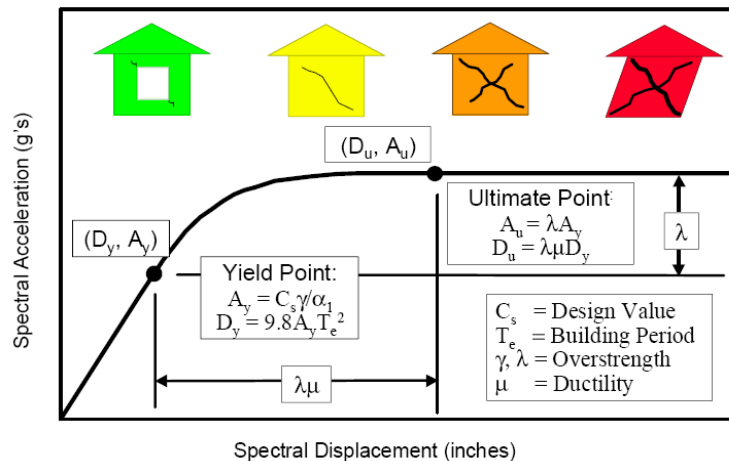


Figure 22. Example building capacity curve and control points (FEMA, 2001)

36 different building structural typologies are considered. For each typology, values of the parameters defining the capacity curves are provided. As an example, see Figure 23 and Figure 24 for C1M building class (Mid-Rise Concrete Moment Frame).

Seismic Design Level	Elastic Period (sec.)	Average Inter-Story Drift Ratio					
		Capacity Curve Control Points		Structural Damage State Thresholds (Fragility Medians)			
		Yield	Plastic	Slight	Moderate	Extensive	Complete
Special High-Code	0.75	0.0038	0.0614	0.0042	0.0083	0.0250	0.0667
High-Code	0.75	0.0026	0.0410	0.0033	0.0067	0.0200	0.0533
Moderate-Code	0.76	0.0013	0.0154	0.0033	0.0058	0.0156	0.0400
Low Code	0.76	0.0006	0.0064	0.0033	0.0053	0.0133	0.0333
Pre-Code	0.76	0.0006	0.0077	0.0027	0.0043	0.0107	0.0267

1. A typical C1M building is 5-stories (i.e., 50 feet) in height. Spectral displacement is equal to 0.75 x roof displacement and base shear is equal to 0.80W x spectral acceleration.

Figure 23. “Elastic” period values and average inter-story drift ratios of capacity curve control points and structural damage state thresholds (fragility medians) for C1M¹ building class (FEMA, 2001)

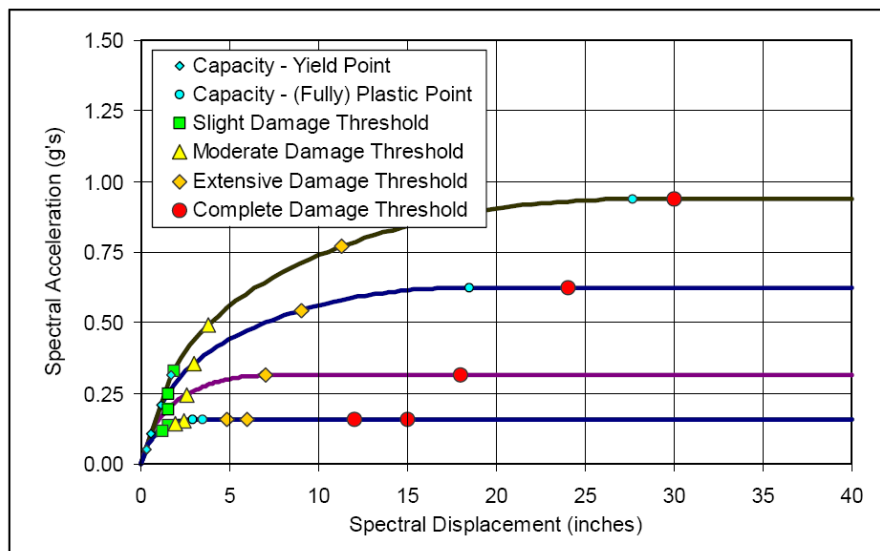


Figure 24. Capacity curves and structural damage-state thresholds (fragility medians) for five seismic design levels (Special High, High, Moderate, Low and Pre-Code) for C1M building class (FEMA, 2001)

Capacity Spectrum Method is adopted in HAZUS to evaluate the demand corresponding to a given seismic intensity. To this end, the inelastic demand spectrum is obtained reducing the 5%-damped elastic response spectrum by means of an effective damping value which is defined as the total energy dissipated by the building during peak earthquake response and is the sum of an elastic damping term and a hysteretic damping term associated with post-yield, inelastic response and influenced by ground motion duration. Then, peak response displacement and acceleration are determined from the intersection between the demand spectrum and the building's capacity curve (see Figure 25).

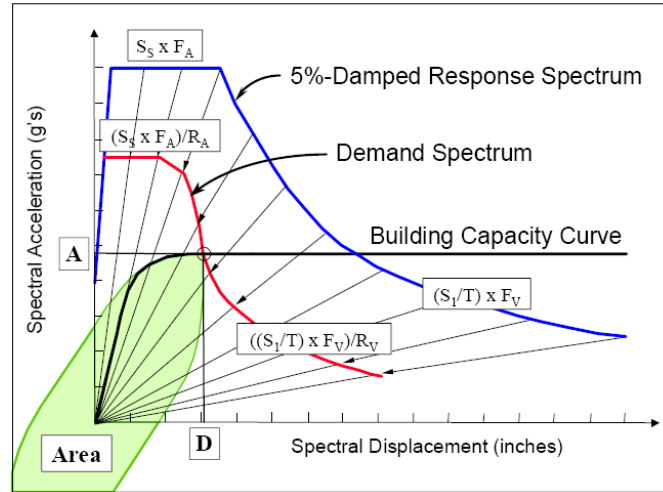


Figure 25. Example demand spectrum construction and calculation of peak response displacement (D) and acceleration (A) (FEMA, 2001)

HAZUS provides fragility curves for damage to structural system, non-structural components sensitive to drift and non-structural components (and contents) sensitive to acceleration. Fragility curves are lognormal functions defined by a median value of the demand parameter, which corresponds to the *threshold* of that damage state, and by the variability associated with that damage state. For example, the spectral displacement S_d that defines the threshold of a particular damage state ds is given by

$$S_d = \bar{S}_{d,ds} \cdot \epsilon_{ds} \quad (1.3.6)$$

where $\bar{S}_{d,ds}$ is the median value of spectral displacement of damage state ds and ϵ_{ds} is a lognormal random variable with a unit median value and a logarithmic standard deviation ϵ_{ds} , which controls the slope of the fragility curve and accounts for the variability and uncertainty associated with capacity curve properties, damage states and ground shaking.

Four damage states are defined: Slight, Moderate, Extensive and Complete (see Figure 26). Median values of spectral displacement associated with each damage state are evaluated calculating the average interstorey drift ratio (i.e., roof displacement divided by building height) corresponding to the step of pushover analysis at which a certain fraction of structural elements reaches a certain deformation limit. The value of this fraction is defined as the repair or replacement cost of components at limit divided by the total replacement value of the structural system.

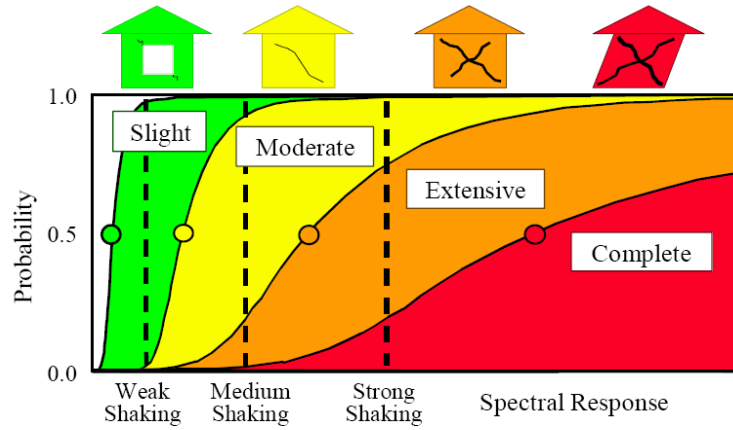


Figure 26. Example fragility curves for Slight, Moderate, Extensive and Complete damage (FEMA, 2001)

The lognormal standard deviation β_{ds} , which describes the total variability of fragility-curve damage state ds , is given by three contributions:

$$\beta_{ds} = \sqrt{(\text{CONV}[\beta_C, \beta_D])^2 + (\beta_{T,ds})^2} \quad (1.3.7)$$

where β_C is the lognormal standard deviation parameter that describes the variability of the capacity curve, β_D is the lognormal standard deviation parameter that describes the variability of the demand spectrum and $\beta_{T,ds}$ is the lognormal standard deviation parameter that describes the variability of the threshold of damage state ds . Since the demand spectrum is dependent on building capacity, a convolution process is required to combine their respective contributions to total variability, while the third contribution to total variability, $\beta_{T,ds}$, is assumed mutually independent of the first two and is combined with the results of the convolution process using the square-root-sum-of-the squares (SRSS) method. The convolution process involves a complex numerical calculation that would be very difficult for most users to perform. To avoid this difficulty, sets of pre-calculated values of damage state Beta's are proposed.

These Beta values are given as a function of building height group, post-yield degradation of the structural system, damage state threshold variability and capacity curve variability.

Estimation of β_C and $\beta_{T,ds}$ must be made by users on a judgmental basis, based on the consideration that these variability values are influenced by uncertainty in capacity curve properties and thresholds of damage states and by building population (i.e., individual building or group of buildings): relatively low variability of damage states would be expected for an individual building with well known properties (e.g., complete set of as-built drawings, material test data, etc.) and whose performance and failure modes are known with confidence. Relatively high variability of damage states would be expected for a group of buildings whose properties are not well known and for which the user has low confidence in the results (of pushover analysis) that represent performance and failure modes of all buildings of the group.

Kappos et al. (2006), within RISK-EU project, propose a mechanical-based method for the vulnerability assessment of RC and URM buildings. Vulnerability curves are determined based on nonlinear analyses of archetype buildings, whose displacement capacity is determined based on pushover analyses, while di displacement demand is determined via incremental dynamic analyses. The method is similar to HAZUS, but capacity thresholds are defined differently. A probabilistic model is defined for the combination of analytical and statistical data.

Lagomarsino and Giovinazzi (2006), within RISK-UE project, propose a method for seismic risk assessment based on the assumption that, dealing with a territorial vulnerability assessment, building seismic response can be represented by simplified bilinear capacity curves defined by three parameters: the yield acceleration, the yield period of vibration and the structural ductility capacity. The yield acceleration can be derived as a function of the seismic code design lateral force, multiplied by another factor in order to consider median values of material strength instead of nominal ones. The period can be evaluated through simplified expressions proposed by code. The ductility capacity can be derived from the behaviour factor adopted in design, if any; otherwise, for buildings non-specifically designed to have dissipation capacity, a value of 2.5 is arbitrarily assumed. For non designed structures, the author states that bilinear capacity curve can be derived taking into account the geometrical and the technological features characterizing on the average the typology (number of floors, code level, material strength, drift capacity, age, etc.) and hypothesizing a certain collapse mode. Displacement demand assessment for a given seismic intensity is carried out according to the Capacity Spectrum Method.

Four damage states are considered. Mean values of the corresponding displacement threshold are proposed as a function of the yielding and ultimate displacements, based on *expert judgement*, and are verified on the basis of the results of pushover analyses performed on prototype buildings.

In order to define fragility curves for the considered damage states, uncertainty in the estimate has to be evaluated. To this end, a different approach from HAZUS is proposed: the overall uncertainty in the damage estimation is evaluated in order to represent the same dispersion of observed damage data that are well fitted by binomial distributions. Repeating this procedure for different buildings typologies a lognormal standard deviation is found, depending on the ductility corresponding the mean damage values.

Grant et al. (2006) also adopt a code-based approach to the evaluation of building seismic vulnerability. In order to carry out a first, rapid and very simplified step of a multi-level screening procedure aimed at defining priorities and timescales for seismic intervention in school buildings, authors evaluate the PGA capacity from the code-prescribed seismic input at the age of construction, based on the assumption of a “perfect” code compliance. To this aim, starting from the design inelastic acceleration capacity prescribed by the seismic code in force at the age of construction, a sort of “back-analysis” is applied, thus calculating the corresponding PGA, also accounting for modern seismic code requirements including adjustments for ductility capacity (i.e., the behaviour factor) and building importance. In a very conservative (but unrealistic) way the authors also assume that buildings designed for Gravity Loads only have a null seismic capacity. Following this procedure, the seismic vulnerability can be evaluated in terms of a “PGA deficit” obtained as the difference between the evaluated PGA capacity and the PGA demand, which is derived from modern seismic hazard studies.

However, a quite critical shortcoming can affect a procedure that evaluate seismic capacity based on the assumption of a perfect code compliance with seismic codes in force at the age of construction, since the actual seismic capacity of a building stock can differ greatly from the prediction of such a code prescription-based model. At least, factors accounting for material overstrength should be accounted for (e.g., Giovinazzi, 2005). Moreover, design conservatism approximations usually should lead to a higher capacity, compared with code prescriptions. Hence, a code-based procedure may systematically underestimate seismic capacity. This approach may be justified as *conservative*, but actually a seismic vulnerability assessment for a large scale earthquake loss model should not be *conservative*; it should rather provide a seismic capacity estimation as reliable as possible.

Ordaz et al. (2000) adopt a vulnerability analysis procedure where the damage level is expressed as a function of the maximum interstorey drift, which is evaluated as a function of the spectral acceleration. The relationship between the maximum expected interstorey drift and the spectral

acceleration demand is evaluated through a simplified model based on the analogy with equivalent cantilever beams subjected to shear and flexural deformations. In this model, coefficients are used to account, among others, for the structural type, for the height of the structure and for the ratio between inelastic and elastic demand. Moreover, further coefficients are used to account for the increase in seismic vulnerability due to some factors including, for instance, irregularities in elevation and/or in plan or the presence of short columns.

Calvi (1999) first proposes an approach for the evaluation of the vulnerability of building classes based on the Displacement-Based method (e.g., Priestley, 1997).

For each limit state, a displacement shape is assumed and a corresponding displacement capacity is evaluated, depending on the attainment of a local deformation limit [material strain capacity \rightarrow section curvature capacity \rightarrow element drift capacity \rightarrow building displacement capacity (on the equivalent SDOF model)]. A possible range of variation for the evaluated capacity is defined. At the same time, a possible range of variation for the period of vibration (secant to the displacement capacity) is defined, too. Hence, for each limit state, rectangles representing the possible “positions” of the points representing the building capacity in a period-displacement plane are obtained. A uniform probability density function over the rectangles is assumed, describing the variability of the capacity.

Seismic demand is represented by displacement response spectra adjusted to include the nonlinear response, wherein a reduction of the spectral ordinates is applied to account for the energy dissipation capacity of the structure as a function of the target displacement and the structural response.

Capacity and demand can be directly compared to each other as a function of the period: the rectangle area below the demand spectrum represents the expected proportion of buildings reaching (or exceeding) the limit state capacity (see Figure 27).

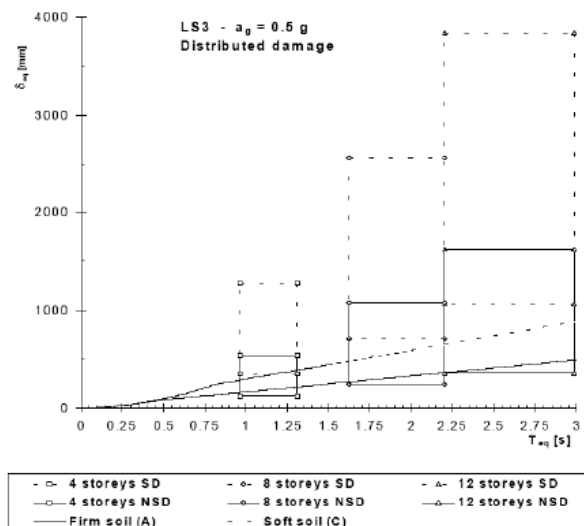


Figure 27. An example of the intersection of capacity areas and demand spectrum (Calvi, 1999)

The methodology proposed by Calvi (1999) is subsequently developed (Pinho et al., 2002; Glaister and Pinho, 2003; Crowley et al., 2004; Crowley et al., 2006) leading to the Displacement-Based Earthquake Loss Assessment (DBELA) procedure.

The main improvements to the original procedure by Calvi (1999) may be summarized in (i) the theoretical improvement of structural and non-structural displacement capacity equations, (ii) the derivation of an equation between yield period and height for European buildings both with and

without infill panels (Crowley and Pinho, 2004, 2006) and (iii) the development of a fully probabilistic framework accounting for uncertainties in geometrical and mechanical properties, in capacity models and in demand spectrum.

In DBELA the displacement capacity can be expressed as a function of the building height; this relationship can be transformed into a direct relationship between displacement capacity and period, through the substitution of an equation relating the height of a building to its limit state period. Hence, a direct comparison is possible at any period between the displacement capacity of a building class and the displacement demand predicted from a response spectrum (see Figure 28).

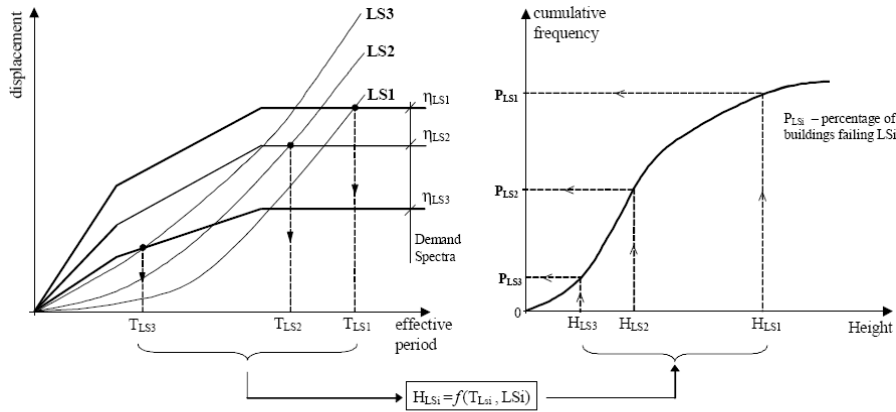


Figure 28. Deformation based seismic vulnerability assessment procedure (Glaister and Pinho, 2003)

The probabilistic treatment of the uncertainties involved in the assessment procedure leads to the definition of a Joint Probability Density Function (JPDF) of displacement capacity and period (see Figure 29), which was originally assumed to be uniform (Calvi, 1999).

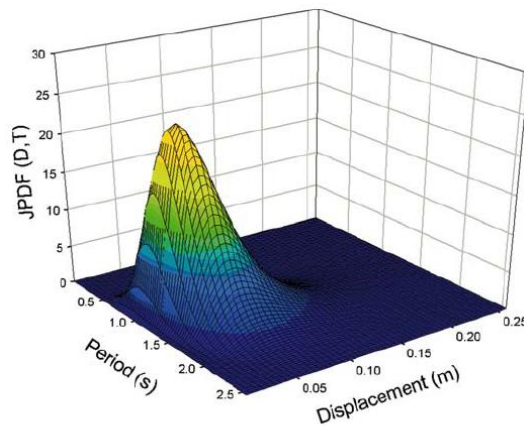


Figure 29. Joint Probability Density Function (JPDF) of displacement capacity and period (Crowley et al., 2004)

The Simplified Pushover-Based Earthquake Loss Assessment (SP-BELA) by Borzi et al. (2008a) combines the definition of a pushover curve using a simplified mechanics-based procedure – similar to (Cosenza et al., 2005) – to define the base shear capacity of the building stock with a displacement-based framework similar to that in DBELA, such that the vulnerability of building classes at different limit states can be obtained.

Simplified pushover curves are derived according to the following procedure: a prototype structure representing the building class is defined first, for which the collapse mechanism and, therefore, the collapse multiplier under a linear distribution of lateral forces is determined. Based on limit conditions given in terms of element chord rotations, the building displacement capacity (in terms of the equivalent SDOF) is evaluated for different Limit States. Then, the period of vibration for each Limit State is calculated, corresponding to the secant stiffness to the displacement capacity.

In order to derive vulnerability curves using this type of analytical procedure, a set of random variables is defined – together with the corresponding probability distributions – including geometrical dimensions, material properties and design loads.

Seismic demand is defined in terms of inelastic displacement demand spectra, and the uncertainty in this demand is taken into account assuming the corner periods of the spectrum and the spectral amplification coefficient as random variables.

A Monte Carlo simulation approach is adopted, and random variables are generated through a Latin Hypercube Sampling procedure. Hence, vulnerability curves can be derived for a class of buildings and for different Limit States, carrying out the following steps:

- definition of a number of building samples through the generation of assumed random variables;
- definition of building capacity through a pushover curve for each generated building;
- definition of the displacement demand;
- comparison between demand and capacity to define the number of buildings – out of the generated population – exceeding the given Limit State conditions.

SP-BELA has been further developed in order to approximately account for the presence of infill panels in (Borzi et al., 2008b). Two possible distributions of the infill panels are considered: a uniform distribution along the height of the building or a “pilotis” distribution. It is assumed that the panels have an influence on the lateral resistance of the building up to the yield limit state. When the frames evolve into the nonlinear range, the panels are considered to collapse and, therefore, they no longer contribute to the base shear resistance. The behaviour of the single strut representing the infill panel is assumed to be linear up to failure. The influence of the panels is not considered in defining the displacement capacity on the pushover curve as the panels are often not perfectly in contact with the frames and they are assumed to play a role on the overall building performance only after the frames have already been deformed beyond their elastic limit. On the other hand, the panels are assumed to collapse before the frames reach the significant damage limit condition.

Hence, the only way the influence of infill panels is accounted for is that they are assumed to increase the lateral strength of the building up to the yielding of the RC structure. In other terms, the presence of infill panels leads to a lower value of the secant period to the yielding Limit State by increasing the yield strength, thus decreasing the corresponding failure probability within the adopted Displacement-Based assessment framework. No influence at all is considered on other Limit States.

However, authors do not clarify how the presence of elements characterized by a brittle behaviour (such as infill trusses) can be accounted for in a mechanisms-based approach, where all the structural elements should have an elastic-perfectly plastic behaviour.

VC (Vulnerabilità Calcestruzzo armato, *reinforced concrete vulnerability*), by Dolce and Moroni (2005), is a simplified procedure – implemented in a spreadsheet software – for the vulnerability assessment of RC buildings. Two Limit States are considered: Slight Damage and Collapse. The vulnerability is expressed as the PGA values leading the attainment of these Limit States. The procedure is based on the evaluation of the storey strength at each storey and on the application of a ductility coefficient accounting for the inelastic displacement capacity.

Soft-storey (concentration of the inelastic demand only in columns in one storey) is the only collapse mechanism considered. In authors' opinion, this is the most probable collapse mechanism for existing RC buildings, due to frequent weak column/strong beam conditions.

Infill elements can be taken into account, both in terms of stiffness and strength.

For the definition of Slight Damage Limit State an interstorey drift limit, based on Italian code prescriptions, is assumed. An elastic behaviour is assumed up to this limit. Hence, interstorey shear stiffness has to be evaluated. To this end, the sum of column stiffness values is calculated, also considering the influence of the restrain condition given by the beams; a cracked stiffness is considered, too. If infill panels are present, their contribution is taken into account assuming the stiffness model provided by Italian code. Hence, a value of interstorey shear leading to the attainment of Slight Damage Limit State (V_{OPER}) is evaluated at each storey, corresponding to the prescribed interstorey drift limit.

For Collapse Limit State the ultimate value of interstorey shear strength (V_{COLL}) at each storey is evaluated. The ultimate interstorey shear strength is calculated as the sum of the ultimate shear strength of each column, given by the flexural capacity of the column section, also considering the influence of the restrain condition given by the beams on the moment distribution along the element and, therefore, on the corresponding shear value. Possible shear failures are considered, too. If infill panels are present, their contribution to the ultimate shear strength is taken into account considering different possible collapse mechanisms of the panels. Subsequently, this value is multiplied by a coefficient accounting for the inelastic displacement capacity in order to evaluate the interstorey shear value leading to Collapse in a spectral elastic approach, thus implicitly applying the equal rule between overstrength and ductility ($R=\mu$).

The procedure can be summarized in the following steps (each step is carried out in both building directions):

- at each storey, interstorey shear leading to Slight Damage drift limit (V_{OPER}) and ultimate interstorey shear strength (V_{COLL}) are evaluated, as above described;
- the interstorey shear demand distribution is evaluated, assuming a base shear demand equal to the weight of the structure (that is, a pseudo-acceleration equal to $1g$) and a linear distribution of lateral displacements;
- at each storey, the ratios between V_{OPER} and V_{COLL} and the interstorey shear demand are evaluated, representing the pseudo-acceleration values $S_{D(OP)}$ and $S_{D(COLL)}$ (expressed in g) leading to the attainment of a shear demand equal to V_{OPER} and V_{COLL} , respectively;
- at each storey, the PGA values corresponding to $S_{D(OP)}$ and $S_{D(COLL)}$ are evaluated by means of different coefficients: α_{PM} (accounting for the participating mass ratio of the first mode), α_{AD} (aimed at evaluating the PGA from the spectral pseudo-acceleration depending on the period of vibration and the shape of the demand spectrum), α_{DS} (accounting for the structural dissipation capacity) and α_{DUT} (accounting for the inelastic displacement capacity). Obviously, α_{DUT} is equal to 1 for Slight Damage Limit State. For Collapse Limit State, a coefficient $\alpha_{DUT,pil}$ is evaluated for each column as a function of the axial load ratio; it is assumed equal to 1 if the column behaviour is controlled by shear. Then, α_{DUT} is given by a weighted average of $\alpha_{DUT,pil}$ extended to all the columns in the storey. α_{DUT} can be reduced by means of coefficients accounting for the presence of a soft storey or for irregularities in strength/stiffness/mass distribution. If the presence of infill panels is taken into account α_{DUT} is assumed equal to 1.5 since in this case in authors' opinion the failure mechanism is controlled by brittle interaction mechanisms between structural and non-structural elements;
- for both Limit States, the minimum PGA value between all the values calculated at each storey and in each direction is evaluated, representing the PGA capacity of the building.

The RE.SIS.TO® (Chinni et al. 2013) method evaluates the collapse acceleration (PGA_c) of buildings by assessing the shear strength at each floor. The collapse spectral acceleration ($S_{a,c}$) is converted to PGA_c using factors such as the modal participation factor (β_{PM}), spectral amplification factor (β_{AD}), dissipation factor (β_{DT}), and structure factor (β_{DUC}). For masonry buildings, the Turnšek and Cacovic formulation is used to calculate the resistant shear ($V_{r,i}$) at each floor, considering the minimum area of resistant walls, the shear strength of masonry (τ_0), and the average normal stress ($\sigma_{0,i}$). The resistant shear is adjusted by a factor (C_{rid}) to reflect the building's current condition based on the GNDT form. The building's capacity in terms of spectral acceleration is defined by the ratio of resistant shear to acting shear at each floor. Five classes of strength and vulnerability are determined from the ratio of PGA_c to the design acceleration (PGA_d).

PGA_c/PGA_d	Strength Class	Vulnerability Class
0–25%	V	High
25–50%	IV	Medium-High
50–75%	III	Medium
75–100%	II	Medium-Low
>100%	I	Low

Figure 30. Vulnerability classification according to RE.SIS.TO® method (from Ceroni et al. 2020)

As reported in Martins and Silva (2020) The GEM Foundation conducted a survey among structural and earthquake engineering experts to create a global catalogue of representative building classes. They developed a web application to classify building stocks based on structural parameters such as material, lateral load-resisting system, height, ductility level, and irregularities. Users also provide the relative frequency of each building class in rural and urban areas and classify buildings by use (e.g., residential, commercial). This application is accessible via the OpenQuake platform.

As of the survey, nearly 600 entries from over 70 countries were collected. To enhance the catalogue, additional sources were consulted, including past regional and national projects, World Housing Encyclopaedia reports, the PAGER-WHE project, and regional workshops conducted by GEM. At 2020, the list of building classes includes almost 500 typologies categorized by construction material, lateral load-resisting system, ductility level, and height.

The classification includes materials like masonry, reinforced concrete, adobe, timber, steel, and composites. Lateral load-resisting systems are divided into moment resisting frames, infilled frames, wall systems, and dual systems, each with varying ductility levels. Buildings are also categorized by height into low-, mid-, high-rise, and tall structures.

For fragility assessments, nonlinear time-history analyses on SDOF systems were performed using the Risk Modellers Toolkit, integrated with OpenSees software. The analyses defined capacity curves based on spectral acceleration and displacement, considering different materials' and systems' behavior under seismic loads.

For the fragility assessment, each SDOF's hysteresis behavior is characterized by a capacity curve showing spectral acceleration (S_a) versus spectral displacement (S_d). For building classes like steel frames, timber, and composite structures, where base shear capacity does not significantly reduce due to damage, a trilinear elasto-plastic model is used. This model is defined by yielding displacement ($S_{d,y}$), ultimate displacement ($S_{d,ult}$), elastic period (T_1), and yielding period (T_y), with T_y assumed to be 1.5 times T_1 if no direct calculation formula is available.

For building classes with significant base shear capacity reduction due to damage in masonry panels (e.g., confined masonry, reinforced concrete with infills), a quadrilinear capacity curve is used. This curve accounts for reduced displacement capacity due to the added stiffness from masonry walls, applying reduction factors from Bal et al. (2010a). These classes assume a regular distribution of infill walls, leading to post-peak behavior similar to that in Villar-Vega et al. (2017). The initial two points on the curve are calculated as in the trilinear model, with the elastic range ending at $0.5S_d$ and T_1 , and the peak defined by yield displacement and T_y . The third point aligns with the yield displacement of the equivalent bare frame, and the final point is the ultimate displacement.

In the Acceleration Displacement Response Spectrum (ADRS) format, the mean capacity is derived from the roof displacement (δ_{roof}) of the multi-degree-of-freedom structure using specific equations, with (T) as the vibration period and (Γ) as the first mode participation factor.

In this way, capacity curves of each building class were defined, based on research and experimental data. The classification follows the GEM taxonomy guidelines (Brzev et al. 2013) and revisions by Silva et al. (2017).

The methodology included defining damage states from slight to complete and considering uncertainties in damage criteria as shown in Figure 31.

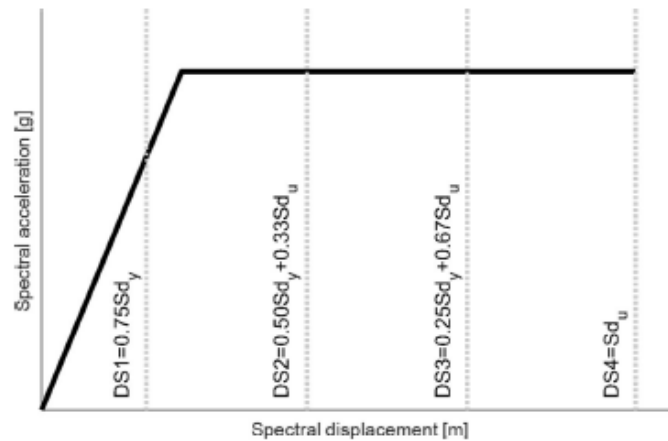


Figure 31. Damage thresholds (from Martins and Silva 2020)

Fragility functions were derived using a cloud analysis approach, and censored regression methods were employed to avoid biases from extreme deformation data points. The fragility parameters for masonry building classes are reported, for example, in the table shown in Figure 32.

Building class	IM	DS1		DS2		DS3		DS4	
		θ	β	θ	β	θ	β	θ	β
MUR/LWAL + DNO/H1	SA(0.3 s)	0.53	0.60	1.05	0.60	1.49	0.60	1.88	0.60
MUR/LWAL + DNO/H2	SA(0.3 s)	0.43	0.58	0.91	0.58	1.36	0.58	1.78	0.58
MUR/LWAL + DNO/H3	SA(0.3 s)	0.41	0.57	0.96	0.57	1.47	0.57	1.95	0.57
MUR/LWAL + DNO/H4	SA(0.6 s)	0.18	0.56	0.46	0.56	0.74	0.56	1.02	0.56
MUR/LWAL + DNO/H5	SA(0.6 s)	0.20	0.54	0.50	0.54	0.80	0.54	1.09	0.54
MUR + ADO/LWAL/DNO/H1	SA(0.3 s)	0.34	0.59	0.73	0.59	1.04	0.59	1.33	0.59
MUR + ADO/LWAL/DNO/H2	SA(0.3 s)	0.27	0.56	0.66	0.56	1.02	0.56	1.35	0.56
MUR + ADO/LWAL/DNO/H3	SA(0.6 s)	0.12	0.54	0.32	0.54	0.51	0.54	0.70	0.54
MUR + STRUB/LWAL + DNO/H1	SA(0.3 s)	0.37	0.60	0.81	0.60	1.16	0.60	1.48	0.60
MUR + STRUB/LWAL + DNO/H2	SA(0.3 s)	0.36	0.56	0.77	0.56	1.15	0.56	1.50	0.56
MUR + STRUB/LWAL + DNO/H3	SA(0.3 s)	0.35	0.58	0.82	0.58	1.24	0.58	1.65	0.58
MUR + STRUB/LWAL + DNO/H4	SA(0.6 s)	0.16	0.54	0.39	0.54	0.61	0.54	0.84	0.54
MUR + STRUB/LWAL + DNO/H5	SA(0.6 s)	0.17	0.53	0.42	0.53	0.68	0.53	0.94	0.53
MUR + STDRE/LWAL + DNO/H1	SA(0.3 s)	0.50	0.60	0.92	0.60	1.29	0.60	1.61	0.60
MUR + STDRE/LWAL + DNO/H2	SA(0.3 s)	0.36	0.58	0.81	0.58	1.21	0.58	1.59	0.58
MUR + STDRE/LWAL + DNO/H3	SA(0.3 s)	0.40	0.58	0.87	0.58	1.31	0.58	1.72	0.58
MUR + STDRE/LWAL + DNO/H4	SA(0.6 s)	0.16	0.56	0.40	0.56	0.64	0.56	0.88	0.56
MUR + STDRE/LWAL + DNO/H5	SA(0.6 s)	0.18	0.53	0.45	0.53	0.72	0.53	0.99	0.53
MUR + CL99/LWAL + DNO/H1	SA(0.3 s)	0.47	0.59	0.87	0.59	1.21	0.59	1.51	0.59
MUR + CL99/LWAL + DNO/H2	SA(0.3 s)	0.35	0.56	0.81	0.56	1.23	0.56	1.63	0.56
MUR + CL99/LWAL + DNO/H3	SA(0.3 s)	0.38	0.59	0.87	0.59	1.32	0.59	1.74	0.59
MUR + CL99/LWAL + DNO/H4	SA(0.6 s)	0.17	0.55	0.42	0.55	0.68	0.55	0.93	0.55
MUR + CL99/LWAL + DNO/H5	SA(0.6 s)	0.18	0.53	0.46	0.53	0.73	0.53	1.01	0.53
MUR + CB99/LWAL + DNO/H1	SA(0.3 s)	0.53	0.60	1.16	0.60	1.70	0.60	2.19	0.60
MUR + CB99/LWAL + DNO/H2	SA(0.3 s)	0.41	0.58	0.98	0.58	1.50	0.58	1.99	0.58
MUR + CB99/LWAL + DNO/H3	SA(0.3 s)	0.48	0.56	1.08	0.56	1.62	0.56	2.15	0.56
MUR + CB99/LWAL + DNO/H4	SA(0.6 s)	0.20	0.56	0.52	0.56	0.83	0.56	1.14	0.56
MUR + CB99/LWAL + DNO/H5	SA(0.6 s)	0.53	0.60	1.16	0.60	1.70	0.60	2.19	0.60

PGA peak ground acceleration, SA(X) spectral acceleration at T=X s, θ median, β logarithmic standard deviation

Figure 32. Fragility parameters for masonry building classes (from Martins and Silva 2020)

These functions were converted into vulnerability functions through damage-to-loss models, using beta distributions to represent loss ratios. The results, especially for unreinforced masonry structures, are available in a public repository for further analysis.

2.1.1.2.3. Hybrid and judgment-based methods

Singhal and Kiremidjian (1996) estimate vulnerability curves and DPMs for different RC frames (from Low-Rise, Mid-Rise and High-Rise classes, respectively) through nonlinear dynamic analyses and using the Monte Carlo simulation technique.

Hybrid methods allow to produce DPMs and vulnerability curves as a combination of analytical data from mechanical models and empirical data from observed damage, thus allowing, for example, to calibrate analytical models or to provide for the lack of empirical damage data at certain intensity levels for the geographical area under consideration.

In (Kappos et al., 1995; Kappos et al., 1998) DPMs are provided which are partially derived from observed damage data from past earthquakes, through the vulnerability index procedure, and partially obtained from nonlinear dynamic analyses carried out on building models representing different building classes.

In order to include such analytical results into the DPMs, an empirical correlation between intensity and PGA values at which the accelerograms were scaled is used, and a correlation is also established

between an analytical global damage index obtained from the analyses and the damage expressed as the cost of repair. 6 structural models representing existing Greek buildings, 10 accelerograms and 2 intensities are considered, thus leading to a total number of 120 nonlinear dynamic analyses. The damage results are then combined with the observed damage from the 1978 earthquake in Thessaloniki.

In (Singhal and Kiremidjian, 1998) the analytical vulnerability curves proposed in (Singhal and Kiremidjian, 1996) for Low-Rise RC frames are updated based on the observational data obtained on 84 buildings damaged during the 1994 Northridge earthquake, by means of a Bayesian updating technique accounting for the reliability of different data sources.

Nevertheless, special attention should be addressed to the treatment of uncertainties when using hybrid methods since analytical and empirical vulnerability data include different sources of uncertainty and are thus not directly comparable. Hence, in order to improve an analytical model through a comparison with an empirical model, it probably would be better to calibrate the former in order to obtain only median values equal to the ones provided by the latter. In this way, each source of uncertainty can be properly taken into account through a specific and explicit modelling (Calvi et al., 2006).

An example of Damage Probability Matrices derived from expert judgement can be found in ATC-13 (ATC, 1985), where DPMs are provided which were derived from the judgement of more than 50 senior earthquake engineering experts. Each expert provided, according to his engineering judgement and experience, an estimate of low, best and high values of the damage ratio for each of 36 different building classes, as a function of the seismic intensity expressed according to the MMI scale. These values were assumed as corresponding to 5th, 50th and 95th percentiles, respectively, of a lognormal distribution representing the estimated damage factor for a given seismic intensity. The estimates provided by the experts were also weighted according to the experience and confidence level of each expert for the considered building class.

2.1.1.3. Specificity related to buildings social function

The above methods have been developed thinking about the most diffused buildings, i.e., residential buildings. This is understandable, since residential buildings include people dwellings, and their vulnerability is strictly connected to the most important impacts: above all, human life loss; hence, injuries to people, then, dislocation of people and related impact on emergency management.

However, other buildings exist, and their importance for community cannot be neglected: hospital buildings, that play a key role in emergency management; school buildings, with their importance recognized in all cultures of the world, as well as for the fact that they mostly hold the vulnerable population of children and young people, whose harm is largely deemed unacceptable; industrial facilities, with their economic importance and role in the urban fabric; cultural heritage buildings (churches, monuments, etc.), for their immeasurable value and social role.

Basically, physical vulnerability of these buildings is evaluated as for residential buildings. However, especially within empirical methods, specific vulnerability indicators or weights to vulnerability scores are assigned based on peculiarities of these kinds of structures. These specificities or “vulnerability (underlying) drivers” (Rodgers 2012) are described in the following subsections. Also, in some cases, physical vulnerability is strictly connected to (or even less important than) functional vulnerability. This implies that physical assets assuring functionality are the core issue of physical vulnerability. This occurs, above all, for the case of hospital buildings.

Many papers exist in the literature focusing on applications (potentially with slight modifications) of already described vulnerability assessment methods on this kind of buildings. In the following, we

will focus on original methodologies or, as already stated, on literature notes about specific vulnerability drivers that should be taken into account.

2.1.1.3.1. School buildings

As highlighted by Lang et al. (2009), schools are in general spacious facilities, sometimes consisting of a number of separate buildings. Their areal extension may play a role in their vulnerability, as well as the fact that a school may be an aggregate of buildings, which requires appropriate techniques for combining the vulnerability of its parts (i.e., of the single buildings constituting it). Also, they are characterized by diffused nonstructural members, such as desks, chairs, blackboards, whose presence may obstruct escape routes, as well as by pending devices that can become hazardous falling objects, or objects attached to the walls, whose collapse may be harmful to children. In the assessment of a school vulnerability, the presence, number, distribution of escape routes and emergency exits should be appropriately considered. Lang et al. (2009) also proposed a questionnaire for the assessment of a Structural Vulnerability Index (SVI) whose base value is potentially amplified by an age factor and by an actual state factor accounting for potential presence of degradation.

Rodgers (2012) elaborated a precious opinion paper highlighting, based on observed data and experts' judgment, the specific vulnerabilities of school buildings (in addition to those already highlighted in Lang et al. 2009). Namely, To ensure cost-efficiency and clear sight lines, classrooms are usually large rooms without interior supports. Preferences for cross-ventilation and natural light result in school buildings that are one or two classrooms wide, with classrooms adjacent to corridors and exterior windows on the other sides. Irregular shapes emerge from maximizing classroom space on available land, with few cross walls to support earthquake resistance, weakening the structure if it relies on walls for support. Selecting the lowest bidder for school construction can lead to poor quality if contractors are not properly qualified, as cost pressures can force them to cut corners. Inadequate construction inspection further reduces adherence to plans and specifications, resulting in substandard construction.

Underlying drivers of structural vulnerability for schools are listed in the table reported in Figure 33. As shown in the table, these drivers have been specifically identified by some Authors in some countries, often belonging to developing economy countries.

Underlying driver	Location	Specific observations
Community built buildings	Nepal	Construction quality poor because communities forced to build schools without technical support. (Tamang and Dharam, 1995)
	Bhutan	Community built school buildings damaged by 2009 earthquake (RGoB, 2009)
Scarcity of resources	Global	Other pressing demands limit education department resources (Kenny, 2009)
	Canada	Retrofit or replacement of unsafe schools perceived to compete with basic educational needs of children for same limited funds (Monk, 2006)
	India	School administrators struggle to provide basic facilities (Jain, 2004)
Inadequate codes or seismic zoning	Italy	Inadequate codes before 1996; inadequate zoning (Dolce, 2004)
	Algeria	Seismic hazard underestimated (Bendimerad, 2004)
	China	Seismic hazard underestimated; codes inadequate prior to 1992 (CEA, 2008)
Lack of code enforcement	Algeria	Little enforcement after centralized govt construction ended (Bendimerad, 2004)
	Turkey	No construction site inspections (Gulkan, 2004)
Corruption of enforcement	Global	Corruption circumvents regulatory mechanisms intended to provide safe buildings and renders them ineffective (Kenny, 2009)
Unskilled or unaware building professionals	Algeria	Rural contractors less skilled; most professionals can't design and build properly detailed RC frame buildings (Bendimerad, 2004)
	India	No licensing or proficiency requirements for engineers; building professionals generally not competent in seismic safety related aspects (Jain, 2004)
	Nepal	Most new schools built by convention, not designed (Bothara and Sharpe, 2003)
	Pakistan	Unskilled builders built poorly despite good materials (Mumtaz et al., 2008)
	Turkey	No requirements for engineers, architects or contractors (Gulkan, 2004)
Lack of accountability	Turkey	Engineer of record is paid by developer, no independent inspection, no liability (Gulkan, 2004)
Lack of risk awareness	Algeria	Those responsible for school safety not aware of earthquake threat; parents unaware but very interested in seismic safety once informed (Meslem, 2007)
	India	Many government officials unaware of earthquake threat (Jain, 2004)
	Pakistan	Professionals and builders unaware of earthquake threat (Mumtaz et al., 2008)
Failure to prioritize schools	Canada	Schools not considered critical infrastructure, politicians uninterested; many other buildings retrofitted before schools (Monk, 2006)
Urgent need for large numbers of new schools	Global	Education for all initiatives create demand for many new schools in developing countries; earthquake safety not usually mentioned Wisner (2006), Kenny (2009)
	Algeria	Rapid expansion of education system led to poor construction (Bendimerad, 2004)
	India	2001 earthquake badly damaged government precast schools built rapidly (Rai, 2001)

Figure 33. Observed underlying vulnerability drivers for school buildings (from Rodgers 2012)

The role of nonstructural members in the assessment of school buildings vulnerability has already been highlighted. De Angelis and Pecce (2015) propose a nonstructural vulnerability form for rapid assessment. Each nonstructural element vulnerability is scored and each score is weighting based on their importance and potential hazardousness.

2.1.1.3.2. Hospital buildings

As highlighted by Lang et al. (2009), hospitals are in general spacious facilities, sometimes consisting of a number of separate buildings. Their areal extension may play a role in their vulnerability, as well as the fact that a hospital may be an aggregate of buildings, which requires appropriate techniques for combining the vulnerability of its parts (i.e., of the single buildings constituting it).

Hospitals have a key role during an emergency. Hence, they are primary strategic buildings: they must be fully operational during and immediately after the earthquake. This has a primary consequence: in any case, capacity thresholds for both structural and nonstructural elements should be more severe than those adopted for a residential building (Monti and Nuti 1996). Also, it should be noted that hospital buildings are characterized by a functional vulnerability (Miniati and Iasio 2012) which can be deemed even more “important” than physical vulnerability: in other words,

vulnerability assessment should be performed with special attention to how the vulnerability of physical parts may influence, increase or interact with functional vulnerability. For example, as stated by Monti and Nuti (1996), the collapse threshold for interior partitions should be set to very low values in hospitals (e.g., to a displacement demand equal to 0.002 times the panel height) because they also have to keep aseptic and sterilized, e.g., operating rooms. All the parts of the elevator systems are characterized by a very low collapse thresholds, because lift may be in use, during the earthquake, for patient transportation from one ward to the other. Menoni et al. (2000) highlight that a hospital, even if localized in a single building, is organized in units of treatment, each of which may be characterized by a specific vulnerability both for its content in terms of nonstructural elements or hazardous materials and for its function and potential role during a seismic emergency.

In addition, a hospital often contains valuable devices or hazardous machines and substances that must be adequately protected, since their collapse may increase economic loss and harm people.

On the other hand, a hospital is often part of a system of hospitals sharing the impact of disasters' consequences: in this sense, systemic vulnerability and resilience assessment is fundamental for a complete vulnerability assessment of hospitals (Cimellaro 2009).

In 2006, the United Nations World Health Organization published a handbook dedicated to "Health facility seismic vulnerability evaluation" (WHO, 2006). Basically, it proposes a method for the seismic vulnerability of hospitals via a fast procedure based on vulnerability scores and weights, in which the role of the nonstructural elements listed in the table reported in Figure 34 is appropriately accounted for.

Architctural elements	Installations	Equipment and furnishings
<ul style="list-style-type: none"> • Divisions and partitions • Interiors • Facades • False ceilings • Covering elements • Cornices • Terraces • Chimneys • Glass • Attachments • Ceilings • Antennas 	<ul style="list-style-type: none"> • Drinking-water • Industrial water • Steam • Medical gasses • Industrial fuel • Vacuum network • Air conditioning • Piping • Waste disposal 	<ul style="list-style-type: none"> • Medical equipment • Industrial equipment • Office equipment • Furnishings • Supplies • Clinical files • Pharmacy shelving • Laboratory shelving

Figure 34. Nonstructural elements in a health facility (from WHO, 2006)

The final vulnerability index, named Total Vulnerability Index, is introduced in Lagormarsino and Giovinazzi (2006)'s equation, with Q equal to 2.3 and 6.25 substituted by 0.125, thus testifying that the TVI is different from the Vulnerability Index by Lagomarsino and Giovinazzi as it is evaluated by appropriately accounting for the role of nonstructural elements and contents.

Also, the TVI accounts for the so-called "architctural vulnerability": due to the necessity of assuring adequate natural lighting and aeration to all areas, hospital buildings are often characterized by complex and irregular plans and shapes, as shown in Figure 35.

The WHO handbook also highlights the fundamental role of functional and systemic vulnerability for a complete assessment that, in this case, is not dominated by physical vulnerability. The complexity of the hospital system in terms of internal and external relationships is shown in Figure 36: this testifies that, as these components are functionally, systemically and physically connected to each other, also their vulnerability is connected and interdependent.

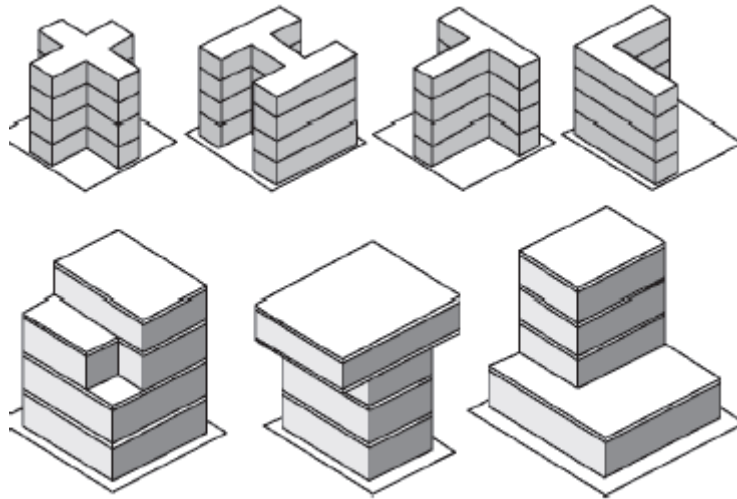


Figure 35. Samples of complex plans and irregular vertical shapes (from WHO, 2006)

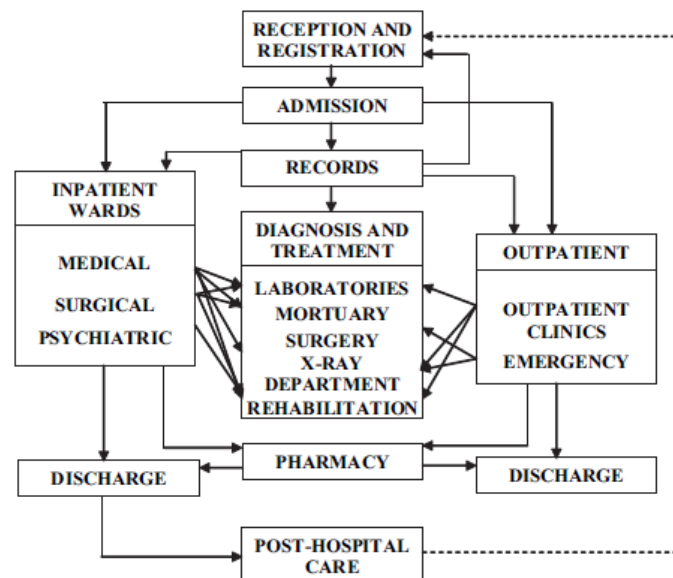


Figure 36. Major clinical relationship (from WHO, 2006)

Perrone et al. (2015) propose a Rapid Visual Screening (RVS) method for evaluating a Safety Index for hospital buildings, adapting the Hospital Safety Index by the Pan American Health Organization to fit the Italian context. The aim is to identify hospitals with the highest seismic risk needing urgent assessment, not to replace detailed analysis.

The method considers three aspects of seismic risk: vulnerability (VULN), exposure (EXP), and hazard (HAZ). It assesses structural, nonstructural, and organizational elements, based on surveys of Italian hospitals and guidelines from WHO. The parameters are calibrated against Italian building codes and national investigations on hospital seismic risk.

The safety evaluation involves calculating six indices: three Primary Indices (ISTR for structural elements, INSTR for nonstructural elements, and IORG for organizational aspects) and three combined indices incorporating Hazard and Exposure. Evaluators use a checklist of 86 questions, with risk levels associated with each. A detailed guideline will assist evaluators, using examples and descriptions for accurate risk assessment. The on-site evaluation should take about six hours, involving a team of professionals with expertise in structural engineering, hospital design, medical

equipment, and administration. The Structural Primary Index (ISTR) assesses structural configurations, materials, and past earthquake exposure. The Nonstructural Index (INSTR) checks the stability of nonstructural elements and critical networks like fire sprinkler systems and HVAC. The Organizational Index (IORG) evaluates hospital management, disaster preparedness, and staff training.

Unlike previous methods, this RVS includes parameters affecting seismic risk comprehensively. The combined indices FUNC and VULN integrate the primary indices, and the final Safety Index (SI) also accounts for hazard and exposure. This holistic approach acknowledges that hospital vulnerability extends beyond physical components to include human and organizational factors.

Moran-Rodriguez et al. (2018) propose a method for assessing seismic vulnerability in hospitals founded on a system of indicators derived from a TF (Task Force) based on various assessments, scoring systems, and international standards and recommendations for risk management in hospitals. This tool is recommended to be applied by a multidisciplinary team, including at least one member of the hospital's maintenance personnel (technicians, engineers, architects) and members from local civil protection and medical staff. It's also beneficial to include one or two external institution members.

Structural, non-structural, functional and administrative-organizational vulnerabilities are considered. Failures in each of these areas are quantified and weighed in order to calculate theoretical indicators for structural (TIA) non-structural (TIB), functional (TIC), and administrative-organizational (TID) vulnerabilities. Failures are weighted based on their impact on life (DL), hospital functioning (DF), and optimal operation (DO), with weights assigned as 0.50, 0.40, and 0.10 respectively. Areas within hospitals are classified into A (vital for life), B (necessary for functioning), and C (less critical). Weights are applied accordingly, considering the expected damage by construction type, seismic hazard, calibration constants, and failures.

Based on the values assumed by these indicators, a vulnerability index is finally calculated. The primary goal is to provide a tool for identifying seismic vulnerability and prioritizing actions to reduce vulnerability in the short, medium, and long term.

2.1.1.3.3. Industrial buildings

Generally, typical vulnerability methods are adopted for the assessment of structural seismic vulnerability of industrial buildings (Magliulo et al. 2008, Ercolino et al. 2018, Ntaliakouras et al. 2018), provided that the adequate weight is given to some well-known weaknesses of these typically prefabricated structures, as listed and documented by Bathalia et al. (2019), as also shown in Figure 37: short-column effect due to the interaction with irregular exterior partitions; connection failure; failure due to loss of support of the beam; cladding panels collapse, industrial storage racks failure. Many studies applied analytical methods, while empirical vulnerability approaches were less adopted.



Figure 37. Some failures in industrial buildings, as reported in Bathalia et al. (2019): short column effect (top left); connection failure (top right); loss of support of beam (bottom left); vertical cladding panel collapse (bottom right).

2.1.1.3.4. Cultural heritage buildings

Generally, cultural heritage buildings can be divided in three categories: churches, historical centers, castles and special structures. Note also that museums, for their precious cultural content, are also included in cultural heritage buildings.

Also in this case, empirical and mechanical methods are the same as those adopted for residential buildings. What changes is, in the case of empirical methods, the fact that specific vulnerable and vulnerability elements not present in residential buildings are included; in the case of mechanical methods, simplified mechanical models should be avoided, while detailed and geometrically complex 3D structural models are needed for nonlinear assessment of capacity and demand. Recently, Zizi et al. (2021) proposed a comprehensive state-of-the-art review for masonry churches.

Lagomarsino (2004) within GNDT and Lagomarsino (2006) within RISK-UE Project, elaborated a methodology for the calculation of the vulnerability scores and index for historical masonry churches (to be adopted within the empirical-based method proposed in Lagomarsino and Giovinazzi (2006)).

Lagomarsino and Giovinazzi (2006) vulnerability curves are adopted also for historical centres by Rapone et al. (2018). Also in this case, a methodology is proposed for the assessment of the vulnerability index to be included in that equation. The method identifies potential fragilities, termed "vulnerability parameters," which depend on building types. Fourteen vulnerability parameters have been identified, influencing building stability during an earthquake. Each parameter is assigned a coefficient, ranging from 0 (no influence) to 1.5 (maximum influence), based on engineering judgment and previous studies. Six potential damage levels (D0 to D5) are defined according to the criteria introduced by Grünthal (1998). These range from no damage (D0) to very heavy damage with near total collapse (D5).

Again, Onescu et al. (2019) propose the use of Lagomarsino and Giovinazzi (2006) equation, with vulnerability index V calculated by considering the cultural values of the (historical) building based on the vulnerability scores and weights shown in the table reported in Figure 38.

%	Criteria	No.	Element	Class				Weight
				A	B	C	D	
70%	STRUCTURAL	1	Organization of vertical structures	0	5	20	45	1
		2	Nature of vertical structures	0	5	25	45	0.25
		3	Location of the building and type of foundation	0	5	25	45	0.75
		4	Distribution of plan resisting elements	0	5	25	45	1.5
		5	Plan regularity	0	5	25	45	0.5
		6	Vertical regularity	0	5	25	45	1
		7	Type of floors	0	5	15	45	0.75
		8	Roofing	0	15	25	45	0.75
		9	Details	0	0	25	45	0.25
		10	Physical conditions	0	5	25	45	1
15%	ARCHITECTURAL ARTISTIC							I_{v10}
		11	Representative architectural style for the area	0	5	25	45	1.5
		12	Originality (global, elements)	0	5	15	25	1.2
		13	Original woodwork/joinery	0	5	15	25	1
		14	Original stucco	0	5	25	45	1
		15	Original statues	0	5	25	45	1
		16	Original gable/fronton	0	5	25	45	1
		17	Original balconies	0	5	15	25	1
		18	Original mosaics	0	5	15	25	1
		19	Original paintings	0	5	15	25	1.2
		20	Actual state of decorative elements	0	5	15	25	0.5
		21	Authenticity/ unauthorised interventions	-15	0	25	45	1.2
		22	Official monument (national, regional, local, protected area)	0	5	25	45	1.5
		23	Particular construction techniques/materials	0	15	25	45	0.5
		24	Actual state of original materials	0	5	15	25	0.5
		25	Representative historical events connected with the building	-5	0	15	25	0.75
		26	Archaeological site	0	5	15	25	1.5
		27	Representative/ original wooden framework	0	5	25	45	1
		28	Restoration work already made on the building	0	5	15	25	1
10%	URBANISTIC							$I_{v \text{ ARCH-ART}}$
		29	Representative for the street profile	0	5	15	45	1.5
		30	Representative for the urban silhouette	0	5	15	45	1.5
		31	Annexes	0	5	15	25	1
		32	Located in touristic area	0	5	25	45	1.5
5 %	SOCIAL ECONOMIC							$I_{v \text{ URB}}$
		34	Public/social functions	0	5	25	45	1.2
		35	Importance for the local community	0	5	15	25	0.5
		36	Economical value	0	5	15	25	1.5
		37	Cultural functions	0	5	25	45	1.2

Figure 38. Seismic vulnerability assessment form considering the cultural influence (from Onescu et al. 2019).

D'Alpaos and Valluzzi (2020) propose the use of the Analytic Hierarchy Process (AHP), a multi-criteria decision-making method that derives ratio scales from pairwise comparisons, for the assessment of vulnerability of cultural heritage and artistic assets. It is particularly useful in contexts where there is limited quantitative information on the effects of actions being evaluated. The AHP is grounded in two fundamental principles: the value of experience and knowledge alongside data for

decision-making, and the ability to measure criteria using actual measurements or a fundamental scale reflecting relative strengths or importance.

AHP allows for the inclusion of both tangible and intangible criteria and enables the evaluation of quantitative and qualitative criteria and alternatives on a unified preference scale. The method assumes that decision-makers can always express a preference and judge the relative importance of evaluation parameters. It structures decision problems into hierarchical levels, with the main goal at the top, criteria and sub-criteria in the middle, and alternatives at the bottom. Pairwise comparisons are conducted at each hierarchical level, converting semantic judgments into numerical values using a fundamental scale, which ranges from 1 (equal importance) to 9 (extreme importance) with intermediate values of 2, 4, 6, and 8.

Pairwise comparisons result in square, reciprocal matrices of preferences, where the elements on the main diagonal are equal to 1, reflecting reflexive binary preference relations, and off-diagonal elements represent the relative importance of one component over another. The method computes priorities (weights) from these matrices, seeking to maintain consistency in judgments, as measured by the consistency index (CI) and consistency ratio (CR). A CR less than 0.10 indicates acceptable consistency, whereas higher values suggest a need for revision.

In practical applications, such as the evaluation of church structures for seismic risk, AHP involves extensive expert input to define criteria, sub-criteria, and their hierarchical relationships. The method combines individual expert judgments to form group decisions, ensuring diverse perspectives are captured. Experts conduct pairwise comparisons of criteria, sub-criteria, and sub-sub-criteria, calculate CI to ensure consistency, and aggregate judgments to determine final priorities.

In conclusion, the AHP provides a systematic approach to decision-making by breaking down complex problems into manageable sub-problems, allowing for the integration of diverse criteria and expert judgments to determine the relative importance and priorities of different components and alternatives.

2.1.1.4. Dynamic seismic vulnerability

Dynamic, time-dependent, or state-dependent vulnerability of buildings refers to the idea that a building's susceptibility to earthquake damage can vary depending on its current state or condition. This concept acknowledges that a building's structural integrity and performance under seismic loads can be influenced by several factors, which can change over time. These factors can be different.

For example, the present condition of the building, including any wear and tear, **previous damage** (from earthquakes or other events), and maintenance history, affects its seismic vulnerability. For example, a building with unrepaired significant damage and, so, weakened components will be more vulnerable.

Temporary changes, such as ongoing renovations, **temporary loading conditions** (e.g., heavy snow, volcanic ashes, or equipment), or changes in building occupancy, can also affect a building's vulnerability.

The cumulative impact of minor seismic events over time can degrade the building's structural components, leading to increased vulnerability.

The natural **aging** process and environmental factors (e.g., corrosion of steel, degradation of concrete) can weaken a building's structural elements.

In a certain sense, also upgrading and retrofitting a structure can be considered within a dynamic vulnerability assessment framework. However, generally, retrofit effects are investigated with a “before-vs-after” approach both with analytical and empirical methods, not with a time-dependent approach.

State-dependent seismic vulnerability assessments are dynamic and need to consider these varying factors to provide an accurate estimate of how a building would perform in the event of an earthquake. This approach contrasts with traditional assessments that might consider vulnerability as a static property based on the original design and construction without accounting for changes over time. This change can be in seismic capacity and seismic demand: some approaches proposed in the literature account for both, others only for one (typically, the latter).

Some major literature works investigating dynamic vulnerability methods are recalled in the following.

Choe et al. (2008) proposed a method for the assessment of seismic fragility of RC columns (and, so, buildings) accounting for the effect of steel rebars corrosion. Basically, steel corrosion is considered in terms of reduction of rebars' area (variation of steel-concrete bonding and crack openings are neglected) during time and a mechanical model with empirical corrections for the assessment of columns' shear force capacity and drift capacity is updated based on the expected reduction of rebars' resisting area from zero to 100 years after the realization. Fragility curves are then estimated, with an analytical approach, at different time distance from the realization of the structure: at each time, structural capacity is updated based on the updated capacity of columns.

Kumar et al. (2008) proposed probabilistic models for the assessment of seismic fragility of columns accounting for cumulative seismic damage, i.e., for the effect of damage due to successive seismic shocks without repair carried out in the meanwhile. Basically, the expected seismic for each seismic shock is expressed in terms of maximum displacement demand. The displacement demand is then converted in an equivalent number of constant amplitude inelastic cycles, N . Then, the basic number of cycles necessary to failure, N_{fl} , accounting for low-fatigue is calculated based on the ductility capacity of the column. In this way, since each event is transformed in N equivalent cycles, it is possible to calculate the updated N_{fm} (i.e., the number of cycles necessary to failure at the m -th earthquake) by subtracting to N_{fl} the number of equivalent cycles of the previous $m-1$ events. The number of cycles to failure for each event allows the definition of a Damage Index, while, based on the ductility demand for each event, the column stiffness, force, and deformation capacity for fragility assessment are updated. The proposed model can also account for the contemporary effects of corrosion.

A similar approach was adopted by Jia et al. (2020) to account for damage cumulation, corrosion and alkali-silica reaction in concrete.

As reported by Haas (2019), cumulative damage and increased fragility are crucial for assessing the safety of structures after a mainshock. Numerous studies have addressed probabilistic monitoring post-seismic events. Yeo and Cornell (2005, 2009) developed a method to estimate a building's lifetime losses considering aftershocks using an inhomogeneous Poisson model combined with a Markov Chain model for damage accumulation. Recent studies have developed fragility models to account for cumulative damage on individual buildings. Trevelopoulos and Guéguen (2016) proposed a vulnerability assessment based on period elongation, showing a probability increase of up to 107% for exceeding a 60% period elongation due to aftershocks. The increase in exceedance probability varies by building type, from 10% to 207%. For severe damage states, the increase ranges from below 5% for low-rise, low-code buildings to 30% for mid-rise, low-code buildings. Iervolino et al. (2016) developed a stochastic model for seismic damage accumulation using a Markov chain, considering

the damage state at each event. Transition probabilities between damage states are derived from a single degree of freedom (SDOF) model. Iervolino et al. (2016) suggested using a time-variant ground motion rate for aftershock sequences and incorporating repair probabilities, though this framework does not account for long-term seismic risk effectively. Tesfamariam and Goda (2017) assessed non-code conforming RC buildings in British Columbia, focusing on sequence-based loss assessment. They found a 13% increase in collapse probability for 2-story low-rise buildings due to aftershocks, with the highest losses from interface events. Larger structures showed no significant increase. Papadopoulos and Bazzurro (2018) conducted a regional-scale risk assessment in Umbria, Italy, demonstrating that parameter choices for an ETAS seismicity model significantly impact estimated losses, emphasizing the need for careful consideration.

Vulnerability curves for case-study reinforced concrete frames accounting for damage cumulation were analytically derived by Aljawhari et al. (2019). Basically, after an appropriate selection of mainshock-aftershock events, cloud analyses were performed by comparing the displacement demand at the end of the first event and at the end of the second event: in the unique signal adopted for the numerical analyses (so-called back-to-back approach), 40 seconds of free vibrations were allowed between the first and the second event. Note that within this approach fragility changes only due to the increase of seismic demand observed during the second event (during the first events, structural stiffness was reduced due to cracking and sometimes yielding of members), not due to a variation of capacity. A similar back-to-back analysis method was adopted by Di Domenico et al. (2023) to assess period elongation as a proxy to the evaluation of damage states and occupancy of reinforced concrete structures in case of first-second event couples with the same seismic intensity.

A simplified approach, for the assessment of state-dependent seismic fragility via pushover analyses on SDOF systems was proposed by Orlacchio et al. (2020). In this case, back-to-back analysis is substituted by incremental dynamic analyses on SDOF systems whose basic properties (stiffness, hardening ratio, force capacity, etc.) are previously modified to account for different possible damage scenarios based on a certain ductility demand value (the ductility demand hypothetically registered during the previous event).

Similarly, a probabilistic framework was proposed by Iacoletti et al. (2023). In this case, SDOF systems representative of the vulnerability classes defined by GEM (Martins and Silva 2020) are adopted for the back-to-back dynamic analyses yielding to the assessment of a probability of observing a certain damage state at the end of the first event and at the end of the second event. Seismic demand during the second event is of course influenced by damage attained during the first event, while damage thresholds are defined based on significant displacement demand values read on the capacity curves.

2.1.2. Tsunami vulnerability

2.1.2.1. Description of Hazard

Tsunamis are rare but potentially devastating natural hazards. They are defined as a series of long period waves, mostly triggered by earthquake induced uplift or subsidence of the seabed. Tsunami can be also caused by large landslides near the coast, underwater volcanic eruptions or meteorological events (i.e. meteotsunami). Typical wavelength ranges from 20 to 300 km are observed in tsunamis generated by earthquakes while ranges from hundreds of metres to kilometres characterize tsunamis generated by landslides where the wavelength is usually shorter.

Probabilistic hazard analysis methods have been developed in past years and have proved useful. However, large gaps and uncertainties still exist and many steps in the assessment methods lack information, theoretical foundation, or commonly accepted methods (Beherens et al. 2021).

Tsunami hazard maps have been produced so far only in some counties like US and Australia. For the Mediterranean area the TSUMAPS-NEAM project produced in 2018 the first homogeneous region-wide long-term Probabilistic earthquake-induced Tsunami Hazard Assessment (Seismic PTHA, S-PTHA) for the coastlines of the North East Atlantic, the Mediterranean, and connected seas (NEAM), and trigger a common tsunami-risk management strategy in the region (Basili et al. 2018). The hazard results are provided through the online platform TSUMAPS by hazard curves calculated at 2,343 Points of Interest (POI), distributed in the North-East Atlantic (1,076 POIs), the Mediterranean Sea (1,130 POIs), and the Black Sea (137 POIs) at an average spacing of ~20 km. For each POI, hazard curves are given for the mean, 2nd, 16th, 50th, 84th, and 98th percentiles. Maps derived from hazard curves are Probability maps for Maximum Inundation Heights (MIH) of 1, 2, 5, 10, 20 meters; Hazard maps for Average Return Periods (ARP) of 500, 1,000, 2,500, 5,000, 10,000 years. For each map, precalculated displays are provided for the mean, the 16th percentile, and the 84th percentile. Such maps provide MIH at the coastline, while ingressions models onshore are not available and should be derived for the specific area of interest.

2.1.2.2. Physical and functional vulnerability assessment methods for residential buildings

Empirical vulnerability and fragility methods are developed by fitting a statistical model to observational data from past tsunami events. Charvet et al. (2017) present a detailed review of available empirical fragility models and shows that these derive from observations made after a small number of recent tsunami events, given the low frequency of occurrence of this hazard.

Empirical tsunami fragility functions are specific to the event and the location affected by the tsunami, as well as the typical construction practice of the affected regions. Damage scales (e.g. MLIT, 2014, EEFIT, 2006, Fraser et al. 2013) are used to record levels of damage. These are then used in the definition of fragility functions associated to a specific Damage State (DS). The Japanese Ministry of Land, Infrastructure, and Transport (MLIT) defined a damage scale based on post tsunami surveys in the Tohoku region in 2011, reported in Figure 39. However, each empirical fragility model adopts a own definition of damage states, which makes their comparison not immediate. Existing fragility models are developed for different structural typologies, such as masonry, timber and reinforced concrete structures, based on the amount of recorded data.



Damage State		Description	Use	Image
DS1	Minor Damage	Inundation below ground floor The building can be reused by removing mud below the floor boards	Possible to use immediately after minor floor and wall cleanup.	
DS2	Moderate Damage	The building is inundated less than 1m above the floor (can be reused after a repair)	Possible to use after moderate repairs.	
DS3	Major Damage	The building is inundated more than 1m above the floor (below the ceiling)	Possible to use after major repairs.	
DS4	Complete Damage	The building is inundated above the ground floor level.	Major work is required for re-use of the building.	
DS5	Collapsed	The key structure is damaged, and difficult to repair to be used as it was before	Not repairable.	
DS6	Washed Away	The building is completely washed away except for the foundation	Not repairable.	

Figure 39. Damage scale based on post tsunami surveys.

Most empirical fragility functions adopt maximum inundation depth as an IM (e.g., Reese et al. 2011; Suppasri et al. 2011, Charvet et al. 2014a; De Risi et al. 2017a), since the inundation depth is measurable in the aftermath of a tsunami and can also be simulated numerically with a relatively good accuracy. In empirical models, the values of the selected IMs are recorded through visual inspections in the aftermath of an event. However, it is often difficult to accurately determine the exact values of the IM, especially in the case of collapsed and washed away buildings. In the case of earthquake triggered tsunami, damage observations for buildings may reflect the cumulative damage of both earthquake ground shaking and tsunami inundation, increasing the uncertainty of empirical tsunami fragility models.

Recent advances in tsunami structural analysis approaches have led to the development of tsunami analytical fragility functions. The loading imparted by a tsunami inundation on buildings is complex due to the combination of unsteady and quasi-steady flow regimes that characterise the different stages of the incoming and outgoing tsunami flow around buildings. However, Foster et al. and McGovern et al. have shown that due to the extremely large wavelengths of tsunamis, the tsunami inundation is prolonged and sustained, leading to large hydrostatic and hydrodynamic forces acting on the structure. The corresponding flow regime can be considered quasi-steady since the temporal variation of the flow is small, especially with respect to the length scale of a building.

Tsunami on-shore flows induce a complex combination of loads on buildings, comprising horizontal and vertical forces, scour and debris effect (ASCE 7). Tsunami-induced horizontal loads on structures mainly consist of unbalanced hydrostatic pressure, hydrodynamic or drag pressure, bore forces and

debris impact loads, while vertical loads are mainly related to hydrostatic buoyancy and hydrodynamic surge. Equations to compute tsunami load components are ported in the ASCE 7 or can be found in recent studies that provide empirical formulations based on hydraulic testing (Qi et al., Foster et al. 2017).

Several parameters can be used as IM for analytical tsunami fragility functions, such as the inundation depth, the momentum flux or the tsunami force (Rossetto). However, the inundation depth is the largely adopted IM in the existing analytical models for the same considerations previously mentioned for the hazard analysis.

Most of existing analytical studies mainly focus on RC buildings. A partial review of existing analytical methods is provided by Rossetto et al. (2019). Such methods mainly adopted simplified assumptions for structural analysis, based on the concepts adopted for the seismic case, which concentrate lateral forces at storey level. More recent analytical methods are based on the application of the tsunami loads in their actual distribution either in a dynamic regime according to tsunami inundation simulations or in a static load regime that reproduces the effects of tsunami loads. Petrone et al. (2017) demonstrated that static analysis is able to well reproduce the structural performance simulated through dynamic analysis, suggesting the use of such static approaches for tsunami fragility analysis. In particular, two static analysis methods are specifically developed for tsunami loading: Constand Depth Pushover (CDPO) and Variable Depth Pushover (VDPO), being the latter the most accurate. In the VDPO, the inundation depth is monotonically increased keeping constant the Froude number, defined as: $Fr = u / \sqrt{g H_w}$. This means that the velocity increases as well during the VDPO analysis as a function of the inundation depth.

Such analytical methods consider the structure as waterproof, assuming infinitely resisting claddings, and consider only lateral loads (hydrostatic and hydrodynamic). Del Zoppo et al. (2017) extended the VDPO analytical method to the case of buildings with breakaway claddings, presenting the VDPO-BI analysis for RC buildings with infill walls. The VDPO-BI allows for a realistic assessment of the structural performance during a tsunami inundation, accounting for the actual distribution and capacity of infills in the outer perimeter of a building. In the VDPO-BI, the tsunami inundation depth (H_w) at the site of the structure is monotonically increased (assuming a constant Froude number, as in the VDPO). The corresponding horizontal forces are imparted to the building until the out-of-plane capacity of exterior infill walls (appropriately accounting for openings if any) in the plane normal to the tsunami flow direction is achieved. Up until this point, the water is assumed to act solely on the exterior of the building, and hence only the seaward columns are directly loaded by tsunami-induced drag forces. Once the exterior infill walls fail, it is assumed that the water can pass through the building, inducing drag forces on interior columns, in proportion to their impacted surfaces. The new lateral loads on the interior and exterior members are calculated at the inundation depth at which the infill walls have failed. Within this analysis model, partitions are not considered to contribute to the structural capacity. Typically, interior partitions are weaker than external infill walls, and hence they are herein assumed to be washed away when the inundation depth causes the failure of exterior infill walls. From this point, the inundation depth is again monotonically increased, and corresponding forces applied to the interior and exterior structural components. When the inundation depth reaches the soffit of the first storey beams, vertical loads due to internal buoyancy (i.e., uplift loads) also begin to be applied to the slabs and beams, as required by ASCE 7-16. This procedure is repeated for each storey of the building during the non-linear incremental analysis until the maximum lateral capacity of the structure is reached.

The VDPO and VDPO-BI analysis can be implemented in refined structural analysis software like OpenSees, as such any commercial software up to now is able to perform tsunami analyses. Del Zoppo et al. (2022) also proposed a mechanics-based method for the performance assessment of RC frames with breakaway infill walls subjected to tsunami and flow-type loads, called SAFETI

(Structural Assessment to Flows and Extreme Tsunami Inundation), implemented in Matlab and easily applicable for the analysis of building portfolios.

Some steps of the VDPO-BI analysis are reported below, in Figure 40:

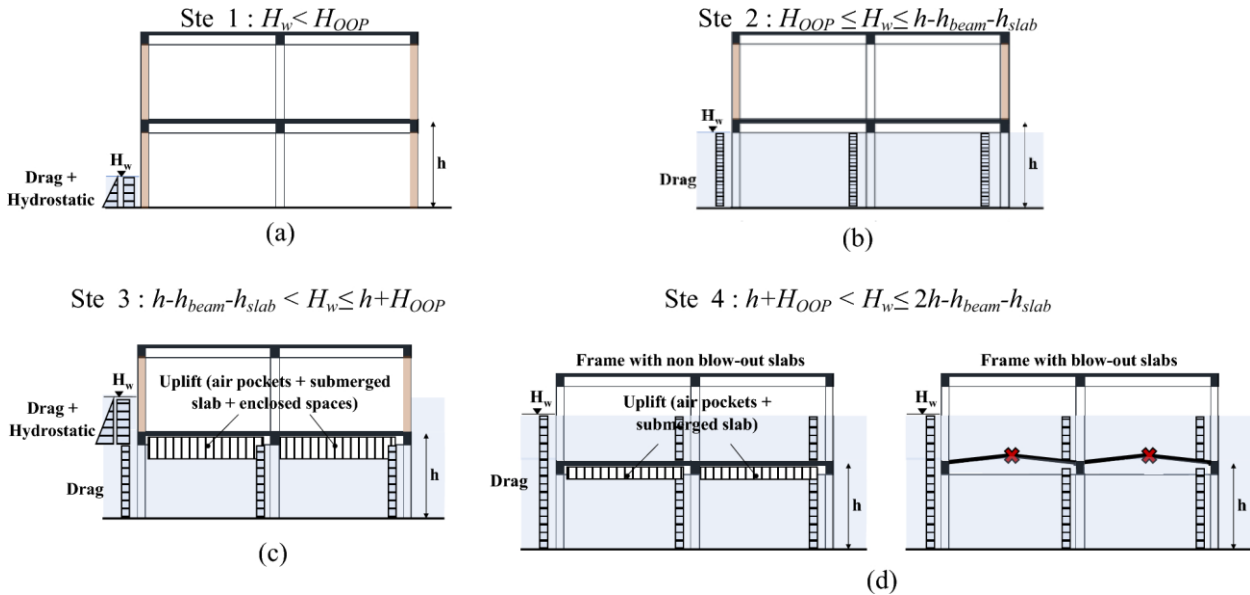


Figure 40. Steps o VDPO-BI analysis.

For masonry buildings, Belliazzi et al. (2021) proposed simplified mechanical models for principal local mechanisms in order to assess the vulnerability of masonry walls in-plane and out-of-plane. In general, a masonry wall under tsunami loads could reach failure for out of plane collapse mechanism (bending and overturning) or in plane collapse mechanism (sliding, cracking by diagonal tension and crushing by diagonal compression), depending on the direction of the flow (Figure 41), if it is parallel or perpendicular to the masonry wall plane. After the tsunami event in 2004, field investigations showed a high vulnerability of masonry structures subjected to tsunami load, especially against out of plane mechanisms.

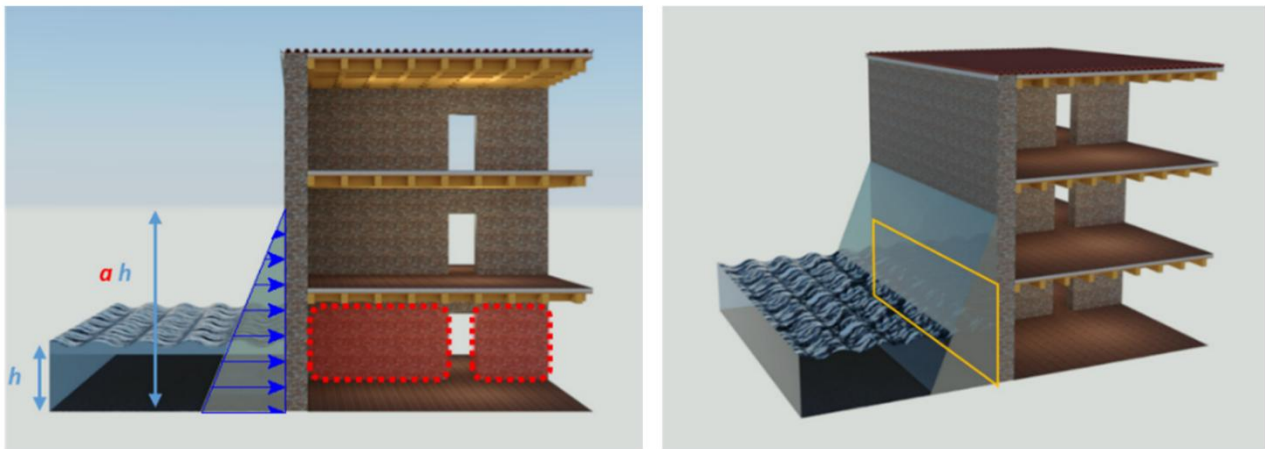


Figure 41. Different impacts on masory walls based on the direction of the flow.

Limited studies have been conducted so far for different structural typologies, such as steel structures (Karafagka et al.) or timber structures.

To develop analytical fragility functions, a damage scale should be defined based on mechanical considerations and Engineering Demand Parameters (EPD) should be properly identified and monitored during the analysis.

While empirical fragility functions curves are typically obtained at community-scale for many buildings and assets, analytical fragility curves can be either developed at single-building level (e.g., Petrone et al. 2017; Alam et al. 2018; Karafagka et al. 2018) and at community level (e.g., Park et al. 2013; Aránguiz et al. 2018, Belliazzi et al., Del Zoppo et al.).

Alternatively to analytical methods, judgement-based methods based on indicators may be used for tsunami vulnerability assessment. One of the most-established indicators-based methods for tsunami focusing on physical vulnerability is the Papathoma Tsunami Vulnerability Assessment (PTVA). This method was first proposed in 2003 and has been applied to case-studies in Greece (Papathoma and Dominey-Howes, 2003). It was further developed following the 2004 Indian Ocean Tsunami (Dominey-Howes and Papathoma, 2007). The weighting method has been improved in further versions of the PTVA (Dall'Osso et al. 2009a; Dall'Osso et al. 2016) and has become a popular method as it has been validated and used in several countries. Indicators-based methods could also be expanded to include indicators related to the functionality of a building. Baiguera et al. (2021) proposed a simple but quantitative approach for the assessment of the resilience of healthcare systems to tsunamis. This is based on indicators that relate not only to hospital building fragility, but also to the maintenance of hospital functionality.

2.2. Climate hazards

2.2.1. Urban heat waves vulnerability

2.2.1.1. Description of Hazard

An extreme climate phenomenon that occurs with greater frequency and intensity as the years go by and that has a direct impact on people's health is, without a doubt, heat waves. Heat waves occur when very high temperatures are recorded for several consecutive days, often associated with high levels of humidity, strong solar radiation and lack of ventilation. These climatic conditions can represent a risk to the health of the population.

Although there is no single definition at a global level, in our country the ISPRA - Higher Institute for Environmental Protection and Research defines the phenomenon as: "episodes of intense and prolonged heat, the frequency of which in the hottest months of the summer season represent a risk, of a cardiac nature and not only, for the health of the population, especially the elderly and frail, due to the stress to which the body is subjected".

To determine a heat wave scenario, the following daily climate parameters were taken into consideration: the maximum temperature (T_{\max}) and the minimum temperature (T_{\min}) of the atmosphere, the Heat Index (HI) and the surface temperature gradient between day and night (ΔT). Table 8 shows the individual parameters with their relative threshold values.

Hazard characteristics	Parameters	Thresholds
P₁	T_{\max}	≥ 30
P₂	T_{\min}	≥ 20
P₃	HI -Heat index	≥ 32
P₄	ΔT - Surface temperature difference	< 10

Table 8 – Heatwave hazard parameters and thresholds

The HI parameter was synthesized by NOAA - National Oceanic and Atmospheric Administration of the United States starting from the maximum temperature and the percentage of relative humidity of the air; it estimates the real temperature perceived by the population, as the maximum temperature and relative humidity vary.

The surface temperature gradient is a parameter that measures the difference in surface temperature between hours of day and night. It is related to the thermal absorptions and emissions of the material during the day depending on its thermal capacity.

A hazard scenario related to the heat wave phenomenon is characterized by a period in which the phenomenon persists on the study area; it is determined by four characteristics linked respectively to the four parameters.

Each characteristic P_i is represented by the number of days in which the value of the climate parameter exceeds a predefined threshold, established by models or calibrations from scientific literature. To define a heatwave hazard scenario, all four parameters must exceed the thresholds for at least 3 consecutive days. The characteristics P_1 , P_2 , P_3 of the hazard scenario are calculated through analysis processes of the results of projective models up to 2100 of the estimates of the maximum temperature, minimum temperature and Heat Index values on the site where the weather station is located, determining the number of consecutive days in which the parameter exceeds the threshold value.

As regards the surface temperature gradient, it was assumed that over time there are no changes in the urban layout and changes in land use, so it was considered that the distribution of the surface temperature gradient

in the study area between day and night in a summer period in which there was a heat wave does not vary over time.

To develop medium- and long-term hazard scenarios, we chose to use the Representative Concentration Pathways (RCP) 4.5 scenario, a climate forecasting model developed by the IPCC, which predicts a slowdown in greenhouse gas emissions but not in their concentrations in the atmosphere, which will increase further. This scenario is the one that today seems most likely, as current trends predict a decrease in greenhouse gas emissions produced by human activities.

The evaluation of the hazard is obtained combining the time and the spatial indexes, following the processes described in (Apreda et al. 2019) in which are considered three types of hazard scenarios: Short term (period 2020-2040), Medium term (period 2041-2070) and Long term (period 2071-2100).

For each of the two climate forecasting scenarios, 3 hazard scenarios were identified, one related to the forecast of a heat wave phenomenon of short duration, in terms of number of continuous days, one of intermediate intensity, and one of high intensity. In this way, it is possible to analyze the distribution of a hazard index related to three scenarios, one more moderate, one medium and one of high intensity (Table 9).

Hazard scenario (RCP 4.5 model)	Heatwave mean duration in days
Short-term	6
Medium-term	30
Long-term	60

Table 9 – Number of days of heatwave phenomenon using RCP 4.5 model

In a short-term scenario, in which the duration of heatwave period is between 3 and 8 days, in (Apreda et al. 2019) after a calibration process is defined the hazard indicator described in the following table (Tab 10):

Data representation	Class	Label
$\Delta T \leq 7$	1	High
$7 < \Delta T \leq 10$	2	Medium-high
$10 < \Delta T \leq 15$	3	Medium
$15 < \Delta T \leq 20$	4	Medium-low
$\Delta T > 20$	5	Low

Table 10 – Thematic hazard classification related to the surface thermal difference in a heatwave with a temporal intensity of less than 6 consecutive days

2.2.1.2. Physical and functional vulnerability assessment methods for residential buildings

To evaluate the vulnerability of the two subsystems residential building, a set of indicators was computed that recognizes the main characteristics of the settlements in the type-morphological and technological aspects, as well as in the presence and intensity of greenery and urban elements, capable of affecting the aspects of temperature, ventilation and relative humidity during intense climatic phenomena (EEA 2012).

To execute our framework the following datasets have been imported into the framework:

- Digital Terrain Model and Digital Surface Model raster dataset of the study areas (cell size 1 m x 1 m);
- Topographic database of the study areas (geographical scale 1:5000);
- ISTAT last census dataset of 2011(geographical scale 1:10.000);
- satellite NDVI, Albedo and in raster format in Geo-Tiff format (cell extension equal to 1x1);

- Temperature Gradient raster data collected in a heatwave period (with a cell extension equal to 1x1).

In Table 11, for each indicator, are described the classification methods applied to and their weights necessary to summarize the intrinsic vulnerability of each subsystem, attributed following a specific calibration.

Subsystem	Indicators	Weights
Residential buildings	Thermal lag	5
	Thermal decrement factor	4
	Building volume	2
	Solar exposure of building envelope	5

Table 11 - Classification of residential buildings indicators with weights

The indicators are aimed at assessing the performance of building envelope related to its overheating.

Thermal lag is defined as the time delay between the maximum heat flow entering the internal environment and the maximum temperature of the external environment. The indicator used estimates the contribution of the characteristic in increasing the thermal insulation of the building envelope. The estimate is carried out with a partitioning into five classes ordered by severity.

Thermal decrement factor is defined as the ratio between the dynamic thermal transmittance module and the thermal transmittance in stationary conditions. The indicator used estimates the contribution of the characteristic in increasing the thermal insulation of the building envelope. The estimate is carried out with a partitioning into five classes ordered by severity.

Solar exposure of building envelope represents the exposure of the facades and roofs of a building to direct solar rays; the duration of such exposure, which in residential buildings must be the most suitable from the dual point of view of lighting and heating, depends on the shape and position of the building as well as on various factors, such as, for example, the presence of other buildings or trees along roads that are not sufficiently.

Thermal lag and *thermal decrement factor* are closely related, depending on the materials of envelope (roof and external walls) that determine the ability of building to delay the transfer of heat from open into indoor spaces. Both parameters are evaluated for each construction technique through the thermal simulation with technical software and the following attribution of values to each building. The *solar exposure of building envelope* is linked to the orientation of the building and is assessed considering the different exposure of the facades to solar radiation during the day and the possible shading provided by surrounding buildings.

To obtain the final indicator of vulnerability of residential buildings to heat waves, a weighted average is calculated based on the weights assigned in Table 4. The weights were set by expert urban planners following appropriate calibrations on a series of analyses carried out.

$$V_{RB} = \frac{(I_{Tl} * W_{Tl}) + (I_{Tdf} * W_{Tdf}) + (I_{Bv} * W_{Bv}) + (I_{Se} * W_{Se})}{W_{Tl} + W_{Tdf} + W_{Bv} + W_{Se}}$$

Where *I* is the indicator's value; *W* is the weight value of the indicators; *W* is the weight value of the indicators; *Tl* is *Thermal lag*; *Tdf* is *Thermal decrement factor*; *Bv* is *Building volume*; *Se* is *Solar exposure of building envelope*.

The indicators are all returned non-dimensional and normalized in order to allow the impact assessment operations, making them comparable to each other. All indicators foresee a partitioning into 5 classes. The values assumed by each class of each indicator are calibrated locally; consequently, in other contexts, as the values assumed by the indicator vary, the ranges of values attributed to the 5 classes may also vary. In the experimentation, it was decided to partition into 5 classes, and it was decided to assign a value from 1 to 5 to each class, where a lower value corresponds to a greater contribution to the vulnerability of the subsystem element. Table 12 shows the values and labels assigned to the 5 classes.

Class	Label
1	High
2	Medium-high
3	Medium
4	Medium-low
5	Low

Table 12 - Classification of indicators with labels

References

- American Society of Civil Engineers (ASCE) (2016). "Minimum Design Loads and Associated Criteria for Buildings and Other Structures." ASCE/SEI 7-16.
- ATC, 1985. Earthquake damage evaluation data for California. Report ATC-13, Applied Technology Council, Redwood City, California, USA.
- Barbat, A. H., Carreño, M. L., Pujades, L. G., Lantada, N., Cardona, O. D., & Marulanda, M. C. (2010). Seismic vulnerability and risk evaluation methods for urban areas: A review with application to a pilot area. *Structure and Infrastructure Engineering*, 6(1-2), 17–38. DOI: 10.1080/15732470802663763.
- Basili, R., Brizuela, B., Herrero, A., Iqbal, S., Lorito, S., Maesano, F. E., ... & Oueslati, F. (2018). NEAM Tsunami Hazard Model 2018 (NEAMTHM18): online data of the Probabilistic Tsunami Hazard Model for the NEAM Region from the TSUMAPS-NEAM project.
- Basili, R., Brizuela, B., Herrero, A., Iqbal, S., Lorito, S., Maesano, F.E., et al. (2018). "NEAM Tsunami Hazard Model 2018 (NEAMTHM18): Online Data of the Probabilistic Tsunami Hazard Model for the NEAM Region from the TSUMAPS-NEAM Project." Istituto Nazionale di Geofisica e Vulcanologia (INGV).
- Behrens, J., Løvholt, F., Jalayer, F., Lorito, S., Salgado-Gálvez, M.A., Sørensen, M.B., et al. (2021). "Probabilistic Tsunami Hazard and Risk Analysis: A Review of Research Gaps." *Frontiers in Earth Science*, 9:764922.
- Behrens, Jörn, et al. "Probabilistic tsunami hazard and risk analysis: A review of research gaps." *Frontiers in Earth Science* 9 (2021): 628772.
- Belliazzi, S., De Risi, R., Del Zoppo, M., & Lignola, G.P. (2021). "Simplified approach to assess the vulnerability of masonry buildings under tsunami loads." *Bulletin of Earthquake Engineering*, 19(12), 4999–5030.
- Benedetti D., Petrini V., 1984. Sulla vulnerabilità di edifici in muratura: proposta di un metodo di valutazione. *L'industria delle Costruzioni*, 149(1), 66-74. (in Italian)
- Bernardini, A., & Lagomarsino, S. (2008). The seismic vulnerability of architectural heritage. *Proceedings of the Institution of Civil Engineers - Structures & Buildings*, 161(4), 171–181. DOI: 10.1680/stbu.2008.161.4.171
- Borzi B., Crowley H., Pinho R., 2008b, The influence of infill panels on vulnerability curves for RC buildings. *Proceedings of the 14th World Conference on Earthquake Engineering*, Beijing, China, October 12-17. Paper 09-01-0111.
- Borzi B., Pinho R., Crowley H., 2008a. Simplified pushover-based vulnerability analysis for large scale assessment of RC buildings. *Engineering Structures*, 30(3), 804-820.
- Bourcet, J., Kubilay, A., Derome, D., Carmeliet J. (2023). Representative meteorological data for long-term wind-driven rain obtained from Latin Hypercube Sampling – Application to impact analysis of climate change. <https://doi.org/10.1016/j.buildenv.2022.109875>
- Braga F., Dolce M., Liberatore D., 1982. A statistical study on damaged buildings and an ensuing review of the MSK-76 scale. *Proceedings of the 7th European Conference on Earthquake Engineering*, Athens, Greece. Pp. 431-450.
- Bursi, O. S., Nardin, C., Marelli, S., Sudret, B., & Broccardo, M. (2024). UQ state-dependent framework for seismic fragility assessment of industrial components.
- Burton C.G. and Silva V. (2014). Integrated Risk Modelling within the Global Earthquake Model (GEM): Test Case Application for Portugal. *Proceedings of the Second European Conference on Earthquake*

Engineering and Seismology, European Association of Earthquake Engineering and European Seismological Commission, Istanbul, Turkey.

- Cabeza, L.M. & Chàfer, M. (2020). Technological options and strategies towards zero energy buildings contributing to climate change mitigation: A systematic review. *Energy and Buildings* 219, 110009, <https://doi.org/10.1016/j.enbuild.2020.110009>
- Calvi G.M., 1999. A displacement-based approach for vulnerability evaluation of classes of buildings. *Journal of Earthquake Engineering*, 3(3), 411-438.
- Calvi G.M., Pinho R., Magenes G., Bommer J.J., Restrepo-Veléz L.F., Crowley H., 2006. The development of seismic vulnerability assessment methodologies for variable geographical scales over the past 30 years. *ISSET Journal of Earthquake Technology*, 43(3), 75-104.
- Calvi, G. M., Pinho, R., Magenes, G., Bommer, J. J., Restrepo-Veléz, L. F., & Crowley, H. (2006). Development of seismic vulnerability assessment methodologies over the past 30 years. *ISSET Journal of Earthquake Technology*, 43(3), 75–104.
- Carreño, M. L., Cardona, O. D., & Barbat, A. H. (2007). A disaster risk management performance index. *Natural Hazards*, 41(1), 1–20. DOI: 10.1007/s11069-006-9008-y.
- Carreño, M. L., Cardona, O. D., & Barbat, A. H. (2007). Urban seismic risk evaluation: A holistic approach. *Natural Hazards*, 40(1), 137–172. DOI: 10.1007/s11069-006-0008-8.
- Castelluccio, R., Fraiese, M., Diana, L., Vitiello, V. (2022). L'identificazione del Rischio Edilizio come fase necessaria per la gestione degli scenari multi-rischio. In: Fatiguso F et al. (eds.) *Colloqui.AT.e 2023 - In Transizione: sfide e opportunità per l'ambiente costruito*, pp. 727–744. EdicomEdizioni, Monfalcone.
- Castori, G., Borri, A., De Maria, A., Corradi, M., & Sisti, R. (2017). Seismic vulnerability assessment of a monumental masonry building. *Engineering Structures*, 136, 454–465. DOI: 10.1016/j.engstruct.2017.01.035
- Catulo, R., Falcão, A. P., Bento, R., & Ildefonso, S. (2018). Simplified evaluation of seismic vulnerability of Lisbon Heritage City Centre based on a 3D GIS-based methodology. *Journal of Cultural Heritage*, 32, 108–116. DOI: 10.1016/j.culher.2017.11.014
- Ceroni, F., Caterino, N., & Vuoto, A. (2020). Simplified seismic vulnerability assessment methods: A comparative analysis with reference to regional school building stock in Italy. *Applied Sciences*, 10, 6771
- Charvet, I., Ioannou, I., Rossetto, T. (2017). "Empirical Fragility Assessment of Buildings Subjected to Earthquake Tsunami Hazard." *Natural Hazards*, 88(3), 1451-1484.
- Charvet, I., Macabuag, J., Rossetto, T. (2014). "Estimation of Tsunami-Induced Building Damage Using Empirical Fragility Curves." *Proceedings of the 2nd European Conference on Earthquake Engineering and Seismology, Istanbul, Turkey*.
- Chioccarelli E., Cito P., Iervolino I., Giorgio M. (2018) REASSESS V2.0: software for single- and multi-site probabilistic seismic hazard analysis. *Bulletin of Earthquake Engineering*. DOI 10.1007/s10518-018-00531-x
- Cimellaro, G. P., Reinhorn, A. M., & Bruneau, M. (2009). Seismic resilience of a hospital system. *Structure and Infrastructure Engineering: Maintenance, Management, Life-Cycle Design and Performance*, 6(1-2), 127-144. DOI: 10.1080/15732470802663847.
- Colombi M., Borzi B., Crowley H., Onida M., Meroni F., Pinho R., 2008. Deriving vulnerability curves using Italian earthquake damage data. *Bulletin of Earthquake Engineering*, 6(3), 485-504.
- Cosenza E., Manfredi G., Polese M., Verderame G.M., 2005. A multi-level approach to the capacity assessment of existing RC buildings. *Journal of Earthquake Engineering*, 9(1), 1-22.

- Crowley H., Colombi M., Borzi B., Faravelli M., Onida M., Lopez M., Polli D., Meroni F., Pinho R., 2009. A comparison of seismic risk maps for Italy. *Bulletin of Earthquake Engineering*, 7(1), 149-190.
- Crowley H., Pinho R., 2004. Period-height relationship for existing european reinforced concrete buildings. *Journal of Earthquake Engineering*, 8(1), 93-119.
- Crowley H., Pinho R., 2006. Simplified equations for estimating the period of vibration of existing buildings. *Proceedings of the 1st European Conference on Earthquake Engineering and Seismology*, Geneva, Switzerland, September 3-8. Paper No. 1122.
- Crowley H., Pinho R., Bommer J.J., 2004. A probabilistic displacement-based vulnerability assessment procedure for earthquake loss estimation. *Bulletin of Earthquake Engineering*, 2(2), 173-219.
- Crowley H., Pinho R., Bommer J.J., Bird, J.F., 2006. Development of a displacement-based method for earthquake loss assessment. ROSE Research Report No. 2006/01, IUSS Press, Pavia, Italy.
- D'Ayala, D., Galasso, C., Minas, S., & Novelli, V. (2015). Review of Methods to Assess the Seismic Vulnerability of Buildings, with Particular Reference to Hospitals and Medical Facilities. Evidence on Demand. DOI: 10.12774/eod_hd.june2015.dayaladetal
- De Angelis, A., & Pecce, M. (2015). Seismic nonstructural vulnerability assessment in school buildings. *Natural Hazards*, 79, 1333–1358.
- De Risi, R., Goda, K., Mori, N., Yasuda, T. (2017). "Tsunami Damage Assessment of Buildings in Kesennuma City Following the 2011 Tohoku Earthquake." *Journal of Earthquake and Tsunami*, 11(4), 1740009.
- De Sortis, G., et al. (2009). Linee guida per la riduzione della vulnerabilità di elementi non strutturali arredi e impianti, Presidenza del Consiglio dei Ministri, Dipartimento della Protezione Civile, Rome, Italy, 2009.
- Del Zoppo, M., De Risi, R., Rossetto, T. (2017). "Analytical Fragility Functions for Italian RC Buildings Considering the Effects of Infill Walls." *Bulletin of Earthquake Engineering*, 15(12), 5435-5459.
- Del Zoppo, M., De Risi, R., Rossetto, T. (2022). "SAFETI: A Mechanics-Based Method for the Performance Assessment of RC Frames with Breakaway Infill Walls Subjected to Tsunami and Flow-Type Loads." *Engineering Structures*, 252, 113592.
- Despotaki, V., Silva, V., Lagomarsino, S., Pavlova, I., & Torres, J. (2018). Evaluation of Seismic Risk on UNESCO Cultural Heritage sites in Europe. *International Journal of Architectural Heritage*, 12(7-8), 1231–1244. DOI: 10.1080/15583058.2018.1503374
- Di Pasquale G., Orsini G., 1997. Proposta per la valutazione di scenari di danno conseguenti ad un evento sismico a partire dai dati ISTAT. Atti dell'VIII convegno ANIDIS "L'ingegneria sismica in Italia", Taormina, Italy, September 21-24. Vol. 1, pp. 477–486. (in Italian)
- Di Pasquale G., Orsini G., Romero R.W., 2005. New developments in seismic risk assessment in Italy. *Bulletin of Earthquake Engineering*, 3(1), 101-128.
- Diana, L. (2017). Seismic vulnerability assessment at urban scale: state of the art and perspectives. *Rivista Valori e Valutazioni*, 18, 69.
- Dolce M., Masi A., Marino M., Vona M., 2003. Earthquake damage scenarios of the building stock of Potenza (southern Italy) including site effects. *Bulletin of Earthquake Engineering*, 1(1), 115-140.
- Dolce M., Moroni C., 2005. La valutazione della vulnerabilità e del rischio sismico degli edifici pubblici mediante le procedure VC (vulnerabilità c.a.) e VM (vulnerabilità muratura), Atti del Dipartimento di Strutture, Geotecnica, Geologia applicata all'ingegneria, N. 4/2005. (in Italian)
- Domaneschi, M., Zamani Noori, A., Pietropinto, M. V., & Cimellaro, G. P. (2021). Seismic vulnerability assessment of existing school buildings. *Computers and Structures*, 248, 106522.

- Earthquake Engineering Field Investigation Team (EEFIT) (2006). "The Indian Ocean Tsunami of 26 December 2004: Mission Findings in Sri Lanka and Thailand."
- Elnashai, A. S. (2006). Assessment of seismic vulnerability of structures. *Journal of Constructional Steel Research*, 62(11), 1134–1147. DOI: 10.1016/j.jcsr.2006.06.024.
- Ercolino, M., Bellotti, D., Magliulo, G., & Nascimbene, R. (2018). Vulnerability Analysis of Industrial RC Precast Buildings Designed According to Modern Seismic Codes. *Engineering Structures*, 158, 67–78. DOI: 10.1016/j.engstruct.2017.12.005
- Estephan, J., Feng, C., Gan Chowdhury, A., Chavez, M., Baskaran, A., & Moravej, M. (2021). Characterization of wind-induced pressure on membrane roofs based on full-scale wind tunnel testing. *Engineering Structures*, 235, 112101. <https://doi.org/10.1016/j.engstruct.2021.112101>
- Faccioli E., Pessina V. (editors), 2000. The Catania project: earthquake damage scenarios for a high risk area in the Mediterranean. CNR-Gruppo Nazionale per la Difesa dai Terremoti, Rome, Italy.
- Faccioli E., Pessina V., Calvi G.M., Borzi B., 1999. A study on damage scenarios for residential buildings in Catania city. *Journal of Seismology*, 3(3), 327-343.
- Fajfar P., 1999. Capacity spectrum method based on inelastic demand spectra. *Earthquake Engineering and Structural Dynamics*, 28(9), 979-993.
- FEMA E-74 (2012), Reducing the Risks of Nonstructural Earthquake Damage - A Practical Guide, Federal Emergency Management Agency, Washington, D.C.
- FEMA, 2001. HAZUS99 Technical Manual. Service Release 2. Federal Emergency Management Agency, Washington, D.C., USA.
- Ferranti, G., Greco, A., Pluchino, A., Rapisarda, A., & Scibilia, A. (2024). Seismic vulnerability assessment at an urban scale by means of machine learning techniques. *Buildings*, 14(2), 309. DOI: 10.3390/buildings14020309.
- Formisano, A., & Marzo, A. (2017). Simplified and refined methods for seismic vulnerability assessment and retrofitting of an Italian cultural heritage masonry building. *Computers & Structures*, 180, 13–26. DOI: 10.1016/j.compstruc.2016.07.005
- Foster, H., Rossetto, T., Allsop, W. (2017). "An Experimental Study of Tsunami Bore Forces on Walls." *Coastal Engineering*, 128, 44-57.
- Fraser, S., Raby, A., Pomonis, A., Goda, K., Chian, S.C., Macabuag, J., et al. (2013). "Tsunami Damage to Buildings in Sri Lanka: Observations and Data Collection." *Natural Hazards*, 63(2), 575-613.
- Giovinazzi S., 2005. The vulnerability assessment and the damage scenario in seismic risk analysis. PhD Thesis, Technical University Carolo-Wilhelmina at Braunschweig, Braunschweig, Germany and University of Florence, Florence, Italy.
- Giovinazzi S., Lagomarsino S., 2004. A macroseismic method for the vulnerability assessment of buildings. *Proceedings of the 13th World Conference on Earthquake Engineering*, Vancouver, Canada, August 1-6. Paper No. 896.
- Glaister S., Pinho R., 2003. Development of a simplified deformation-based method for seismic vulnerability assessment. *Journal of Earthquake Engineering*, 7(SI1), 107-140.
- GNDT, 1993. Rischio sismico di edifici pubblici. Parte I: aspetti metodologici. CNR-Gruppo Nazionale per la Difesa dai Terremoti, Rome, Italy.
- Grant D., Bommer J.J., Pinho R., Calvi G.M., 2006. Defining priorities and timescales for seismic intervention in school buildings in Italy. ROSE Research Report No. 2006/03, IUSS Press, Pavia, Italy.

- Grünthal G., 1998. Cahiers du Centre Européen de Géodynamique et de Séismologie: Volume 15 – European Macroseismic Scale 1998. European Center for Geodynamics and Seismology, Luxembourg.
- Guéguen, P. (2013). Seismic Vulnerability of Structures. ISTE Ltd and John Wiley & Sons, Inc. ISBN: 978-1-84821-524-5.
- Guéguen, P., Michel, C., & LeCorre, L. (2007). A simplified approach for vulnerability assessment in moderate-to-low seismic hazard regions: Application to Grenoble (France). *Bulletin of Earthquake Engineering*, 5(4), 467–490. DOI: 10.1007/s10518-007-9036-3.
- Hassan A.F., Sozen M.A., 1997. Seismic vulnerability assessment of low-rise buildings in regions with infrequent earthquakes. *ACI Structural Journal*, 94(1), 31-39.
- Iacoletti, S., Cremen, G., & Galasso, C. (2023). Modeling damage accumulation during ground-motion sequences for portfolio seismic loss assessments. *Soil Dynamics and Earthquake Engineering*, 168, 107821. DOI: 10.1016/j.soildyn.2023.107821.
- Iervolino I., Manfredi G., Polese M., Verderame G.M., Fabbrocino G., 2007. Seismic risk of R.C. building classes. *Engineering Structures*, 29(5), 813-820.
- INGV-DPC S1, 2007. Progetto S1. Proseguimento della assistenza al DPC per il completamento e la gestione della mappa di pericolosità sismica prevista dall'Ordinanza PCM 3274 e progettazione di ulteriori sviluppi. Istituto Nazionale di Geofisica e Vulcanologia – Dipartimento della Protezione Civile, <http://esse1.mi.ingv.it> (in Italian)
- JBDPA, 1990. Standard for seismic capacity assessment of existing reinforced concrete buildings. Japanese Building Disaster Prevention Association, Ministry of Construction, Tokyo, Japan.
- Kaewunruen, S., Wu, L., Goto K., and Najih, Y. (2018). Vulnerability of Structural Concrete to Extreme Climate Variances. *Climate*, 6(2):40. <https://doi.org/10.3390/cli6020040>
- Kappos A.J., Pitilakis K., Stylianidis K.C., 1995. Cost-benefit analysis for the seismic rehabilitation of buildings in Thessaloniki, based on a hybrid method of vulnerability assessment. *Proceedings of the 5th International Conference on Seismic Zonation*, Nice, France, October 17-19. Vol. 1, pp. 406-413.
- Kappos A.J., Stylianidis K.C., Pitilakis K., 1998. Development of seismic risk scenarios based on a hybrid method of vulnerability assessment. *Natural Hazards*, 17(2), 177-192
- Kappos, A. J., Panagopoulos, G., Panagiotopoulos, C., & Penelis, G. (2006). A hybrid method for the vulnerability assessment of R/C and URM buildings. *Bulletin of Earthquake Engineering*, 4(4), 391–413. DOI: 10.1007/s10518-006-9023-0.
- Kircher C.A., Nassar A.A., Kustu O., Holmes W.T., 1997. Development of building damage functions for earthquake loss estimation. *Earthquake Spectra*, 13(4), 663-682.
- Kircher C.A., Reitherman R.K., Whitman R.V., Arnold C., 1997. Estimation of earthquake losses to buildings. *Earthquake Spectra*, 13(4), 703-720.
- Kumar, R., Gardoni, P., & Sanchez-Silva, M. (2008). Effect of cumulative seismic damage and corrosion on the life-cycle cost of RC bridges. *Earthquake Engineering and Structural Dynamics*, 38, 887–905. DOI: 10.1002/eqe.873.
- Lagomarsino, S. (2006). On the vulnerability assessment of monumental buildings. *Bulletin of Earthquake Engineering*, 4(4), 445–463. DOI: 10.1007/s10518-006-9025-y
- Lagomarsino, S., & Giovinazzi, S. (2006). Macroseismic and mechanical models for the vulnerability and damage assessment of current buildings. *Bulletin of Earthquake Engineering*, 4(4), 415–443. DOI: 10.1007/s10518-006-9024-z.

- Lagomarsino, S., & Podestà, S. (2004). Seismic Vulnerability of Ancient Churches: I. Damage Assessment and Emergency Planning. *Earthquake Spectra*, 20(2), 377–394. DOI: 10.1193/1.1737735
- Lagomarsino, S., & Podestà, S. (2004). Seismic Vulnerability of Ancient Churches: II. Statistical Analysis of Surveyed Data and Methods for Risk Analysis. *Earthquake Spectra*, 20(2), 395–412. DOI: 10.1193/1.1737736
- Lang, D. H., Verbicaro, M. I., & Singh, Y. (2009). Seismic vulnerability assessment of hospitals and schools based on questionnaire survey. Norwegian Geotechnical Institute Technical Report.
- Magliulo, G., Fabbrocino, G., & Manfredi, G. (2008). Seismic Assessment of Existing Precast Industrial Buildings Using Static and Dynamic Nonlinear Analysis. *Engineering Structures*, 30(2580–2588). DOI: 10.1016/j.engstruct.2008.02.003
- Martins, L., & Silva, V. (2021). Development of a fragility and vulnerability model for global seismic risk analyses. *Bulletin of Earthquake Engineering*, 19, 6719–6745. DOI: 10.1007/s10518-020-00885-1.
- Masi A., 2003. Seismic vulnerability assessment of Gravity Load Designed R/C frames. *Bulletin of Earthquake Engineering*, 1(3), 371-395.
- Menoni, S., Meroni, F., Pergalani, F., Petrini, V., Luzi, L., & Zonno, G. (2000). Measuring the seismic vulnerability of strategic public facilities: response of the health-care system. *Disaster Prevention and Management: An International Journal*, 9(1), 29-38. DOI: 10.1108/09653560010316041.
- Miniati, R., & Iasio, C. (2012). Methodology for rapid seismic risk assessment of health structures: Case study of the hospital system in Florence, Italy. *International Journal of Disaster Risk Reduction*, 2, 16-24. DOI: 10.1016/j.ijdr.2012.07.001.
- Miniati, R., Capone, P., & Hosser, D. (2014). Decision Support System for Rapid Seismic Risk Mitigation of Hospital Systems: Comparison Between Models and Countries. *International Journal of Disaster Risk Reduction*, 9(12–25). DOI: 10.1016/j.ijdr.2014.03.008
- Ministry of Land, Infrastructure, Transport and Tourism (MLIT) (2014). "Guidelines for Tsunami Evacuation Buildings." Tokyo, Japan.
- Moghtadernejad, S., Mirza, S. (2014). Performance of building facades. Presented at the Proceedings of CSCE - 4th International Structural Specialty Conference, Canadian Society for Civil Engineers, Halifax, NS (2014), pp. 28-31
- Moran-Rodriguez, S., & Novelo-Casanova, D. A. (2018). A Methodology to Estimate Seismic Vulnerability of Health Facilities: Case Study in Mexico City, Mexico. *Natural Hazards*, 90(1349–1375). DOI: 10.1007/s11069-017-3101-2
- Mouroux P., Le Brun B., 2006. Presentation of RISK-UE project. *Bulletin of Earthquake Engineering*, 4(4), 323-339.
- Nikolic, Ž., Benvenuti, E., & Runjic, L. (2022). Seismic risk assessment of urban areas by a hybrid empirical-analytical procedure based on peak ground acceleration. *Applied Sciences*, 12, 3585. DOI: 10.3390/app12073585.
- Ntaliakouras, I., & Pnevematikos, N. (2018). Seismic Vulnerability Curves for Industrial Steel Structures. [TEI of Athens, Greece]
- Onescu, I., Onescu, E., & Mosoarca, M. (2019). The impact of the cultural value on the seismic vulnerability of a historical building. *IOP Conference Series: Materials Science and Engineering*, 603, 042031. DOI: 10.1088/1757-899X/603/4/042031

- Ordaz M., Miranda E., Reinoso E., Pérez-Rocha L.E., 2000. Seismic Loss estimation model for Mexico City. Proceedings of the 12th World Conference on Earthquake Engineering, Auckland, New Zealand, January 30-February 4. Paper No. 1902.
- Orsini G., 1999. A model for buildings' vulnerability assessment using the Parameterless Scale of Seismic Intensity (PSI). *Earthquake Spectra*, 15(3), 463-483.
- Ozdemir P., Boduroglu M.H., Ilki A., 2005. Seismic safety screening method. Proceedings of the International Workshop on Seismic Performance Assessment and Rehabilitation of Existing Buildings (SPEAR), Ispra, Italy, April 4-5. Paper No. 23.
- Papathoma-Köhle M., Ghazanfari A., Mariacher R., Huber W., Lücksmann T., Fuchs, S. (2023). Vulnerability of Buildings to Meteorological Hazards: A Web-Based Application Using an Indicator-Based Approach. *Applied Sciences*, 13, 6253. DOI: 10.3390/app13106253
- Park Y.J., Ang A.H.S., 1985. Mechanistic seismic damage model for reinforced concrete. *ASCE Journal of Structural Engineering*, 111(4), 722-739.
- Perrone, D., Aiello, M. A., Pecce, M., & Rossi, F. (2015). Rapid Visual Screening for Seismic Evaluation of RC Hospital Buildings. *Structures*, 3(57-70). DOI: 10.1016/j.istruc.2015.03.002
- Petrone, C., Rossetto, T., Goda, K. (2017). "Fragility Assessment of a RC Structure under Tsunami Actions via Nonlinear Static and Dynamic Analyses." *Engineering Structures*, 136, 36-53.
- Pinho R., Bomber J.J., Glaister S., 2002. A simplified approach to displacement-based earthquake loss estimation analysis. Proceedings of the 12th European Conference on Earthquake Engineering, London, UK, September 9-13. Paper No. 738.
- Priestley M.J.N., 1997. Displacement-based seismic assessment of reinforced concrete buildings. *Journal of Earthquake Engineering*, 1(1), 157-192.
- Qi, Z., van de Lindt, J.W., Liu, H., Do, T.Q., Dao, T.N. (2014). "Experimental Study of Tsunami Wave Impact Forces on Wood-Frame Walls." *Journal of Performance of Constructed Facilities*, 28(1), 201-210.
- Rapone, D., Brando, G., Spacone, E., & De Matteis, G. (2018). Seismic vulnerability assessment of historic centers: Description of a predictive method and application to the case study of Scanno (Abruzzi, Italy). *International Journal of Architectural Heritage*, 12(7-8), 1171-1195. DOI: 10.1080/15583058.2018.1503373
- Reese, S., Cousins, W.J., Power, W.L., Palmer, N.G., Tejakusuma, I.G., Nugrahadi, S. (2011). "Tsunami Vulnerability of Buildings and People in South Java – Field Observations after the July 2006 Java Tsunami." *Natural Hazards and Earth System Sciences*, 11(2), 605-614.
- Rodgers, J. E. (2012). Why schools are vulnerable to earthquakes. *GeoHazards International*.
- Rossetto T., Elnashai A., 2003. Derivation of vulnerability functions for European-type RC structures based on observational data. *Engineering Structures*, 25(10), 1241-1263.
- Rossetto T., Elnashai A., 2005. A new analytical procedure for the derivation of displacement-based vulnerability curves for populations of RC structures. *Engineering Structures*, 27(3), 397-409.
- Rossetto, T., De Risi, R., Del Zoppo, M., Foster, H., Macabuag, J., Ioannou, I., et al. (2019). "The Influence of Out-of-Plane Infill Walls on the Seismic Vulnerability Assessment of RC Frame Buildings." *Earthquake Engineering & Structural Dynamics*, 48(4), 438-459.
- Rosti, A., Rota, M., & Penna, A. (2022). An empirical seismic vulnerability model. *Bulletin of Earthquake Engineering*, 20, 4147-4173. DOI: 10.1007/s10518-022-01374-3.

- Rota M., Penna A., Strobbia C., Magenes G., 2008. Direct derivation of fragility curves from Italian post-earthquake survey data. Proceedings of the 14th World Conference on Earthquake Engineering, Beijing, China, October 12-17. Paper 09-01-0148.
- Ruggiero, G., Marmo, R., Nicoletta, M. (2021). Methodologies for Service Life Prediction of Buildings. *Sustainability*, 13(5), 2812.
- Ruiz F, Aguado A, Serrat C, Casas J. R (2019). Condition assessment of building façades based on hazard to people. *Structure and Infrastructure Engineering* 15(10):1346-1365.
- Sabetta F., Goretti A., Lucantoni A., 1998. Empirical fragility curves from damage surveys and estimated strong ground motion. Proceedings of the 11th European Conference on Earthquake Engineering, Paris, France, September 6-11.
- Sabetta F., Pugliese A., 1987. Attenuation of peak horizontal acceleration and velocity from Italian strong-motion records. *Bulletin of the Seismological Society of America*, 77(5), 1491-1513.
- Sabetta F., Pugliese A., 1996. Estimation of response spectra and simulation of nonstationary earthquake ground motions. *Bulletin of the Seismological Society of America*, 86(2), 337-352.
- Salerno, E., Carpanese, P., Pernechele, V., & da Porto, F. (2019). A priority ranking procedure to assess seismic vulnerability of school buildings at territorial scale. Dipartimento di Ingegneria Civile, Ambientale e Meccanica, Università di Trento.
- Shooraki, M. K., Bastami, M., Abbasnejadfar, M., & Motamed, H. (2024). Development of Seismic Fragility Curves for Hospital Buildings Using Empirical Damage Observations. *International Journal of Disaster Risk Reduction*, 108(104525). DOI: 10.1016/j.ijdr.2024.104525
- Silva, A., de Brito, J., Gaspar, L.P. Methodologies for Service Life Prediction of Buildings, Springer, Switzerland, 2016.
- Singhal A., Kiremidjian A.S., 1996. Method for probabilistic evaluation of seismic structural damage. *ASCE Journal of Structural Engineering*, 122(12), 1459-1467.
- Singhal A., Kiremidjian A.S., 1998. Bayesian updating of fragilities with application to RC frames. *ASCE Journal of Structural Engineering*, 124(8), 922-929.
- Sinha, A. K., & Siddharth. (2021). A review paper on seismic vulnerability and evaluation methodology of buildings. In *Advances in Geotechnics and Structural Engineering* (pp. 533–546). Springer. DOI: 10.1007/978-981-33-6969-6_45.
- Smith, D. J., & Masters, F. J. (2015). A study of wind load interaction for roofing field tiles. In: [Presented at 14th International Conference on Wind Engineering]. 02744. pp. 1-9. From: ICWE14: 14th International Conference on Wind Engineering, 21-26 June 2015, Porto Alegre, Brazil.
- Spence R.J.S., Coburn A.W., Sakai S., Pomonis A., 1991. A parameterless scale of seismic intensity for use in the seismic risk analysis and vulnerability assessment. *International Conference on Earthquake, Blast and Impact*, Manchester, UK, September 19-20. Pp. 19-30.
- Suppasri, A., Koshimura, S., Imai, K., Katada, T., Matsuoka, M., Tanaka, N., et al. (2011). "Tsunami Fragility Curves: A Comprehensive Review." *Natural Hazards and Earth System Sciences*, 11(8), 2313-2327.
- Suzuki, A., Iervolino, I., Kurata, M., & Shimmoto, S. (2017). State-dependent fragility curves for aftershock seismic risk assessment of Japanese steel frames.
- Taghavi, S., & Miranda, E. (2003). Response Assessment of Nonstructural Building Elements, Pacific Earthquake Engineering Research Center, University of California, Berkeley, CA, 2003.

- UNDRR and ISC. (2020). *Hazard Information Profiles (HIPs)*. Supplement to the *Hazard Definition and Classification Review: Technical Report*. United Nations Office for Disaster Risk Reduction.
- Varum, H., Batalha, N., & Rodrigues, H. (2019). Seismic Performance of RC Precast Industrial Buildings—Learning with the Past Earthquakes. *Innovative Infrastructure Solutions*, 4(4). DOI: 10.1007/s41062-018-0191-y
- Verderame G.M., De Luca F., Ricci P., Manfredi G., 2010. Preliminary analysis of a soft storey mechanism after the 2009 L'Aquila earthquake. *Earthquake Engineering and Structural Dynamics*. DOI: 10.1002/eqe.1069
- Whitman R.V., Anagnos T., Kircher C.A., Lagorio H.J., Lawson R.S., Schneider P., 1997. Development of a national earthquake loss estimation methodology. *Earthquake Spectra*, 13(4), 643-661.
- Whitman R.V., Reed J.W., Hong S.T., 1973. Earthquake Damage Probability Matrices. *Proceedings of the 5th World Conference on Earthquake Engineering*, Rome, Italy, June 25-29. Vol. 2, pp. 2531-2540.
- World Health Organization (WHO) (2006). *Health facility seismic vulnerability evaluation: A handbook*. WHO Regional Office for Europe, Copenhagen, Denmark. Disponibile su: WHO Europe.
- Yakut A., 2004. Preliminary seismic performance assessment procedure for existing RC buildings. *Engineering Structures*, 26(10), 1447-1461.

Authors contribution

Even if the Deliverable are unified in their aspects of conception, knowledge framework, methodological approach and experimentation, the contributions have been elaborated as follows:

Introduction	Rossella Marmo and Roberto Castelluccio
Seismic vulnerability	Mariano Di Domenico and Gerardo Mario Verderame
Tsunami vulnerability	Marta Del Zoppo
Heat wave vulnerability	Cristina Visconti, Valeria D'Ambrosio, Ferdinando Miraglia